

ISSN 1407-5806

**COMPUTER
MODELLING
AND
NEW TECHNOLOGIES**

**Volume 7
No 1**

2003

Transporta un sakaru institūts
(Transport and Telecommunication Institute)

Computer Modelling and New Technologies

Volume 7, No.1- 2003

ISSN 1407-5806

ISSN 1407-5814

(On-line: www.tsi.lv)

Riga – 2003

EDITORIAL BOARD:

Prof. Igor Kabashkin (Chairman of the Board), *Transport & Telecommunication Institute, Latvia*;
Prof. Yuri Shunin (Editor-in-Chief), *Transport & Telecommunication Institute, Latvia*;
Prof. Adolfas Baublys, *Vilnius Gediminas Technical University, Lithuania*;
Dr. Brent Bowen, *University of Nebraska at Omaha, USA*;
Prof. Olgierd Dumbrajs, *Helsinki University of Technology, Finland*;
Prof. Eugene Kopytov, *Transport & Telecommunication Institute, Latvia*;
Prof. Arnold Kiv, *Ben-Gurion University of the Negev, Israel*;
Prof. Anatoly Kozlov, *Moscow State University of Civil Aviation, Russia*;
Prof. Juris Zakis, *University of Latvia*;
Prof. Edmundas Zavadskas, *Vilnius Gediminas Technical University, Lithuania*.

Technical editors:

MS Christina Hamroon, *Transport & Telecommunication Institute, Latvia*
MS Cyril Budilov, *Transport & Telecommunication Institute, Latvia*

Host Organization:

Transport and Telecommunication Institute - Eugene Kopytov, Rector

Co-Sponsor Organization:

PAREX Bank, Latvia - Valery Kargin, President

Supporting Organizations:

Latvian Transport Development and Education Association - Andris Gutmanis, President
Latvian Academy of Sciences - Juris Ekmanis, Vice-President
Latvian Operations Research Society – Igor Kabashkin, President
University of Nebraska at Omaha, USA - Brent Bowen, Director of Aviation Institute
“The Khaim Kordonsky Charitable Foundation”- Inna Kordonsky-Frankel

THE JOURNAL IS DESIGNED FOR PUBLISHING PAPERS CONCERNING THE FOLLOWING FIELDS OF RESEARCH:

- mathematical and computer modelling
- mathematical methods in natural and engineering sciences
- physical and technical sciences
- computer sciences and technologies
- semiconductor electronics and semiconductor technologies
- aviation and aerospace technologies
- electronics and telecommunication
- navigation and radar systems
- telematics and information technologies
- transport and logistics
- economics and management
- social sciences

Articles are presented in the journal in English (preferably), Russian, German and Latvian languages (at the option of authors). All articles are reviewed.

EDITORIAL CORRESPONDENCE

Transporta un sakaru institūts (Transport and Telecommunication Institute)
Lomonosova iela 1, LV-1019, Riga, Latvia. Phone: (+371)-7100593. Fax: (+371)-7100535.
E-mail: journal@tsi.lv, <http://www.tsi.lv>

COMPUTER MODELLING AND NEW TECHNOLOGIES, 2003, Vol. 7, No.1

ISSN 1407-5806, ISSN 1407-5814 (on-line: www.tsi.lv)

Scientific and research journal of Transport and Telecommunication Institute (Riga, Latvia).
The journal is published since 1996.

Copyright © Transport and Telecommunication Institute, 2003

CONTENT

EDITORS' REMARKS	5
SOLID STATE PHYSICS	7
DFT SIMULATIONS ON A REGULAR <i>O/Al(001)</i> INTERFACE Yu.F. Zhukovskii, A. Kovalevska, P.W.M. Jacobs, Yu.N. Shunin	7
DFT SIMULATIONS OF THE INTERACTION BETWEEN OXYGEN AND A STEPPED <i>Al(111)</i> SUBSTRATE P.W.M. Jacobs, Yu.F. Zhukovskii, A. Kovalevska, Yu.N. Shunin	18
PREDICTION OF PHASE FORMATION IN <i>Mg-Ag</i> IN NON-EQUILIBRIUM CONDITIONS ON THE BASIS OF <i>ab initio</i> CALCULATIONS I.G. Brown, M.M. Talianker, D.L. Fuks, A.E. Kiv, L.Yu. Kutsenko	24
CORRELATION EFFECTS IN ATOM-VACANCY "ALLOY" D. Fuks	28
APPLIED STATISTICS	37
DEA SUPER EFFICIENCY MULTISTAGE RANKING Y. Hadad, L. Friedman, Z. Sinuany-Stern, A. Mehrez	37
DECISION-MAKING SIMULATION MODEL FOR CONTROLLING SEVERAL STOCHASTIC PROJECTS Z. Laslo, D. Golenko-Ginzburg, A. Gonik, A. Malisheva	47
MATHEMATICAL PHYSICS	55
ONE SIMPLE METHOD FOR SOLUTION OF SOME CLASS OF INVERSE PROBLEMS S. Guseinov	55
Authors' index	59
Personalia	60
Patrick Jacobs - 80 <i>Congratulations</i>	62
Preparation of publications	63



Editors' Remarks

The "good old times" - all times when old are good -
Are gone; the present might be if they would;
Great things have been, and are, and greater still
Want little of mere mortals but their will:
A wider space, a greener field, is given
To those who play their "tricks before high heaven."
I know not if the angels weep, but men
Have wept enough — for what? — to weep again!

George Gordon Byron **THE AGE OF BRONZE,**
1822-1823

Since this 7th volume we change the format of our journal. It will be published four times per year. This new format will allow us to present new scientific results of contributors in a shorter time. This also means that we evidently divide the main topics of the journal into different issues. But this does not mean that the edition strategy is transformed sufficiently.

This edition is the continuation of our publishing activities. We hope our journal will be interesting for research community, and we are open for collaboration both in research and publishing.

EDITORS



Yu. N. Shunin



I.V. Kabashkin



DFT SIMULATIONS ON A REGULAR O/Al(001) INTERFACE

Yu.F. ZHUKOVSKII^a, A. KOVALEVSKA^a, P.W.M. JACOBS^b, Yu.N. SHUNIN^c

^a*Institute of Solid State Physics, University of Latvia, 8 Kengaraga, LV-1063, Riga, Latvia*

^b*Department of Chemistry, University of Western Ontario, London, ON, N6A 5B7, Canada*

^c*Department of Natural Sciences and Computer Technologies, Information System Institute & Transport and Telecommunication Institute, 1 Lomonosova, LV-1019, Riga, Latvia*

Slab models of the regular O/Al(001) interface with 1/4 monolayer (ML), 1/2 ML and 1 ML oxygen coverages have been calculated using *ab initio* density functional method as implemented in the CRYSTAL 98 code. The preliminary stage of molecular oxygen adsorption leads to the dissociation of O₂ molecules and arrangement of O_{ads} atoms above the hollow positions on the (001) substrate. The second stage of the simulation performed included the penetration of adatoms into the substrate and their further localization on octahedral and tetrahedral sites in the aluminium lattice. Unlike the regular O/Al(111) interface, absorption of O_{ads} adatoms on the Al(001) surface occurs readily without any steric restrictions on the density of their surface overlayer, in agreement with the failure to observe a distinct chemisorption stage for oxygen on Al(001). The calculated properties of interface energetics and its electronic structure are analyzed for the O/Al(001) interface to interpret the stages of the initial oxidation which were simulated.

Keywords: O/Al(001) interface, periodic slab model, dissociation of oxygen molecules, chemisorption, absorption, DFT-LCGTF method

1. Introduction

Because of its great practical importance, the oxidation of aluminium by oxygen continues to be an active field of research. Despite considerable efforts, reliable atomistic description of this process is still not very well developed, especially at the stage between the absorption of oxygen adatoms and the initial oxide nucleation. In our previous paper from a series of publications devoted to the DFT simulations on periodic slab models of densely packed O/Al interfaces, we first described an atomistic mechanism of the interaction between oxygen and the perfect Al(111) surface [1], up to the formation of separate Al₂O₃ formula units.

The interaction of oxygen with a regular Al(001) surface was comprehensively studied earlier both experimentally and theoretically [2-13]. Interpretation of experimental data for the O/Al(001) interface is much more difficult than in the case of O/Al(111). For example, it is not possible to distinguish by any experimental method the elementary stages of chemisorption, absorption and oxide nucleation [2]. In the X-ray photoelectron spectra (XPS) [2,3] from the beginning of oxygen contact with Al(001) a broad peak appears (removed by ~2.5-2.7 eV from that for the metallic state) with a weak shoulder (at ~1.2-1.3 eV) which corresponds to chemical shift (CS) of the 2p(Al) level for oxide and chemisorbed oxygen, respectively. Low-energy electron diffraction measurements (LEED) could not establish any metastable well-ordered oxygen "islands" on the Al(001) substrate [4] as was done for the O/Al(111) interface [14]. Moreover, dramatically different changes of work function ($\Delta\phi$) on both surfaces have been found at the beginning of the interaction of oxygen with aluminium: namely, a slight increase of $\Delta\phi$ on the (111) surface and its essential decrease on (001) [5]. Unlike the O/Al(111) interface, no direct experimental measurements have been done to define the equilibrium position of O_{ads} atoms on Al(001). It has only been concluded (when comparing various experimental and theoretical data [4,6,7,10]) that chemisorbed oxygen on Al(001) most likely occurs within or slightly below the surface plane at four-fold hollow sites. A simple explanation of the faster rate of oxide nucleation on the Al(001) substrate in comparison with Al(111) was given in [8]: because of its lower density compared to (111) the (001) face provides more free space between the aluminium atoms for O atoms to migrate to subsurface sites. In fact, no structural reconstruction of the Al(001) surface is necessary for the penetration of O_{ads} atoms into the substrate: for an adatom, lying in the middle of the square unit cell (UC) of the Al(001) plane, the Al-O bond has a length of 2.025 Å which is larger than the sum of the atomic radii of O and Al atoms (1.85 Å) [2]. Moreover, the Al(111) surface possesses a smaller surface energy than that of Al(001) [15] and, therefore, the former is energetically more stable. Thus, the regular O/Al(111) interface is usually considered as a model system to study the initial aluminum oxidation whereas the O/Al(001) interface represents rather an additional possibility to understand better the oxidation mechanism.

Previous theoretical calculations on the electronic structure of the O/Al(001) interface have been

Solid State Physics

based on either Hartree-Fock (HF) [9-11] or density functional theory (DFT) [12,13] formalisms. In the first case various kinds of finite cluster models were mainly used whereas DFT methods were applied to periodic slabs. Moreover, molecular-dynamic (MD) simulations have also been performed to interpret angle-resolved secondary ion mass spectrometry measurements (ARSIMS) of oxygen interaction with the Al(001) surface [7]. In this paper, using the DFT method as implemented in the *CRYSTAL 98* code [16], we perform systematic simulations of the interaction of oxygen with the perfect Al(001) surface beginning with O₂ molecules (including their adsorption and further dissociation), through the formation of a chemisorbed layer up to the penetration of adatoms into the substrate and their internal diffusion. We consider slab models of both 1/4 ML and 1 ML substrate coverages by oxygen adatoms. Due to the different symmetry of the Al₂O₃ formula units and the Al(001) surface (which are D_{3h} and C_{4h} , respectively) no simple periodic model may be constructed for the [(Al₂O₃)_nO]/Al(001) system as was done in our previous paper devoted to the perfect O/Al(111) interface [1]. Consequently, we did not consider the stage of initial oxide nucleation on the Al(001) substrate at all.

2. Theoretical background

2.1. COMPUTATIONAL DETAILS

Since the computational method used in our current calculations has been described in detail recently [1,17] we consider in this Subsection only the most general points. In the *CRYSTAL 98* code [16] the periodic wave functions are defined as CO LCGTF (crystalline orbitals formed from linear combinations of Gaussian-type functions). To perform DFT calculations on the heterogeneous O/Al(001) interface, we used the non-local exchange potential suggested by Becke [18] and a correlation potential constructed by Perdew and Wang [19] according to the generalized gradient approximation (GGA), which depends not only on the electron density but also on its gradients. The stability of the Fermi level ε_F during the self-consistent-field (SCF) procedure is much improved in the *CRYSTAL 98* code by replacing the Heaviside 0 K occupation function $\Theta\{\varepsilon_F - \varepsilon(\mathbf{k})\}$ by a linear approximation to the finite temperature Fermi-Dirac occupation function $f_T\{\varepsilon_F - \varepsilon(\mathbf{k})\}$. This substitution, when combined with level shifting [20], effectively removes the inherent instability associated with self-consistent field (SCF) calculations on metals and small band-gap semiconductors. We also took advantage of the convergence stabilizer, which mixes current and previous Kohn-Sham matrices at each SCF cycle [21]. One of the crucial points in calculations on metals is a correct choice of reciprocal-space integration parameters: optimum values of shrinking factors for Al were found to be 16 for both the Monkhorst and Pack [22] and Gilat [23] nets.

All-electron basis sets (BSs) consisting of GTFs were used for both aluminum and oxygen. That for Al (8-8-311G) was based on a BS used previously [24], but modified by adding a $3d$ -type polarization function and then re-optimizing valence and virtual shells to achieve a minimum total energy. To take into account quantum size effects the outer valence $3sp$ and virtual $4sp$ and $3d$ shells in the external layers of Al slabs, were made slightly more diffuse (as suggested by Boettger *et al.* [25]) and then these GTFs were again re-optimized. This resulted in a more homogeneous electron distribution and improved SCF convergence. The BS for oxygen (8-511G) was obtained by re-optimizing that used earlier in *CRYSTAL* investigations of MgO polymorphs [26] but modified by adding a $3d$ polarization function. To optimize the basis sets and the geometry of the various slab configurations we used a procedure introduced by Heifets *et al.* [27] that interfaces with *CRYSTAL* calculations a conjugate gradient optimization technique [28] using numerical computation of derivatives.

2.2. SLAB MODELS

In our previous paper [17] we have described in detail the periodic slab model of the regular Al(001) surface. (The key parameter of the aluminium substrate with *fcc* structure is the nearest-neighbor distance $r_{\text{Al-Al}}^{(\text{min})} \approx 2.864 \text{ \AA}$ [29].) The same three-, five- and seven-layer slabs modeling the Al substrate have been used in the current study. We have used the optimized geometry of relaxed Al(001) slabs as an initial guess for further simulation of their interaction with oxygen. 1 ML, 1/2 ML and 1/4 ML adsorbate coverages have been imitated by choosing either primitive 1×1 unit cells (UC) of Al(001) substrate or their 2×2 supercells (SC) *per* oxygen atom. To reduce computational effort and to exploit to the maximum the system's symmetry, we have mainly simulated one-sided or two-sided oxygen chemisorption and absorption when using 3-layer or 5-layer Al(001) slabs, respectively.

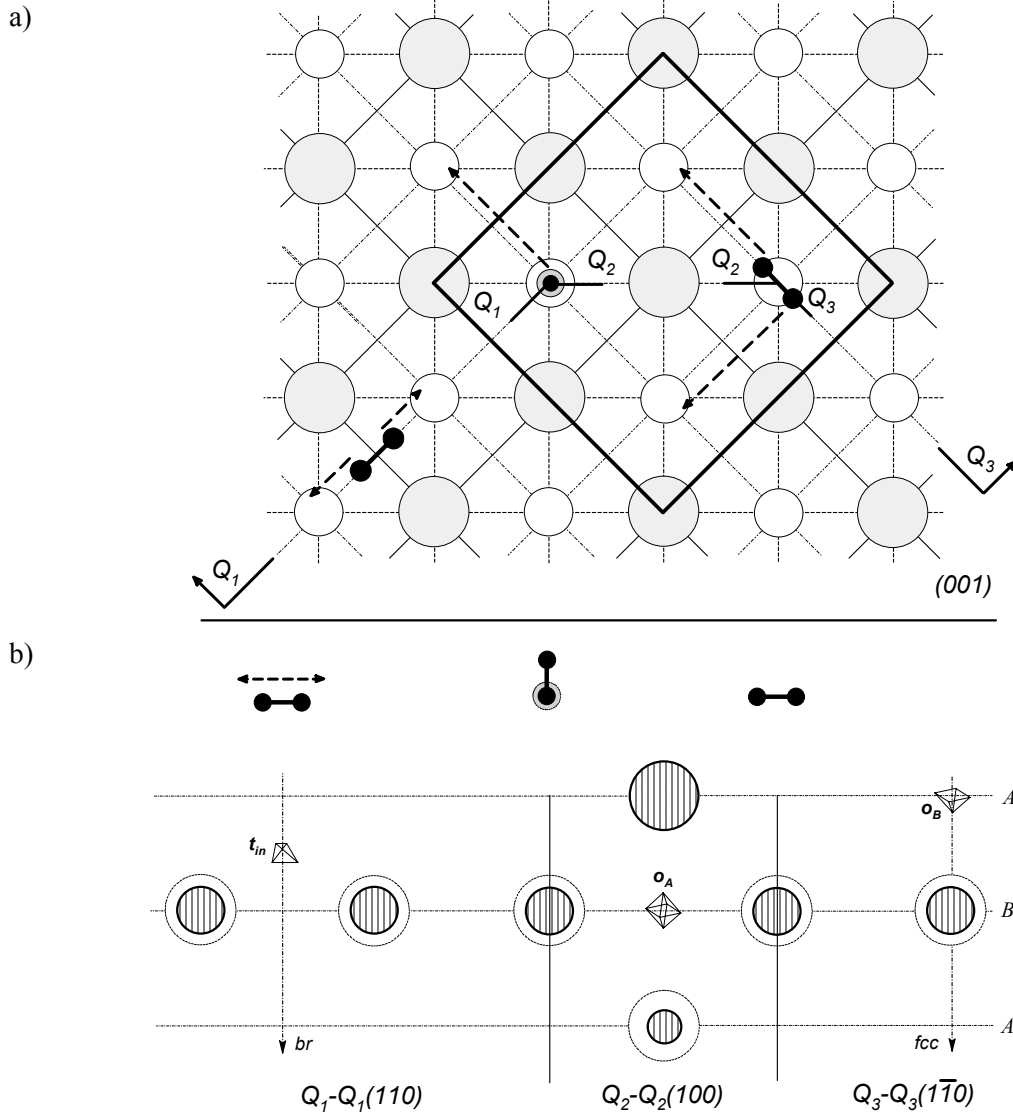


Figure 1. Periodic model for the adsorption of oxygen molecule on the regular Al(001) slab with three possible adsorption sites: two horizontal positions over bridge (between nearest Al atoms) and four-fold (hollow) sites and one vertical position above the same *fcc* hollow site on the substrate. The most probable trajectories for dissociation are shown in a) by dashed arrows.

- a) Top view of the Al(001) substrate. Largest circles denote Al atoms in the top layer *A* and smaller circles Al atoms in the next subsurface layers. All nearest-neighbor atoms are joined with straight solid and dashed lines (in the former case they join surface atoms only). The 2×1 surface supercell is marked by thicker solid lines.
- b) Three joined cross-sections of the same model as shown in a) along the $Q_1-Q_1(110)$, $Q_2-Q_2(100)$ and $Q_3-Q_3(1\bar{1}0)$ planes. The small tetrahedra and octahedra show surface (o_B) and interstitial (t_{in} and o_A) sites of tetrahedral and octahedral symmetry, which are the preferred sites for the metastable location of oxygen ions.

For the models of molecular adsorption (with both normal and parallel orientation of O_2 with respect to the substrate) we have used a 2×2 SC of the Al(001) slab *per* adsorbed molecule by setting intramolecular atoms oriented symmetrically towards the hollow and bridge sites on the substrate (only three layers are shown in Fig. 1). To show all three adsorption configurations in Fig. 1b we have joined three cross-sections. As in our previous study on the regular $O_2/Al(111)$ interface [1], we have fixed both the triplet (*T*) ground state $^3\Sigma_g^-$ and equilibrium bond length ($r_{O-O}^{(0)} \approx 1.21$ Å) for the free oxygen molecule as an initial guess for the simulation of molecular adsorption. The probable dissociation trajectories are shown by dashed arrows on the top view of the $O_2/Al(001)$ interface (Fig. 1a). Along these trajectories, we have considered both triplet and singlet (*S*) states for adsorbed oxygen. (To obtain the proper profiles of energy curves we have set a minimal symmetry for all interface configurations: for molecular adsorption parallel to the surface, the symmetry of the $O/Al(001)$ interface corresponds to C_{2h} .)

Solid State Physics

Dissociation of $(\text{O}_2)_{\text{ads}}$ should be completed by the chemisorption of newly-formed separated adatoms above the Al(001) surface, more probably over four-fold o_B sites of C_{4h} symmetry (Fig. 1b).

Both the equilibrium interface spacing (which is defined by the vertical coordinate of the oxygen adatom z_O) and the first interlayer subsurface spacing (l_{1-2}) have been optimized carefully for each chemisorption configuration, over both o_B and t_{in} sites (Fig. 1b). In this paper we do not discuss the overlayer diffusion of adatoms along O/Al(001) interface because it is useful in explaining the formation of the $(\text{O}_{\text{ads}})_n$ “islands” (if $\theta_O < 1$) but not the initiation of the oxidation of aluminium. Since the interaction of oxygen with the (001) substrate is very large the formation of islands is doubtful.

When simulating trajectories of oxygen penetration into the substrate, vertical relaxation has been considered for both 1/4 ML, 1/2 ML and 1 ML oxygen coverages whereas horizontal structural reconstruction has been simulated only for the two former cases of quasi-isolated adatoms (we have found a slight expansion of those squares consisting of the four nearest Al atoms on the surface lattice, which are crossed by oxygen adatoms penetrating into the substrate *via* o_B sites, thus reducing the energy barrier for absorption). This is very important in describing real structural transformations and to compensate for the absence of a molecular-dynamic treatment. Beginning with the penetration of O_{ads} into the (001) substrate we have performed an analogous optimization for the reconstructed O/Al interface to describe underlayer diffusion of O atoms. Apart from the optimization of three possible trajectories for the dissociative adsorption of $(\text{O}_2)_{\text{ads}}$ molecules (Fig. 1a) and the chemisorption of O_{ads} atoms over hollow and bridge sites, we have also simulated both absorption and interstitial diffusion of oxygen atoms in the substrate along the following trajectory (Fig. 1b): center of the surface half-octahedron (o_B) \rightarrow center of the nearest subsurface tetrahedron (t_{in}) \rightarrow center of the adjacent tetrahedron (t_{in}) \rightarrow center of the subsurface octahedron (o_A).

2.3. PROPERTIES EVALUATED FOR ANALYSIS

In this paper we discuss the same properties of *interface energetics* and *electronic structure* for both molecular adsorption and atomic chemisorption of oxygen on the Al(001) substrate presented in Tables 1,2 and Figs. 2,3 as described in detail in our previous paper devoted to the regular O/Al(111) interface [1].

To estimate the energetics of the O/Al(001) interface we have constructed potential energy curves upon the energy surface $E_b(\mathbf{r})$ as a function of the position of oxygen molecules or atoms (over or within the substrate). For each point determined by \mathbf{r}_i , the values of E_b have been defined with respect to the asymptotic plateau, which corresponds to remote positions of molecules or atoms. Every point calculated for this energy surface was optimized by both the vertical relaxation of outer Al layers and the structural reconstruction within them, always checking spin multiplicity. A spline technique has been used to construct smooth energy curves (Fig. 2) for different structural transitions over the whole range of $\{\mathbf{r}\}$. To define an optimal value of the binding energy $E_{bind}(\text{O}_2/\text{Al})$ or $E_{bind}(\text{O}/\text{Al})$ using such a curve of $E_b(z)$, where z is the distance from surface, we have applied the so-called universal binding energy relation [30]:

$$E_b(z_i) = E_{bind} k \left(1 + \frac{z_i - z^{(o)}}{z_i}\right) \exp \left[-\frac{z_i - z^{(o)}}{s} \right], \quad (1)$$

where the multiplier k is either 1 or 2, depending on whether a one- or two-side model of adsorption is considered, $z^{(o)}$ the equilibrium interfacial distance, and s a scaling constant. However, such a definition of $E_{bind}(\text{O}/\text{Al})$ is not always the most reliable. For monolayers from adatoms or molecules, a strong repulsion between them at remote distances from the substrate leads to an SCF divergence, and we were forced to be very careful in those cases to obtain a realistic description of the “tails” in the corresponding $E_b(z)$ curves.

The energy of dissociative chemisorption of an $(\text{O}_2)_{\text{ads}}$ molecule is defined by the formula:

$$E_{diss}[(\text{O}_2)_{\text{ads}}] = -(E_{\text{O}_2/\text{slab}}^{\min} - E_{2\text{O}/\text{slab}}^{\min}), \quad (2)$$

where $E_{\text{O}_2/\text{slab}}^{\min}$ and $E_{2\text{O}/\text{slab}}^{\min}$ are the minimized total energies of the corresponding systems *for* the same

Solid State Physics

surface unit cell, taking into account the difference in energies for the S and T electronic states $\Delta E_{bind}^{T \rightarrow S}$. To estimate the total energy gain *per* one chemisorbed adatom due to spontaneous adsorption and further dissociation of oxygen molecule we combine both energies:

$$E_{gain}(O_{ads}) = \{E_{bind}[(O_2)_{ads}] - E_{diss}[(O_2)_{ads}]\} . \quad (3)$$

Together with initial kinetic energy of adsorbed molecule a value of E_{gain} allowed us to estimate the height of the energy barriers for various structural transformations, which need to be overcome by O_{ads} .

Parameters of the electron density distribution in the O/Al(001) interface (induced effective charges Δq_{O_2} and Δq_O on molecules and adatoms as well as two-dimensional (2D) difference electron charge distributions $[\rho(\mathbf{r})]_z$ along planes which cross slabs perpendicular to their surface) have been described in more details in our previous papers [1,17]. We can add only that induced effective charges Δq , which are considered in this paper, are defined as the difference between the total electronic charge of an isolated atom and its total charge in the O/Al(001) interface. The same holds for the chemical shifts of the core levels (we are analyzing CS for $2p(\text{Al})$ and $1s(\text{O})$ states, which are shifted with reference to the isolated substances by chemisorption, absorption and oxidation). Again, we consider here not the absolute values of energy levels but differences $\varepsilon_i^{(s)} - \varepsilon_F$ for both pure substrate and adsorbate as well as the corresponding O/Al interface with reference to a common energy scale with Fermi level $\varepsilon_F' = 0$. Therefore, these CSs were re-defined for the new spectral distributions $\{\varepsilon_i^{(isol)}\}$ and $\{\varepsilon_i^{(interf)}\}$ with respect to their common ε_F' . These $\Delta\varepsilon^{CS}(\varepsilon_i)$ can be compared directly with the corresponding experimental values for $1s(\text{O})$ and $2p(\text{Al})$ energy levels [3].

To construct the energy diagram (Fig. 2), which fixes local minima and saddle points upon the energy surface $E_b(\mathbf{r})$ for the chain of structural transformation in the interface from remote O_2 molecules over the pure Al(001) substrate up to the interstitial diffusion of oxygen atoms in the substrate, we have done calculations on a model of one-sided 1/2 ML coverage of a 3-layer Al slab. In this model we have fixed the position of a chemisorbed O_{ads} atom above an o_B site on a 2×2 SC of Al(001) slab in which a second adatom has been allowed to penetrate into the substrate and to diffuse there between interstices t_{in} and o_A . Thus, we have simulated a particular absorption configuration with an imitation of horizontal reconstruction of the surface, as described in Subsection 2.2. In Fig. 3 for each interface configuration corresponding to an energy level in Fig. 2, we have drawn one or two 2D electron distributions $[\rho(\mathbf{r})]_z$ along (100) and (110) planes that intersect the Al(001) surface (that is, the charge density in the relaxed interface minus the sum of these densities for the isolated atoms).

3. Adsorption of molecular oxygen and its dissociation

The main results obtained in our simulations on several configurations of O_2 molecules over a regular Al(001) substrate, the models for which have been described in Subsection 2.2 (Fig. 1), are presented in Table 1 and Figs. 2, 3. We have checked a number of other possible sites and orientations for the molecular adsorbate, but their bonding with both substrates was found to be noticeably weaker. As explained in Subsection 2.2, calculations on molecular adsorption models have been performed for these systems in both triplet and singlet states. The oxygen interaction with (001) substrate begins with the same initial geometry of a free O_2 molecule as described in Ref. [1] for regular Al(111) surface. Unlike the latter case, the horizontal position of $(O_2)_{ads}$ above the four-fold fcc site on Al(001) surface (o_B center) is preferred (see Table 1). This difference could be the cause of symmetry compatibility of the linear O_2 molecule with the (001) substrate in contrast to the (111) surface. Triplet states of adsorbed oxygen molecules above the (001) surface are even more stable than singlet states (by 1.0-1.1 eV) than above the (111) surface.

Molecular adsorption on Al(001) surface is accompanied by a larger charge transfer from external aluminium atoms than in the $O_2/\text{Al}(111)$ interface (1.15 e *per* molecule *versus* 0.9 e [1]). Estimated values of chemical shifts $\Delta\varepsilon_0^{CS}(1s)$ almost coincide with those obtained for the $O_2/\text{Al}(111)$ interface [1], whereas $\Delta\varepsilon_{Al}^{CS}(2p)$ are considerably less for the $O_2/\text{Al}(001)$ since substrate coverage in the latter case is only half that for $O_2/\text{Al}(111)$.

TABLE 1. Properties of molecular oxygen adsorption on the Al(001) substrate (Fig. 1)

Optimized configurations of $(O_2)_{ads}$ molecule	Distance z_O^a , \AA	Charge $\Delta q_{O_2}^b$, e	Parameters of energy surface			Chemical shifts ^{e)}	
			E_{bind}^c ,	$\Delta E_{bind}^{T \rightarrow S}$,	E_{gain}^d ,	$\Delta \epsilon_O^{CS}(1s)$,	$\Delta \epsilon_{Al}^{CS}(2p)$,
			eV				
four-fold <i>fcc</i> (horizontal)	1.26	1.15	2.73	0.83	4.28	-0.59	-0.35
four-fold <i>fcc</i> (vertical)	1.32	0.89	2.51	0.89		-0.54	-0.32
bridge <i>br</i> (horizontal)	1.34	0.81	2.31	0.81		-0.52	-0.36

a) For vertical configurations, z_O is a distance between the lower intramolecular atom and the surface.

b) Increase of electron charge on an adsorbed molecule (a positive sign for Δq_{O_2} means an excess of electron density compared to a free oxygen molecule); however, the charge on the two intramolecular atoms is not always equal: for vertical orientation ~60-70% of Δq_{O_2} is concentrated on the lower atom.

c) Values of the binding energy are defined according to Eq. (1) for a fixed intramolecular distance.

d) Value of the energy released *per* adatom after adsorption and dissociation of molecular oxygen (E_{gain}) is defined in Eq. (3); this is practically independent of adsorption site for the same interface.

e) For vertical orientations of adsorbed oxygen molecule, this chemical shift is an average (it is larger for the lower atom and smaller for the higher atom).

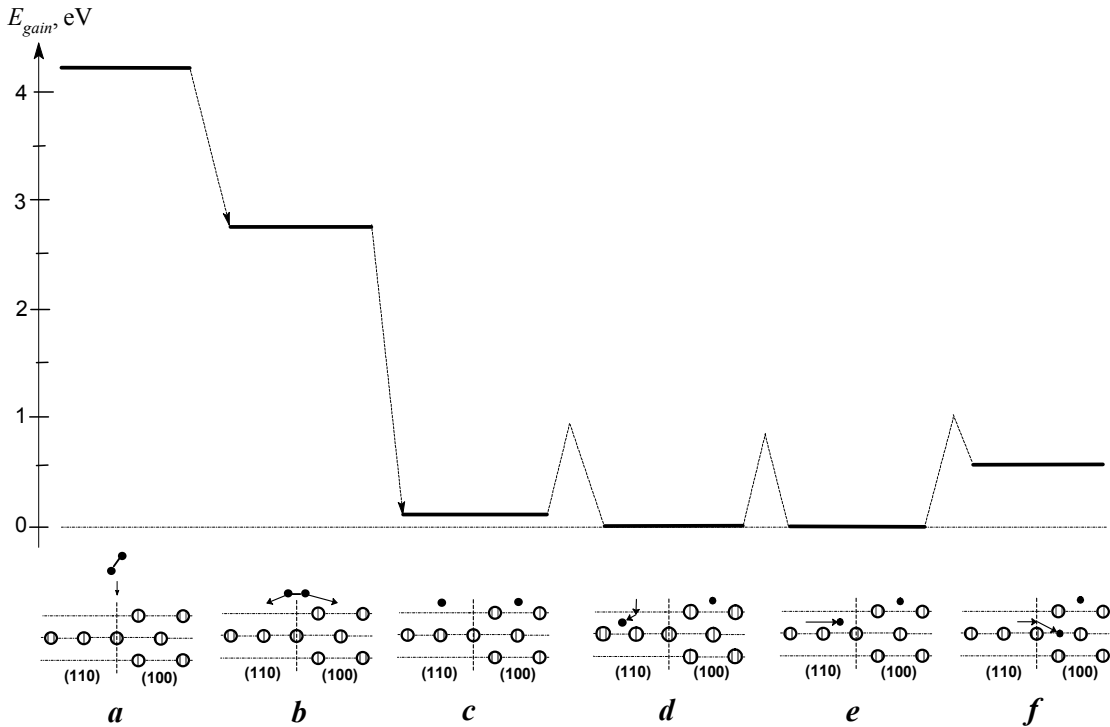


Figure 2. Energy gain *per* one oxygen atom relative to that of a gas-phase O_2 molecule that demonstrates the feasibility of the proposed model for the description of the subsequent reaction of oxygen with an Al(001) substrate: molecular adsorption ($a \rightarrow b$), dissociation ($b \rightarrow c$), atomic chemisorption (c), absorption and localization at t_{in} center ($c \rightarrow d$), interstitial diffusion between two t_{in} centers ($d \rightarrow e$) and interstitial diffusion between t_{in} and o_A centers ($e \rightarrow f$). The corresponding processes may be visualized from the sequence of steps shown by a to e . As in Fig. 1 we use two sections, (110) and (100), to show the possible configurations.

Along the trajectories of spontaneous dissociation of molecular oxygen above an Al(001) substrate shown in Fig. 1a, saddle points on the energy surface are practically absent, even above the bridge (*br*) sites. This is probably due to the higher position of $(O_2^-)_{ads}$ above the (001) surface (1.26 \AA versus 1.16 \AA for the (111) surface [1]). Another reason for this difference could be the different coverages for these substrates (1/2 a molecular ML over Al(111) and 1/4 of an $(O_2)_{ads}$ layer over a Al(001) surface) since the lateral interaction between adjacent molecules may hinder slightly the dissociation process. The change of ground state during $(O_2^-)_{ads}$ dissociation from triplet to singlet is quantitatively similar for both (001) and (111) surfaces. The initial part of the energy diagram shown in Fig. 2 describes the trajectory between the remote oxygen molecule $(O_2)_{ads}$ and the $2O_{ads}$ configurations. It illustrates graphically how the value of E_{gain} , defined by Eq. (3) and presented in Table 1, may be released as the result of both molecular adsorption and dissociation. Figure 3 clearly shows the difference in

Solid State Physics

electron densities for both a remote oxygen molecule and the adsorbed O_2^- molecular ion (with its axis parallel to the surface) above the *fcc* site.

When localizing newly formed adatoms above neighboring o_B centers the transfer of further charge reaches 1.0-1.2 *e per* O_{ads} , *i.e.* results in the formation of oxygen ions. The total value of the net energy *per* O_{ads}^- ion after molecular adsorption and dissociation (Fig. 2) is almost the same as for the $O_2/Al(111)$ interface (4.3 eV *versus* 4.2 eV [1]). Comparison of these data may be considered as additional confirmation of conclusions made in earlier studies about the greater reactivity of the Al(001) surface towards oxidation, even at the initial stage of molecular adsorption.

4. Chemisorption and absorption of atomic oxygen

The main results of our simulations on the interaction between oxygen adatoms and Al(001) substrate are presented in Table 2 and Figs. 2,3 for the relaxed geometry. Both equilibrium values of z_O over *fcc* hollow site have been found to be ~ 0.5 Å, closer to the surface than for the O/Al(111) interface. We also consider oxygen chemisorption above bridge sites on the Al(001) substrate in which the adsorbate is positioned above tetrahedral t_{in} centers of the subsurface lattice (Fig. 1) because some experiments gave indirect confirmation of the existence of these interface configurations [2,6]. The equilibrium position of oxygen above bridge sites is higher (~ 0.85 Å), due to the smaller coordination of surface Al atoms. A smaller induced charge Δq_O is concentrated on an adatom localized above a *br* site since this is not a proper position for chemisorption but rather a saddle point for the surface diffusion of O_{ads}^- ions.

TABLE 2. Chemisorption and absorption of atomic oxygen in the O/Al(001) interface for substrate monolayer and 1/4 coverages.

Oxygen ion over or in:	Type of configuration in interface	Possible structural relaxation ^{a)}	Distance z_O , Å	Charge Δq_O ^{b)} , <i>e</i>	Binding energy $E_{bind}(O/Al)$ ^{c)} ,	Chemical shifts ^{d)} $\Delta \epsilon_{Al}^{CS}(2p)$ ^{e)} ,
----- eV -----						
<i>1 ML coverage</i>						
o_B site	chemisorption (<i>fcc</i> position)	none	0.55	1.12	10.77	-1.9
		included	0.51	1.23	10.84	
t_{in} site	chemisorption (<i>br</i> position)	none	0.88	0.60	9.56	-0.5
		included	0.85	0.64	9.63	
	absorption (t_{in} position)	none	-1.05	1.16	9.39	-1.5
		included	-1.32	1.42	11.12	
o_A site	absorption (o_A position)	none	-2.06	1.52	9.42	-2.0
		included	-2.44	1.64	9.87	
<i>1/4 ML coverage</i>						
o_B site	chemisorption (<i>fcc</i> position)	none	0.56	0.94	10.35	-0.5
		included	0.53	1.01	10.43	
t_{in} site	chemisorption (<i>br</i> position)	none	0.91	0.56	9.44	-0.1
		included	0.88	0.59	9.47	
	absorption (t_{in} position)	none	-1.02	1.07	9.34	-0.4
		included	-1.25	1.35	10.42	
o_A site	absorption (o_A position)	none	-2.03	1.59	9.45	-0.6
		included	-2.30	1.73	9.91	

^{a)} For a 1 ML model this includes surface relaxation normal to the surface only, in the case of a 1/4 ML model both vertical relaxation and horizontal reconstruction are taken into account.

^{b)} Positive sign of Δq_O means an excess of electron density compared to a neutral atom.

^{c)} Values of the binding energy defined according to Eq. (1), at the interface distance z_O .

^{d)} Values of chemical shifts are practically the same for unrelaxed and relaxed substrate.

^{e)} For the experimentally-established chemisorption stage, the value of $\Delta \epsilon_{Al}^{CS}(2p)$ is -1.2-1.3 eV [2,3].

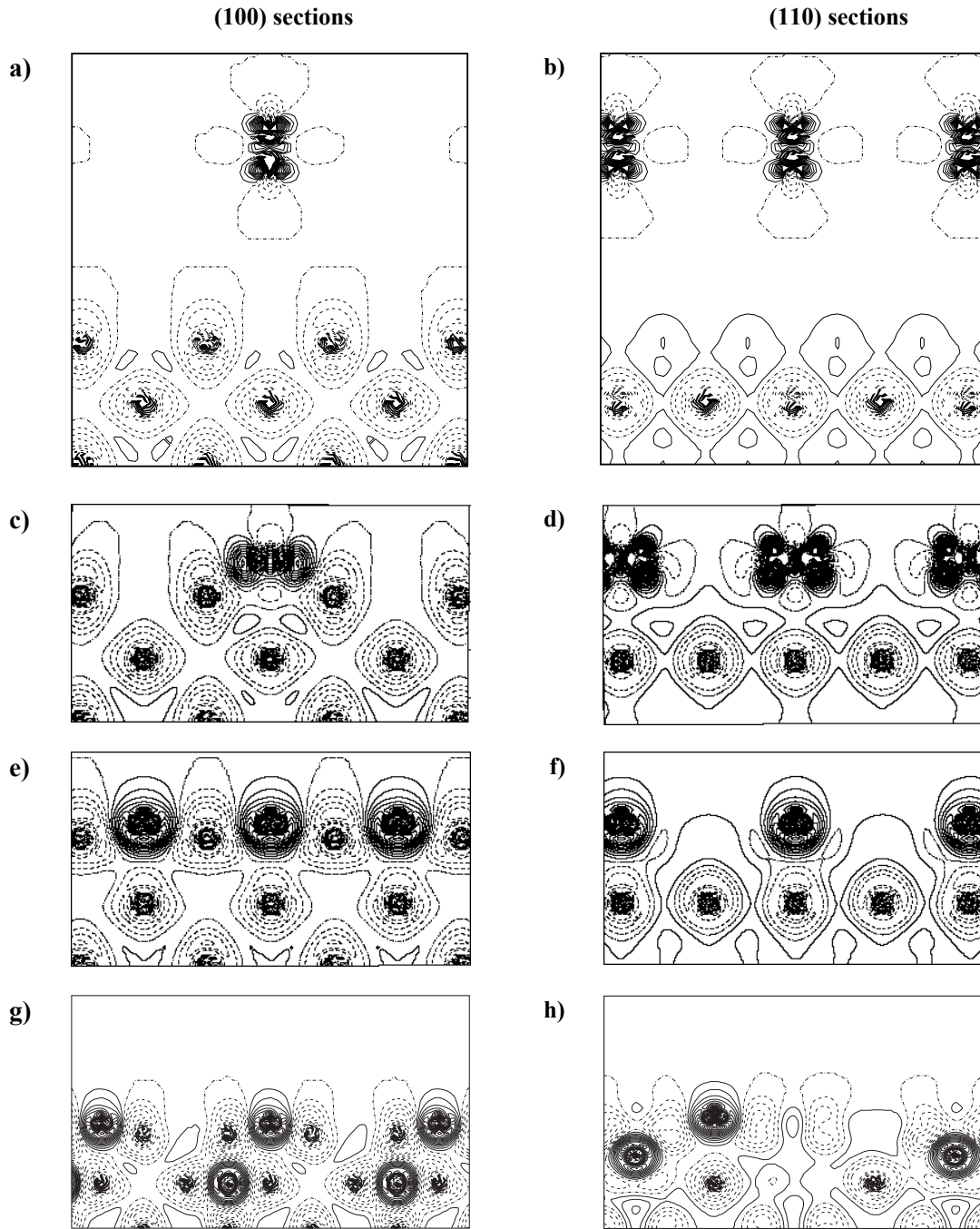


Figure 3. 2D difference electron density plots describing the charge distribution in sections shown in Fig. 2 relative to that in free Al and O atoms. Plots (a) to (f) show charge distributions for configurations of remote O_2 molecule over the Al(001) substrate (a and b), adsorbed O_2^- molecule (c and d) and chemisorbed O_{ads}^- ions (e and f) along (100) and (110) sections, respectively. Plot (g) corresponds to the (100) section for the configuration shown in Fig. 2f (absorption in o_A center) whereas plot (h) for a (110) section corresponds to the localization of oxygen ions in t_m center (Figs. 2d,e). Accumulation of electronic charge is shown by solid lines of equal density, while dashed lines show a deficit of charge with respect to the free atoms. Isodensity curves are drawn from $-1 e \text{ a.u.}^{-3}$ to $1 e \text{ a.u.}^{-3}$ with increment of $0.002 e \text{ a.u.}^{-3}$.

The binding energy E_{bind} per oxygen ion above a four-fold *fcc* site is practically the same as that above a *fcc* site on the Al(111) surface (10.5-10.9 eV). Though the value of z_O for the O/Al(001) interface is smaller, lateral effects are also smaller than for the Al(111) substrate. In the case of monolayer coverage of the Al(001) surface each O atom has four nearest oxygen neighbors instead of six. Obviously,

Solid State Physics

for br sites E_{bind} is considerably smaller (9.6 eV). Outward relaxation of the external substrate layer in the case of 1 ML chemisorption on the Al(001) surface is larger than for the analogous configuration of the O/Al(111) interface: 0.2 Å instead of 0.07 Å, respectively (for the fcc site). For the br site, it is markedly smaller (0.08 Å) since this value obviously depends on the proximity of adsorbate and adsorbent.

As mentioned above, unlike the Al(111) surface, the less dense Al(001) plane does not hinder oxygen ion penetration into the substrate through its fcc hollow sites o_B (Fig. 1). Nevertheless, for the penetration of quasi-isolated O_{ads}^- ions (1/4 ML), we have found a slight expansion of the square formed by the four nearest outer Al atoms (by ~4%) which lowers the activation barrier by ~0.3 eV. As a result, the values of energy barriers for absorption of well-separated oxygen ions into subsurface interstices *via* fcc hollow sites are markedly different for Al(001) and Al(111) substrates (0.8 eV along the penetration trajectory $\rightarrow o_B \rightarrow t_{in}$ as shown in Fig. 2 *versus* 1.4 eV along both trajectories $\rightarrow o_C$ and $\rightarrow t_B$ as described in [1]).

Moreover, unlike the O/Al(111) interface, the binding energy of an oxygen ion localized at the t_{in} center is higher by 0.3 eV than that for O_{ads}^- chemisorbed above the four-fold site on the Al(001) surface (in the model of monolayer coverage; in the case of 1/4 coverage both chemisorption and absorption energies are almost equal). However, this effect may be observed in our simulations only after the marked outward relaxation of the external substrate layer when oxygen ions move towards t_{in} centers (by ~0.6 Å). These calculations confirm results obtained earlier by Bedford and Kunz for a cluster model of the O/Al(001) interface [10] and show that the most stable position for absorbed oxygen ions is just at the t_{in} center. Since incorporation of O_{ads}^- *via* bridge sites is doubtful even with structural reconstruction of the Al(001) substrate, localization of oxygen ions at t_{in} centers is possible by internal diffusion ($o_B \rightarrow t_{in}$). Moreover, outward relaxation of the aluminium surface distorts the initial symmetry of the interstitial tetrahedra and octahedra. The energy barriers for the interstitial migrations $t_{in} \rightarrow t_{in}$ and $t_{in} \rightarrow o_A$ (for 1/4 ML) are found to be 0.9 and 0.5 eV, respectively (Fig. 2). This is quite reasonable, and qualitatively agrees with earlier DFT calculations on hydrogen diffusion in bulk Al [31].

As in the case of the O/Al(111) interface [1], penetration of O_{ads}^- into the (001) substrate (Table 2) leads to both expansion of the subsurface interlayer and the transfer of further charge to oxygen ($\Delta q_O = 1.4-1.75 e$). The similarity of induced charges in both substrates may be explained by a similar coordination of absorbed oxygen ions. Our results as well as earlier periodic simulations of the O/Al(001) interface [10,13] qualitatively confirm the main data from electron spectroscopy experiments [1]. Nevertheless, unlike the model of the O/Al(111) interface, we found that oxygen chemisorbed on the Al(001) surface in fcc position is characterized by a similar chemical shift of the $2p(Al)$ level compared to absorbed oxygen (Table 2). Both are larger than the corresponding experimental value of ~1.2-1.3 eV but smaller than 2.7 eV, which is typical for aluminium oxide [3]. For the br position of O_{ads} , this shift is almost twice as small, which confirms the improbability of stable oxygen chemisorption on this surface site. Table 2 allows us also to compare the values of $\Delta \epsilon_{Al}^{CS}(2p)$ for both 1/4 ML and 1 ML coverages; quite naturally the chemical shift induced by an oxygen monolayer is almost four times larger. On the whole, comparison of data presented in Ref. [1] and Table 2 as well as the difference in the net energies for the whole process beginning with molecular adsorption on both densely packed surfaces up to the interstitial diffusion of oxygen ions in these substrates (*cf.* Fig. 2 and Fig. 4 in Ref. [1]) clearly explains the faster oxidation of the Al(001) surface compared to Al(111) as also observed experimentally [2,6]. This also clarifies why the chemisorption stage of oxidation on an Al(001) substrate is less evident than on Al(111).

5. Conclusions

Periodic DFT CO LCGTF simulations of the initial stage of the oxidation of densely-packed Al(001) surfaces have been performed using the *CRYSTAL 98* code. We have described the following steps of this process:

- Initial contact of free oxygen molecules with a pure aluminium substrate leads to their spontaneous adsorption in the triplet electronic ground state. For the $O_2/Al(001)$ interface oxygen molecules prefer a horizontal orientation across bridge sites with the position of their midpoints above four-fold fcc sites. This adsorption is accompanied by ionization to form $(O_2^-)_{ads}$. Adsorbed molecules are found

Solid State Physics

to be very unstable with respect to further dissociation, which occurs spontaneously on the Al(001) surface. The breaking of O-O bonds on the Al substrate is accompanied by both a release of energy of ~ 4.3 eV per each newly formed adatom and the transition from the triplet to the singlet electronic ground state.

- Dissociation of oxygen molecules leads to the chemisorption of newly formed adatoms above neighboring four-fold *fcc* sites (o_b) on the Al(001) surface, accompanied by both outward relaxation of the external substrate layer (by up to 0.2 Å) and the transfer of further charge amounting to 1.0 - 1.2 *e* per O_{ads} , *i.e.* it results in the formation of oxygen ions. Each O_{ads}^- is localized at $z_O \approx 0.5$ Å above the surface layer with a binding energy of 10.8 eV. The bridge sites (*br*) are less stable ($z_O \approx 0.85$ Å and $E_{\text{bind}} \approx 9.6$ eV) and thus correspond to saddle points on the energy surface for diffusion over the substrate.
- Chemisorbed O_{ads}^- ions can penetrate into the regular (001) substrate with an activation energy of 0.8 eV (although an Al(001) plane does not hinder oxygen ion penetration into the substrate through its four-fold *fcc* sites, an expansion of the square formed from the four nearest outer Al atoms by $\sim 4\%$ lowers the activation barrier for absorption by ~ 0.3 eV). Incorporation of O_{ads}^- into the substrate leads to an expansion of the subsurface interlayer. Outward relaxation for adatoms localized in tetrahedral t_{in} centers amounts to 0.6 Å (these interstices can be reached by O_{ads}^- by subsurface diffusion rather than by direct penetration into the substrate). When adatoms are positioned in the larger octahedral interstices o_A the outward relaxation is markedly smaller (0.2 - 0.3 Å). Absorption is accompanied by further ionization so that the absorbed O_{ads}^- ions have a charge of -1.4 to -1.8 *e* (depending on their location inside the substrate).
- The energy balance for oxygen reactivity is more favorable for the less densely-packed Al(001) surface: unlike the regular Al(111) substrate the local energy minimum, which corresponds to oxygen atoms positioned in the tetrahedral interstitial t_{in} , is 0.3 eV deeper than that for chemisorbed O_{ads} above the four-fold *fcc* site on this substrate. The net energy for the whole process of interaction beginning with molecular adsorption up to the interstitial diffusion of adatoms inside substrate is almost 50% larger for the former case as well. These results clearly confirm why Al(001) substrate is oxidized at a faster rate than Al(111), as is observed experimentally for O/Al systems.

Acknowledgements

This study was supported by the Natural Sciences and Engineering Research Council of Canada and the European Centre of Excellence for Advanced Materials Research and Technology under Contract ICA1-CT-2000-7007. The authors thank M. Causá, E. Heifets, B.I. Lundqvist, and A.M. Stoneham for helpful discussions. The technical assistance of Yu. Matrikov was most valuable.

References

- [1] Zhukovskii Yu.F., Sychev O., Jacobs P.W.M., Shunin Yu.N. (2000) *Computer Modelling & New Technologies* **4**, No.2, 18.
- [2] Batra I.P., Kleinman L. (1984) *J. Electron Spectrosc. Related Phenomena* **33**, 175.
- [3] Bushby S.J. (1992). *Ph.D. Thesis*. University of Western Ontario, London (Ontario).
- [4] Den Boer M.L., Einstein T.L., Elam W.T., Park R.L., Roelofs L.D. (1980) *Phys. Rev. Lett.* **44**, 496.
- [5] Gartland P.O. (1977) *Surf. Sci.* **62**, 183.
- [6] Michel R., Gastaldi J., Allasia C., Jourdan C., Derrien J. (1980) *Surf. Sci.* **95**, 309.
- [7] Lauderback L.L., Lynn A.J., Waltman C.J., Larson S.A. (1991) *Surf. Sci.* **243**, 323.
- [8] Memmert U., Norton P.R. (1988) *Surf. Sci.* **203**, L689.
- [9] Messmer R.P., Salahub D.R. (1977) *Phys. Rev. B* **16**, 3415.
- [10] Bedford K.L., Kunz A.B. (1982) *Phys. Rev. B* **25**, 2119.
- [11] Zhukovskii Yu.F., Smirnov E.P., Lokenbach A.K. (1991) *Russ. J. Phys. Chem.* **65**, 1214.
- [12] Batra I.P., Ciraci S. (1977) *Phys. Rev. Lett.* **39**, 774.
- [13] Krakauer H., Posternack M., Freeman A.J., Koelling D.D. (1981) *Phys. Rev. B* **23**, 3859.

Solid State Physics

- [14] Brune H., Wintterlin J., Trost J., Ertl G., Wiechers J., Behm R.J. (1993) *J. Chem. Phys.* **99**, 2128.
- [15] Vitos L., Ruban A.V., Skriver H.L., Kollar J. (1998) *Surf. Sci.*, **411**, 186.
- [16] Saunders V.R., Dovesi R., Roetti C., Causà M., Harrison N.M., Orlando R., Zicovich-Wilson C.M. (1999) *CRYSTAL 98. User Manual*. University of Torino. Turin.
- [17] Jacobs P.W.M., Zhukovskii Yu.F., Mastrikov Yu., Shunin Yu.N. (2002) *Computer Modelling & New Technologies* **6**, No.1, 7.
- [18] Becke A.D. (1988) *Phys. Rev. A* **38**, 3098.
- [19] Perdew J.P., Wang Y. (1992) *Phys. Rev. B* **45**, 13244.
- [20] Guest M.F., Saunders V.R. (1974) *Mol. Phys.* **28**, 819.
- [21] Moruzzi V.L., Janak J.F., Williams A.R. (1978) *Calculated Electronic Properties of Metals*. Pergamon Press, New York.
- [22] Monkhorst H.J., Pack J.D. (1976) *Phys. Rev. B* **13**, 5188.
- [23] Gilat G. (1972) *J. Comput. Phys.* **10**, 390.
- [24] Towler M.D., Zupan A., Causà M. (1996) *Comput. Phys. Commun.* **98**, 181.
- [25] Boettger J.C., Birkenheuer U., Rösch N., Trickey S.B. (1994) *Intern. J. Quant. Chem.: Quant. Chem. Symp.* **28**, 675.
- [26] Causà M., Dovesi R., Pisani C., Roetti C. (1986) *Phys. Rev. B*, **33**, 1308.
- [27] Heifets E., Kotomin E.A., Eglitis R.I., Maier J., Borstel G. (2001) *Phys. Rev. B* **64**, 235417.
- [28] Press W.H., Teukolsky S.A., Vetterling W.T., Flannery B.P. (1997). *Numerical Recipes in FORTRAN77 (2nd ed.)*. University Press, Cambridge, MA.
- [29] Wyckoff R.W.G. (1963) *Crystal Structures (2nd ed.)*. V. 1. New York: Wiley-Interscience.
- [30] Hong T., Smith J.R., Srolovitz D.J. (1994) *J. Adhes. Sci. Technol.* **8**, 837.
- [31] Popovic Z.D., Stott M.J. (1974) *Phys. Rev. Lett.* **33**, 1164.

Received on the 17th of December 2002

DFT SIMULATIONS OF THE INTERACTION BETWEEN OXYGEN AND A STEPPED *Al(111)* SUBSTRATE

P.W.M. JACOBS^a, Yu.F. ZHUKOVSKI^b, A. KOVALEVSKA^b, Yu.N. SHUNIN^c

^aDepartment of Chemistry, University of Western Ontario, London, ON, N6A 5B7, Canada

^bInstitute of Solid State Physics, University of Latvia, 8 Kengaraga, LV-1063, Riga, Latvia

^cDepartment of Physics, Transport and Telecommunication Institute & Information System Institute,
1 Lomonosova, LV-1019, Riga, Latvia

A periodic stepped O/Al(111) interface may be considered as a model surface for the study of the interaction between atomic oxygen and a defective aluminium substrate. Calculations on different configurations of the stepped interface have been performed using the first-principles DFT method implemented in the *CRYSTAL 98* code. The stepped surface contains both {111} and {001} microfacets. Penetration of oxygen adatoms into the subsurface interstices of the substrate occurs preferentially on the {001} microfacets. The presence of densely-packed microfacets on a stepped (111) substrate allows us to compare results of the current study with simulations on the perfect O/Al(111) and O/Al(001) interfaces performed by us earlier. The binding energy of an oxygen ion adsorbed on the stepped Al(111) substrate was found to be noticeably larger than on the regular interfaces (*cf.* 11.3 eV per adatom with 10.4-10.5 eV for the same 1/4 monolayer coverage of the perfect (111) and (001) surfaces). This confirms conclusions drawn from earlier studies that a defective surface strengthens interfacial bonding. The height of the energy barrier for the penetration of an O adatom into the stepped (111) substrate is 1.1 eV, intermediate between the values for the regular O/Al(001) and O/Al(111) interfaces which are 0.8 eV and 1.4 eV, respectively.

Keywords: stepped O/Al(111) interface, periodic slab model, chemisorption, absorption, interstitial diffusion, DFT-LCGTF method

1. Introduction

In our recent papers we have described in detail the first principles simulations on slab models of the regular densely-packed O/Al(111) [1] and O/Al(001) [2] interfaces using a method based on density functional theory (DFT). However, when comparing results of these and other theoretical simulations with numerous data from experimental studies of the initial stage of the oxidation of aluminium we should take into account that real substrate surfaces are defective. It is well known from different studies of chemisorption that surface defects not only strengthen bonding between a metallic substrate and an adsorbate but also initiate surface reactions [3]. The defective structure of O/Al interfaces has been reliably identified in high-precision scanning tunneling microscopic (STM) studies at the level of atomic resolution combined with Auger electron spectroscopy (AES) and low energy electron diffraction (LEED) experiments [4,5]. An STM study of carefully prepared samples of the Al(111) substrate before its interaction with oxygen [4] showed the presence of terraces, steps and kinks. It has been suggested that terrace step edges are favorable sites for initial oxide nucleation on the Al(111) surface. Nevertheless, we could not find in the literature any attempts at systematic *ab initio* simulations of the interaction between a defective aluminium surface and oxygen.

Recent DFT simulations of the homoepitaxial growth of an Al(111) substrate [6] and its study by STM [7] described such atomic processes as terrace diffusion, corner crossing and kink breaking. In all the cases newly formed three-dimensional (3D) islands consist of two types of steps between neighboring crystallographic (111) planes: the *A* step with a {001} microfacet and the *B* step with a {111} microfacet. This is why we have recently constructed a slab model [8] in which the presence of both {001} and {111} microfacets is realized in periodic surface steps on the Al(111) substrate. These correspond completely with the *A*- and *B*-steps of epitaxially grown islands [6]. Therefore, when using this stepped-surface model we reproduce fragments of the real Al(111) substrate more correctly than by using a perfect surface.

Because of computational limitations we could not simulate the adsorption and dissociation of oxygen molecules on the stepped Al(111) substrate, as carefully as was done in our previous studies on oxygen interaction with regular densely-packed aluminium surfaces [1]. Due to this same restriction we could not follow the reaction of oxygen with the substrate up to the formation of Al₂O₃ formula units [1]. However, we have considered in the current study the same principal questions as in our previous papers [1,2]: how are oxygen atoms chemisorbed and then penetrate into the substrate to become localized in the subsurface interlayer; how easily can they diffuse in the subsurface area; and what is the nature of the

intermediate structure between the absorbed oxygen phase and oxide nuclei? We have considered both the energetics of the stepped interface and its electronic structure, and we have compared these results with the corresponding properties obtained from models of both stepped and regular O/Al interfaces.

2. Theoretical background

In this paper we omit completely details of the computational scheme applied in the *CRYSTAL 98* code [9], used in our DFT calculations, as well as the definition of calculated properties, since these have been described by us in detail elsewhere [1,2,8]. Thus, we limit ourselves in this Section to the description of the model used for the simulation of a stepped O/Al(111) interface. To construct the stepped O/Al(111) slab as a model for the interface (Fig. 1) we cut from the outer layers of a regular Al(111) slab every second row parallel to the [110] crystallographic axis. The symmetry of this slab model with regular steps containing both {111} and {001} microfacets is described by the point group D_{2d} .

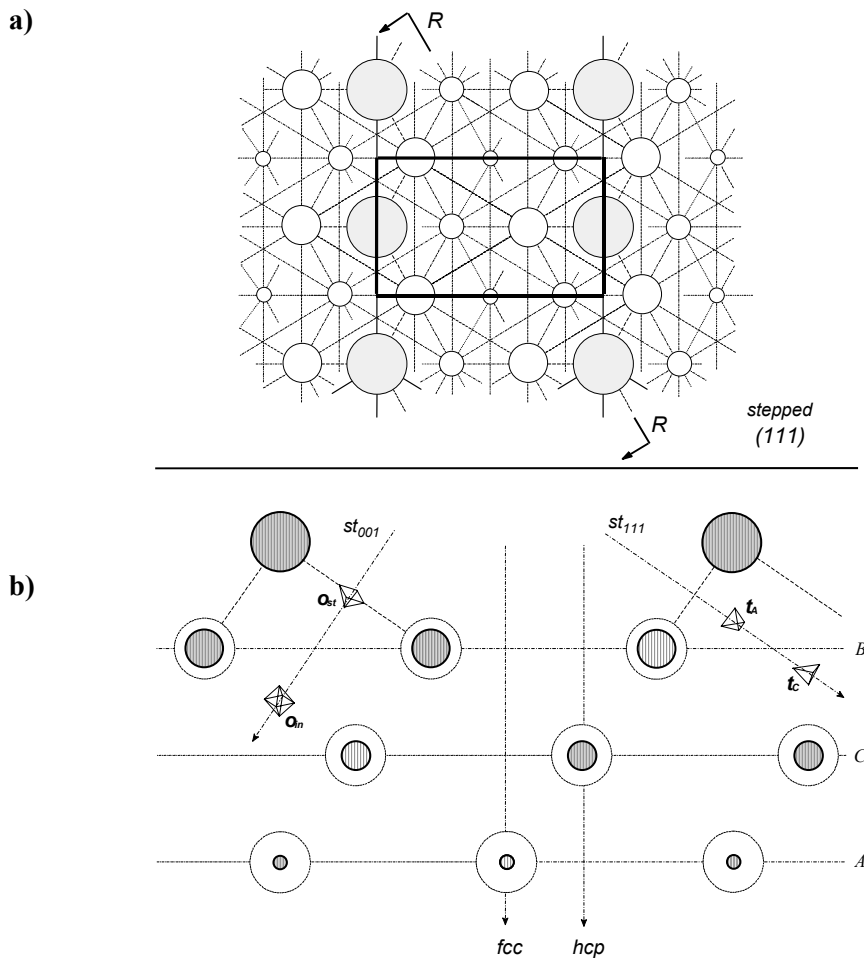


Figure 1. Periodic model of the stepped O/Al(111) interface with possible positions of oxygen ions outside and inside the substrate:
 (a) Top view of the stepped substrate shows that it differs from that for perfect Al(111) surface by both the absence of every second row of outer Al atoms and the rectangular surface unit cell (instead of a rhombic one) marked by thicker lines. Largest circles denote Al atoms in the top layer *A* (at the edge of steps) and smaller circles Al atoms in the next subsurface layers. All nearest-neighbor atoms are joined by straight solid and dashed lines (in the former case they join surface atoms only).
 (b) Dash-dot arrows on the cross-section view (*R-R*) marked by *hcp* and *fcc* (over flat pits) as well as *st₀₀₁* and *st₁₁₁* (over the corresponding microfacets of regular steps) show four energetically favorable sites for chemisorption. The small tetrahedra and octahedra show surface (*o_s*) and interstitial (*t_a*, *t_c* and *o_m*) sites, which are the most suitable for the metastable location of oxygen ions.

The stepped O/Al(111) interface allows us to model possible structural irregularities on the Al(111) surface. It contains both flat fragments of a three-layer Al(111) slab and regular steps on it, the

Solid State Physics

sides of which correspond to $\{111\}$ and $\{001\}$ microfacets. To simulate the stepped O/Al(111) interface we have imitated two-sided 1/4 monolayer (ML) oxygen adsorption on a 2×2 SC model of the substrate (Fig. 1). Both the height of the step's edge over the next continuous subsurface (111) layer ($l_{1,2}$) and the second interlayer spacing under the substrate pit ($l_{2,3}$) have been optimized for the checked configurations of the stepped interface. For the corresponding parameters of the pure stepped Al(111) surface [8], an inward relaxation has been established ($\delta l_{1,2} \approx -5.1\%$ and $\delta l_{2,3} \approx -0.7\%$). As a result, both the equilateral Al triangles on the $\{111\}$ microfacet and the Al squares on the $\{001\}$ microfacet of each step are slightly distorted to isosceles triangles and rectangles, respectively. For oxygen chemisorption we considered sites at the centers of $\{111\}$ triangles (on both surface steps, where we considered only those which contain two Al atoms on the edge, and pits) as well as $\{001\}$ squares (on the second side of steps). For further adatom penetration into the substrate only the hollow sites on the $\{001\}$ microfacet of the step were checked since (as shown in Ref. [2]) O_{ads} absorption on this site does not require any structural reconstruction, so the symmetry of the corresponding configuration is not changed. Within the stepped substrate we have simulated the following trajectory of oxygen diffusion: through the center of the distorted surface half-octahedron (hollow site on $\{001\}$ square, or o_{st}) \rightarrow center of the nearest subsurface tetrahedron (either t_A or t_C) \rightarrow center of the nearest subsurface octahedron (o_m).

3. Chemisorption and absorption of atomic oxygen

Results of calculations on the stepped O/Al(111) interface are presented in Table 1 and Fig.2. Due to computational limitations we could not optimize the equilibrium configuration of oxygen in different chemisorption and absorption positions as carefully as was done for the perfect O/Al(111) [1] and O/Al(001) [2] interfaces. Therefore, these results should be considered rather as a starting point for further more comprehensive studies than as results of the quality of those reported for perfect Al(111) and Al(001) substrates. Nevertheless, two distinctive peculiarities of the model for a stepped O/Al(111) interface can be commented upon:

- the presence of $\{100\}$ microfacets on surface steps makes penetration of oxygen atoms into the substrate much easier than in the perfect O/Al(111) interface, although calculated parameters of oxygen atoms absorbed by the stepped substrate (Table 1) are close to those described above for O_{ads} localized in interstitial sites of the perfect Al(111) substrate (for the same 1/4 ML coverage [1]);
- simulation of oxide nucleation on the stepped surface should show it be more effective than the corresponding model of the perfect O/Al(111) interface, but this would require more extensive computational resources due to its lower symmetry.

We have simulated all four positions for O_{ads} chemisorption shown on Fig. 1 (st_{001} , st_{111} , fcc and hcp) although bonding of O_{ads} over triangular st_{111} sites (with one Al atom positioned on the edge of step as mentioned in Section 2) is much weaker than in the other three positions. (This is why we did not include the corresponding data in Table 1.) A substantial charge transfer to oxygen adatoms localized above various sites on the stepped substrate (0.85-1.05 e) results in the formation of O_{ads}^- ions. Due to the stepped structure of the substrate with the marked influence of its edges on chemisorption, the equilibrium distances from O_{ads}^- down to the corresponding sites on flat pits and microfacets of steps (Table 1) are larger than for the perfect O/Al(111) [1] and O/Al(001) [2] interfaces for the same 1/4 ML coverage. O_{ads}^- ions in both st_{001} and st_{111} penetration trajectories are somewhat higher than at the edges of steps (0.4 and 0.6 Å, respectively) but along fcc and hcp positions they are localized inside substrate pits. The proximity of the corresponding edge to the nearest adatom is also important (Table 1): the O_{ads}^- ion is most affected when in the st_{001} or st_{111} position. The chemisorption trajectories are rather curved in both cases, compared to the straight lines in Fig. 1. The fcc position for oxygen, being more remote from the edge of a step, is less influenced and calculated parameters in this case are close to those for the perfect O/Al(111) interface [1].

It is quite reasonable that the energetically preferred position of O_{ads}^- ion on the stepped Al(111) surface is found to be st_{001} site. The binding energy (E_{bind}) for oxygen chemisorption in this case is noticeably higher than over both the perfect Al(111) and Al(001) surfaces at the same 1/4 ML coverage (*cf.* ~ 11.3 eV vs 10.45 [1] and 10.43 eV [2], respectively). The most preferred absorption position t_A

Solid State Physics

inside the substrate step (Fig. 1) is the one closest to this st_{001} site. Localization of an O_{ads}^- ion in this tetrahedral position leads to an outward relaxation of the edge of the step of up to 0.6 Å. The ratio of energies between absorbed and chemisorbed states at the stepped O/Al(111) interface show that oxygen penetration into the substrate along the $st_{001} \rightarrow t_A$ direction is more favorable than for the perfect O/Al(111) interface, but less favorable than for the O/Al(001) interface, their energies for 1/4 coverage being $-0.8 \text{ eV} < -0.6 \text{ eV} < 0 \text{ eV}$. Thus, the presence of {001} microfacets on the stepped Al(111) surface leads to easier absorption of O_{ads} atoms. The energy barrier for oxygen penetration is $\sim 1.1 \text{ eV}$ through the surface site o_{st} and is thus comparable with the energy barriers (0.8-1.4 eV) given in Refs. [1] and [2] for the perfect interfaces. This energy barrier for oxygen absorption might have been even lower if we could have simulated surface reconstruction, as was done for the perfect O/Al(111) interface with 1/4 ML coverage [1].

TABLE 1. Properties of stepped O/Al (111) interface (Fig. 1) for various locations of chemisorbed and absorbed oxygen ions.

Oxygen ion over or in:	Type of interface	Possible vertical relaxation	Distance z_O^{a} , Å	Charge Δq_O^{b} , e	Binding energy $E_{\text{bind}}(\text{O/Al})$	Chemical shifts $\Delta \epsilon_{\text{Al}}^{\text{CS}}(2p)^{\text{c}}$,
					eV	
o_{st} site	chemisorption (st_{001} position)	none	1.92	0.75	10.87	
		included	1.85	0.83	11.31	-0.3
	absorption (t_C position)	none	-0.59	1.05	8.75	
		included	-0.71	1.39	9.93	-0.5
fcc "pit"	chemisorption (fcc position)	none	0.94	0.98	10.41	
		included	0.87	1.07	10.83	-0.4
hcp "pit"	chemisorption (hcp position)	none	1.17	0.89	10.24	
		included	1.11	0.96	10.61	-0.4
o_{in} site	absorption (o_{in} position)	none	-1.13	1.67	9.31	
		included	-1.31	1.81	10.11	-0.7
	absorption (t_A position)	none	-1.61	1.17	9.12	
		included	-1.85	1.35	10.68	-0.6

^{a)} For chemisorption of oxygen ion above o_{st} center, z_O means a vertical z -projection of the distance between O_{ads}^- and this position; for absorption of oxygen at t_A centre, z_O is a vertical distance between the latter position and the edge of the step; in other chemisorption and absorption positions of O_{ads}^- , z_O is determined with respect to the second (pit) layer of the substrate.

^{b)} Positive sign of Δq_O means an excess of electron density compared to a neutral atom.

^{c)} Calculated values of $\Delta \epsilon_{\text{Al}}^{\text{CS}}(2p)$ are practically the same for non-relaxed and relaxed substrate.

Figure 2 shows difference electron density maps for various chemisorption and absorption configurations of the stepped O/Al(111) interface. Some similarities may be observed between the density distributions around an O_{ads}^- ion over an st_{001} site on the stepped substrate (Fig. 2a) and fcc hollow sites on the perfect Al(001) surface (compare the corresponding electron density plot in Ref. [2]). For other chemisorption and absorption configurations shown on Fig. 2, some similarities in difference electron charge distributions in the proximity of O_{ads}^- ion may be found between analogous sites on the perfect Al(111) substrate [1]. Mulliken charge analysis (Table 1) indicates rather smaller values of Δq_O in chemisorption and absorption positions of oxygen in the vicinity of each step (st_{001} , st_{111} and t_A) compared to both the perfect interfaces [1,2], although in the deeper chemisorption and absorption positions of O_{ads}^- (fcc , hcp , o_{in} and t_C) the values of Δq_O are higher. Probably this is due to either reduced or enhanced electron density around the step or pit of the stepped substrate, respectively, compared to the perfect O/Al interfaces. Penetration of O_{ads}^- into the stepped (111) substrate leads to the transfer of further charge to oxygen ($\Delta q_O = 1.4-1.8 e$). Relaxation of the stepped substrate leads to an increase in the values of both E_{bind} and Δq_O (Table 1). The set of chemical shifts of the core $2p(\text{Al})$ level for different configurations of the stepped interface is rather larger than for the corresponding configurations of the O/Al(001) interface at 1/4 ML coverage [1,2], so not only the energy gain but also chemical bonding is more marked in the

stepped interface. Probably the most realistic results for the O/Al(111) interface could be obtained when simulating “islands” on this substrate, as was considered in Ref. [6]. However, such a model is too complicated for periodic first principles simulations.

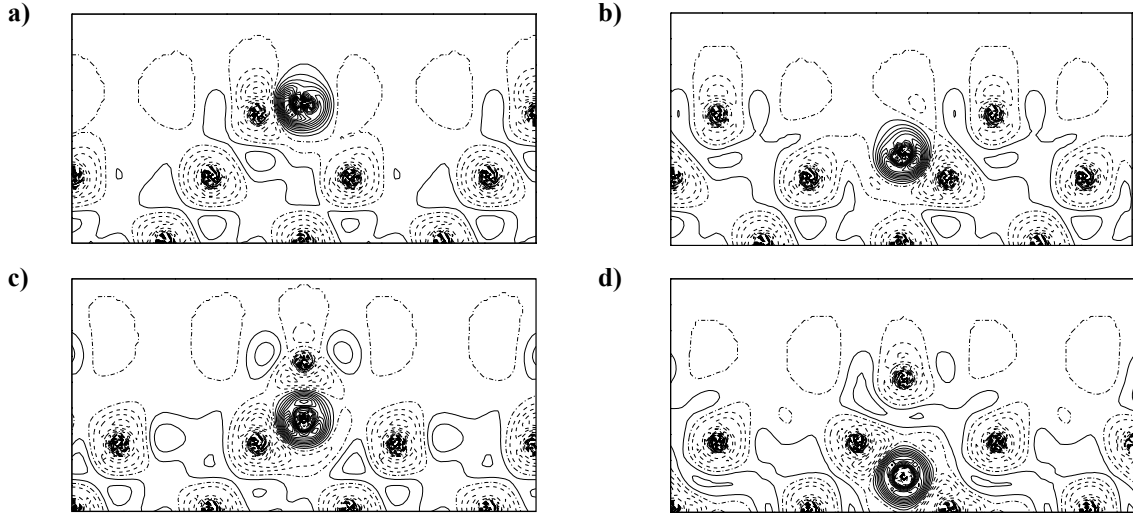


Figure 2. 2D difference electron density plots describing the charge distribution in the section $R-R$ shown in Fig. 1 relative to that of free Al and O atoms. Plots (a) to (d) show charge distributions for configurations of chemisorbed O_{ads}^- ions in $stool$ (a) and hcp (b) positions as well as adsorbed oxygen ions in t_A (c) and o_{in} (d) interstitial sites. Accumulation of electronic charge is shown by solid lines of equal density, while dashed lines show a deficit of charge with respect to the free atoms. Isodensity curves are drawn from $-1 e \text{ a.u.}^{-3}$ to $1 e \text{ a.u.}^{-3}$ with increment of $0.002 e \text{ a.u.}^{-3}$.

4. Conclusions

Periodic DFT simulations of the interaction between oxygen and the stepped Al(111) surface have been performed using the CRYSTAL98 code. It allowed us to consider a more realistic model of the O/Al(111) interface containing steps with $\{001\}$ and $\{111\}$ microfacets, although due to limited computational resources we could not simulate molecular adsorption as well as comprehensive substrate reconstruction. Nevertheless, we can compare our current results with those obtained recently for regular O/Al(111) and O/Al(001) interfaces [1,2].

- A substantial charge transfer to oxygen adatoms localized above various sites on the stepped substrate ($0.85-1.05 e$) results in the formation of O_{ads}^- ions. This is similar to the analogous charge transfers to atomic oxygen chemisorbed over perfect aluminium substrates.
- The energetically most favorable position for chemisorption of O_{ads}^- ions was found to be over the $\{001\}$ microfacet on the stepped Al(111) surface, above the o_{st} center (0.4 \AA over the edge of step). Here $E_{\text{bind}} = 11.3 \text{ eV}$ per ion. This is noticeably larger than for oxygen chemisorption over both perfect Al(111) and Al(001) surfaces at the same $1/4 \text{ ML}$ coverage, which are 10.45 [1] and 10.43 eV [2], respectively.
- On the stepped Al(111) surfaces O_{ads}^- ions can penetrate into the subsurface space via $\{001\}$ microfacets without noticeable surface reconstruction. In all cases examined, incorporation of O_{ads} into the substrate leads to expansion of the subsurface interlayer. This amounts to 0.6 \AA for the edges of the stepped Al(111) substrate when O atoms are localized in tetrahedral t_A interstices inside steps, which is almost the same outward relaxation as observed with the Al(001) substrate for adatoms localized in tetrahedral t_{in} sites [2]. A smaller relaxation is associated with the analogous absorption of O_{ads}^- in the perfect Al(111) substrate (0.45 and 0.35 \AA for t_A and t_B sites, respectively). But when adatoms are positioned in the larger octahedral interstices o_A , o_C , and o_{in} the outward relaxation is naturally smaller ($0.2-0.3 \text{ \AA}$).
- Chemisorbed O_{ads}^- can penetrate into the stepped (111) as well as regular (111) and (001) aluminium substrates with activation energies of 1.1 eV , 1.4 eV and 0.8 eV , respectively. Absorption is

Solid State Physics

accompanied by further ionization so that the absorbed O_{ads}^- ions have a charge of -1.4 to $-1.8 e$ (depending on their location inside all the three types of Al substrate).

- Subsurface tetrahedral interstices t_A in the stepped Al(111) substrate and t_{in} sites inside the Al(001) substrate [2] have been found to be energetically preferred sites for absorbed oxygen atoms. This is probably due to their proximity to the nearest Al neighbors compared to octahedral interstices, despite the higher coordination in the latter sites. Moreover, outward relaxation of both aluminium surfaces distorts the initial symmetry of the interstitial tetrahedra and octahedra. Both t_A and t_{in} interstices can be reached by oxygen atoms as a result of subsurface diffusion rather than by direct penetration into the substrate. Lower energy barriers characterize the diffusion of oxygen ions between adjacent relaxed tetrahedral and octahedral sites (0.3-0.5 eV), but for the transition between adjacent tetrahedral interstices oxygen atoms must overcome barriers of 0.8-1.0 eV.

Acknowledgements

This study was supported by the Natural Sciences and Engineering Research Council of Canada and the European Centre of Excellence for Advanced Materials Research and Technology under Contract ICA1-CT-2000-7007. The authors thank M. Causá, E. Heifets, B.I. Lundqvist, and A.M. Stoneham for helpful discussions. The technical assistance of Yu. Mastrikov was most valuable.

References

- [1] Zhukovskii Yu.F., Sychev O., Jacobs P.W.M., Shunin Yu.N. (2000) *Comput. Model. New Technol.* **4**(2), 18.
- [2] Zhukovskii Yu.F., Kovalevska A., Jacobs P.W.M., Shunin Yu.N. (2003) *Comput. Model. New Technol.* **7**(1), 7.
- [3] Roberts M.W., McKee. C.S. (1978) *Chemistry of the Metal-Gas Interface*. Clarendon Press, Oxford.
- [4] Brune H., Wintterlin J., Trost J., Ertl G., Wiechers J., Behm R.J. (1993) *J. Chem. Phys.* **99**, 2128.
- [5] Schmid M., Leonardelli G., Tscheliebnig R., Biedermann A., Varga P. (2001) *Surf. Sci.* **478**, L355.
- [6] Bogicevic A., Strömquist J., Lundqvist B.I. (1998) *Phys. Rev. Lett.* **81**, 637.
- [7] Barth J.V., Brune H., Fischer B., Weckesser J., Kern K. (2000) *Phys. Rev. Lett.* **84**, 1732.
- [8] Jacobs P.W.M., Zhukovskii Yu.F., Mastrikov Yu., Shunin Yu.N. (2002) *Comput. Model. New Technol.* **6**(1), 7.
- [9] Saunders V.R., Dovesi R., Roetti C., Causà M., Harrison N.M., Orlando R., Zicovich-Wilson C.M. *CRYSTAL 98*. User Manual, (Turin: University of Torino) 1999.

Received on the 17th of December 2002

PREDICTION OF PHASE FORMATION IN *Mg-Ag* IN NON-EQUILIBRIUM CONDITIONS ON THE BASIS OF *ab initio* CALCULATIONS

I.G. BROWN¹, M.M. TALIANKER², D.L. FUKS², A.E. KIV²,
AND L.YU. KUTSENKO²

¹Lawrence Berkeley Laboratory, University of California, Berkeley, California 94720

²Department of Materials Engineering, Ben Gurion University of the Negev,
Beer-Sheva 84105, Israel

Ab initio calculations were performed to study a formation of phases in Mg-Ag alloy obtained by Plasma Immersion Ion Implantation of Ag to Mg matrix. The calculations were carried out within the CPA LMTO procedure. Correlations between the start characteristics of the electronic sub-system of implanted alloy and solid phases, that are formed, were found.

Keywords: Mg-Ag alloys, Plasma Immersion Ion Implantation (PIII), CPA LMTO *ab initio* calculations

1. Introduction

The Plasma Immersion Ion Implantation (PIII) technology opens new ways for the formation of special implantation profiles, for synthesis of new compounds and structures in the near-surface layers of material, thus leading to radical improvement of its properties [1-3].

Knowledge of specific structural changes, which occur in the alloy as a result of PIII treatment, is an essential prerequisite for understanding its performance. To understand better the mechanisms that lead to the modification of materials by PIII it is necessary to study the nature of phases formed in implanted layers. The important factor that has to be accounted is the non-equilibrium conditions, in which a formation of new phases occurs.

In this work we performed a theoretical study of PIII of Silver into Mg matrix. A compilation of crystal structure data of the binary alloy phases in the Ag-Mg system is given in Table 1 [4].

TABLE 1. Binary alloy phases in the Ag-Mg system

Phases	Pearson symbol	Composition, At% Ag	Space group
(Ag) α	CF4	70.7 – 100 %	$Fm\bar{3}m$
Ag_3Mg α'	CP4	75 %	$Pm\bar{3}m$
$AgMg$ β	CP2	34.6 – 64.5 %	$Pm\bar{3}m$
$Ag_{17}Mg_{54}$ ϵ'	OI142	21.2 – 24.1 %	$Immm$
$Ag_{7.96}Mg_{25.04}$ ϵ	CF264	21.2 – 24.1 %	$Fm\bar{3}$
Ag_9Mg_{37} γ	HP92	19.6 %	$P6_3$
(Mg) δ	HP2	0 – 8.9 %	$P6_3 / mmm$

In this paper we demonstrate a possibility to apply *ab initio* calculation technique to bear in a new way on problems of solid phases formation in a non-equilibrium alloy.

The electronic states of atomic configurations in the beginning of the non-equilibrium relaxation of the alloy are the starting conditions for the further transformations in electronic and lattice subsystems. The initial electronic states of the non-equilibrium system depend on the nature of the parent phase and on the nature and concentration of solute atoms. Comparing the start electronic characteristics of non-equilibrium alloy and electronic characteristics of the parent matrix we can analyze how far from the equilibrium state the system is located in the beginning of non-equilibrium relaxation.

In this paper we obtain results based on T=0 K *ab initio* calculations. The zero-temperature study does not yield a complete picture of the phase formation processes, and one might wonder about the

applicability of such an approach. As we show here, considering the results of calculations of total energy and DOS characteristics, the energy differences between various phases are large enough. So the entropy contributions are not likely to influence sufficiently the conditions of the energy competition of the phases.

The Section 2 is devoted to application of *ab initio* calculations for better understanding the processes in electronic and lattice subsystems of the implanted alloy in conditions of PIII. In the Section 3 we discuss the obtained results.

2. *Ab initio* study of non-equilibrium electronic states in Mg-Ag system

Under the PIII of Ag in Mg, lattice structural defects and sites, where Ag substitutes for Mg atoms, arise. As a result of the ion pulse and substitution of Mg by Ag atoms the electronic subsystem of the alloy transits to an excited state. Electronic subsystem reacts immediately on the appearance of extremely non-equilibrium atomic composition in the alloy. The starting state of electronic subsystem determines further processes of lattice and electronic relaxation. So it is important to find correlations between the initial electronic states in the non-equilibrium alloy and the following formation of phases in implanted layers.

The development of the density functional theory (DFT) that is now included in numerous band structure techniques makes possible to obtain reliable results in the calculations of different properties of alloys. The Linear Muffin Tin Orbitals (LMTO) method has proved its ability to describe the density of states (DOS), optical properties, and to characterize the bonding in solids [5].

Band structure calculations based on DFT allow obtain a quantitative description of the ground-state properties of absolutely ordered alloys. Application of these methods to the calculations of thermodynamic properties of partially ordered or random alloys also gives reasonable results [6,7]. The most attractive feature of the single-site coherent potential approximation (CPA) is the ability to apply this scheme to the direct calculations of the electronic structure of random or partially ordered substitution alloys [7]. Recently it was applied to the study of interstitial solid solutions [8] as well.

Band structures for Mg implanted by different atomic fractions of Ag are carried out within the CPA LMTO procedure [7]. We decided to use this code as the fast scheme for the direct calculations of electronic structure of the alloy under consideration. With the self-consistently obtained bands, we calculated the total energies of the Mg alloy with a uniform distribution of Ag atoms in two sublattices of the Mg hexagonal closed-packed crystal. We calculated also the total and partial DOS (density of states) for different atomic fractions of Ag in the alloy.

The exchange-correlation effects were accounted according to Ref. [8]. The individual atomic sphere radii were set equal to the radius of the average atomic Wigner-Seitz sphere of the alloy. There is some uncertainty for the absolute values of the energy gaps. It was the reason for an extended special k-point basis yielded in our calculations. The convergence criterion for the total energy was 0.001 mRy.

First the total energy of the system E_{tot} was calculated for the wide region of concentrations of Ag in Mg lattice. The Ag atoms were situated in the lattice sites of the non-implanted crystal of Mg and the calculations were carried out for the Wigner-Zeitz radius, corresponding to pure Mg. Then the radius of Wigner-Zeitz was varied to find the minimum value of $E_{tot} (E_{tot(\min)})$, and the corresponding lattice parameter was calculated. $E_{tot(\min)}$ gives the value of the energy minimum for the absolutely disordered Mg-Ag alloy. Actually for relatively high atomic fractions of Ag such solid solution does not exist. Instead, the system transfers in the two-phase mixture as follows from the phase diagram. To analyze the real equilibrium states one should perform the calculations for both phases in the mixture. At the same time, the calculations in the hypothetical disordered phase can provide useful information on the role of the electronic sub-system in the alloy on the further structural transformations that may occur when the atomic fraction of the alloying element increases. The value $\Delta E = E_{tot(\min)} - E_{tot}$ characterizes how far (“energy distance”) is the non-equilibrium state after PIII of the alloy from the relaxed state with given concentration of the solute. The results of calculations are presented in Fig. 1.

An interesting correlation may be found by comparison the data displayed in Fig. 1 and the information presented in Table 1. It is seen that for the values of Ag concentration, which correspond to formation of complex phases the sharp increase of the value ΔE occurs. Additional information about the correlation between the starting electronic states and phases formation in the non-equilibrium Mg-Ag system we obtained from the calculations of DOS for all concentrations of interest. Analysis of results

Solid State Physics

obtained in a wide region of concentrations of Ag (0-75 %) shows that the change of Ag concentration does not influence significantly the total and partial DOS at the Fermi level.

The significant dependence of DOS on the concentration of Ag is observed for the deep electronic states in the region 0.15-0.45 Ry. In Figs. 2-4 we demonstrate the change of DOS in this energy region dependently on the concentration of Ag implanted into Mg. Fig. 2 shows that the increase of the total DOS when the concentration of Ag increases, is correlated with the decrease of the partial DOS for d-states of Ag, implanted into Mg.

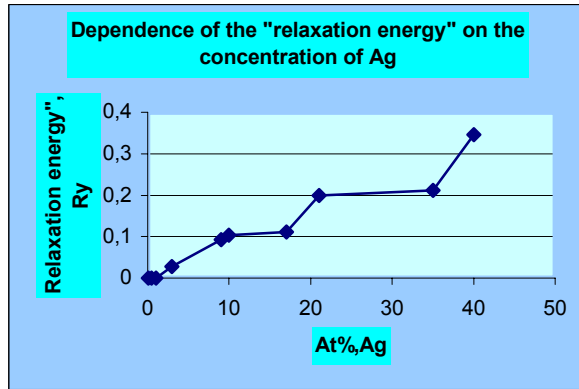


Figure 1. Dependence of the "relaxation energy" ($E_{\text{tot}} - E_{\text{tot}(\text{min})}$) on the concentration of Ag.

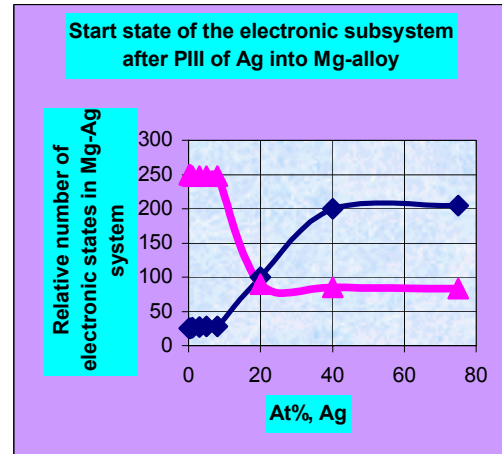


Figure 2. Dependence of the number of electronic states in the region 0.15-0.45 Ry on the concentration of Ag. The red curve corresponds to partial DOS for the d-states of Ag and the black curve corresponds to the total DOS for implanted Mg.

Figs. 3 and 4 show that the partial DOS for s- and p-states are changed insignificantly at the same concentrations. We found only a small increase of the partial DOS for s-states of Mg and a small decrease of DOS for p-states of Mg and Ag at high concentrations of Ag. So we can conclude that d-electrons of Ag are mainly responsible for the further formation of phases after PIII of Ag into Mg alloy.

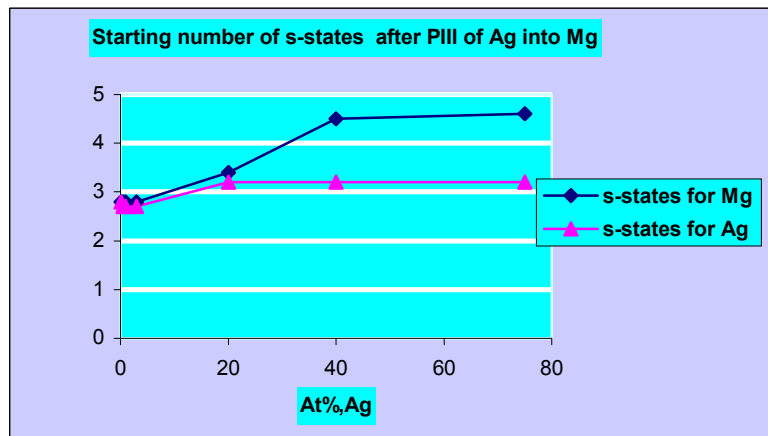


Figure 3. Dependence of the relative number of s-states for Mg and Ag in the region 0.15-0.45 Ry on the concentration of Ag. The red curve corresponds to partial DOS for the s-states of Ag and the black curve corresponds to the partial DOS for the s-states of Mg.

3. Discussion of results

We applied the *ab initio* calculations to clarify the role of different electronic states in non-equilibrium phase formation. In the case of PIII of Ag into Mg alloy we used the *ab initio* approach considering the "starting electronic states" immediately after plasma pulse. This state is hypothetical and cannot be observed experimentally. But further electronic and atomic processes depend essentially on this

Solid State Physics

initial electronic state. We suggest that a formation of more complex phases is accompanied by sufficient changes in the electronic subsystem of interacting components in the alloy. To obtain the corresponding information we have chosen the total energy of the system and the density of electronic states.

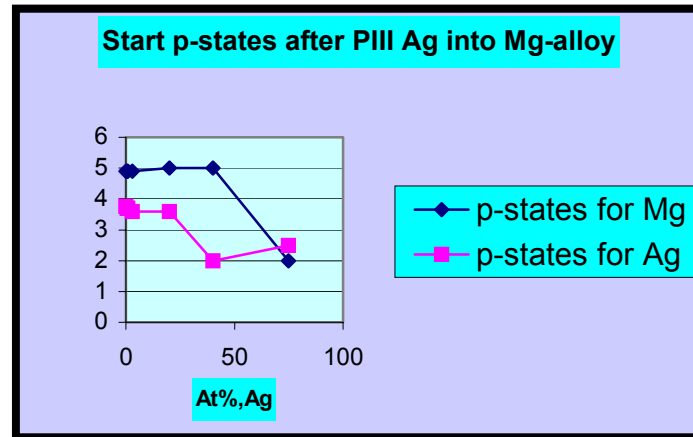


Figure 4. Dependence of the relative number of p-states for Mg and Ag in the region 0.15-0.45 Ry on the concentration of Ag. The red curve corresponds to partial DOS for the p-states of Ag and the black curve corresponds to partial DOS for the p-states of Mg.

In Mg-Ag alloy the increase of the concentration of Ag leads to formation of solid phases with higher symmetry. Our results show that the increase of concentration of Ag leads to decrease of the DOS for d-electrons in Ag. Obviously, d-electrons of Ag promote to the states with higher symmetry and participate the formation of the corresponding electronic orbitals. Fig. 4 shows that the increase of the concentration of implanted Ag in Mg alloy is accompanied by decrease of the partial DOS for d-states in Ag. The further development of this approach enables to shed some light on the nature of electron-atomic interactions in the non-equilibrium phase formation.

4. Conclusion

Using *ab initio* calculations we studied a role of the starting state of the electronic subsystem after the plasma pulse in the formation of complex solid phases in the non-equilibrium processes. It was found that the dependence of the total energy of a non-equilibrium alloy on the concentration of solute enable predict the regions of concentrations that correspond to new complex phases formation. Analysis of DOS plots at different concentrations of solute leads to conclusion that the d-states in Ag are mainly responsible for the formation of phases after PIII of Ag into Mg alloy.

References

- [1] Brown I.G. (1994) Vacuum arc ion sources (Review article). *Rev. Sci. Instrum.* **65** (10)
- [2] Mantese J.VBrown., I.G., Cheung N.W., Collins G.A. (1996) *MRS Bulletin* / August
- [3] Godechot X. and Brown I.G. (1992) Low energy metal ion source. *Journ. Sci. Technol. A* **10** (1)
- [4] Kreiner G., Spiekermann S. (2001) Crystal Structure of e-Ag_{7+x}Mg_{26-x} – A Binary Alloy Phase of the Mackay Cluster Type. *Z. Anorg. Allg. Chem* **677**, 2460
- [5] Andersen O.K. (1975) *Phys. Rev. B* **12**, 3060
- [6] Connolly J.W.D. and Williams A.R. (1983) *Phys. Rev. B* **27**, 5169
- [7] Faulkner J.S. (1982) *Phys. Rev. B* **27**, 1
- [8] Ruban A.V., Abrikosov I.A., Skriver H.L. (1995) *Phys. Rev. B* **51**, 12958

Received on the 17th of December 2002

CORRELATION EFFECTS IN ATOM-VACANCY "ALLOY"

D. FUKS

Materials Engineering Department, Ben-Gurion University of the Negev,
P.O.Box 653, 84105, Beer Sheva, Israel

The formation of the complexes of vacancies in metals is described in terms of interactions. These interactions are reflected by the correlations in atom-vacancy-type defects (VTD) solid solution. It is shown that the sign of the potential of mixing in such an "alloy" defines the curvature of the dependence of the logarithm of diffusivity on the reverse temperature. Formation of the complexes of vacancies that is known as one of the explanations of this curvature is associated with the correlation effects in the atom-VTD alloy in the vicinity of the temperature of phase transition in metals.

Keywords: vacancies in metals, atom-vacancy-type defects (VTD), Ising lattice

1. Introduction

Correlation effects play substantial role in numerous physical effects in alloys, including magnetic and mechanical properties, electric resistance, etc. [1]. Atomic long-range or short-range order affects surface segregation in binary metallic alloys [2]. It is a reason of the film-thickness dependence of the Curie temperature in thin transition metal films [3]. Recently the observation of highly enhanced Curie temperature at Ni-Al alloy surfaces was reported in Ref.[4], where it was associated with the correlation effects in atomic re-arrangement. Basic short-range order effects were accounted by means of the Cluster Variation Method (CVM) [5,6], the free energy expansion method [2,7] or Monte Carlo simulations [8-13]. Correlation effects are also important in explanation of the experimentally observed curvature of Arrhenius plot in self-diffusion in terms of mono- and di-vacancies [14] (or with the participation of more complicated complexes of vacancies [15]). Formation of such complexes of vacancies even when their concentration is extremely low justifies the existence of vacancies interactions. The clustering of vacancies in metals was reported in Ref. [16] and supports the assumption about vacancies interaction (see also Refs.[17-19]). This interaction may be of long-range and non-pair-wise nature leading to the considerable correlation effects in the vicinity of phase transition. In the high-temperature region this may be the pre-melting state of metal. In the low-temperature limit the order-disorder phase transition in atom-vacancy solid solution may occur. Even if the interaction between vacancies has the finite radius and their concentration in a metal is extremely small, the influence of other vacancies on the fixed vacancy may be sufficient. It may be realized indirectly by a long chain of surrounding ions of metal and other vacancies that exert coherent influence upon the vacancy under consideration. The effect of ordering of vacancies is also a direct consequence of the vacancies interaction (see, for example, Refs. [20,21]). In [22] the displacements of atoms in tetrahedral semiconductor structures were reported. It was explained in [22] by the formation of the super-lattice of vacancies at very small concentrations.

The starting point in the analysis of the vacancies interaction is usually based on the model of pair-wise interaction between vacancies. The term, which describes the interaction energy of the metal atoms with vacancies is concentration-dependent and is proportional to c_v^2 (see, for example, Ref.[23]). Some theoretical efforts were undertaken [24] to predict the possibility of formation of vacancies super-lattice in metals. The vacancy-vacancy interaction energy was computed in Ref. [25]. The theory of elastic interaction of point defects that accounts the discrete atomic structure of the crystal may be found in Ref. [26]. Considering the electronic structure of a crystal, the energy of the interaction of defects appears due to the corresponding changes of the electron charge distribution in the vicinity of the interacting vacancies. First-principles calculations [27,28] show that the formation of the vacancy in a metal is accompanied by the electron density redistribution that results in the electron charge transfer. This effect leads to the formation of charged quasi-particles at the "empty" sites of the crystal lattice. In this case not only the vacancy-vacancy interaction appears to become considerable but also the ion-vacancy interaction in a metal has to be accounted for. Thus an assumption about the vacancies interaction is based on the consideration of vacancy-type-defects (VTD) as quasi-particles at the lattice sites, leading to

Solid State Physics

the existence of the atom-VTD solid solution. In such a solution the effective mixing potentials may be introduced as in Ref. [23] where the theory of atom-VTD absolutely uncorrelated solid solution was formulated in pair-wise approximation for the interactions. Even this rough approximation allowed to ascertain the links of thermodynamics of atom-VTD solid solution with the diffusion and to explain the deviation of the Arrhenius plot from the straight line in the self-diffusion in metals.

In this paper we will explore these results. We formulate the theory of atom-VTD "alloy" accounting for the correlation effects in it. This allows to describe the interactions of quasi-particles in a more accurate manner and to explain the formation of complexes of vacancies in terms of correlations in such "alloys".

In this paper we illustrate the influence of the vacancies interaction on the self-diffusion process. We determine the concentration and temperature dependence of vacancies (quasi-particles) interactions as well as physical consequences of non-pair-wise vacancy-vacancy interactions. We show that the correlation in atom-VTD solid solution reflects itself in the non-Arrhenius behavior of self-diffusion.

2. Theory of correlations in atom-VTD solid solution

We start our study with the representation of the atom-VTD alloy assuming it to be of the substitutional type. The energy of this solution may be written as

$$E = \frac{1}{2} \sum_{\vec{r}, \vec{r}'} [V_{vv}(\vec{r}, \vec{r}') C_v(\vec{r}) C_v(\vec{r}') + V_{aa}(\vec{r}, \vec{r}') C_a(\vec{r}) C_a(\vec{r}') + 2V_{va}(\vec{r}, \vec{r}') C_v(\vec{r}) C_a(\vec{r}')] \quad (1)$$

where $V_{vv}(\vec{r}, \vec{r}')$, $V_{aa}(\vec{r}, \vec{r}')$, and $V_{va}(\vec{r}, \vec{r}')$ are the interaction potentials between two vacancies, between two atoms, and between atom and vacancy respectively. Summation is produced over vectors \vec{r} and \vec{r}' which are the lattice sites of the Ising lattice.

The values $C_v(\vec{r})$ and $C_a(\vec{r})$ are accidental spin-like functions, which are determined in the following way:

$$C_v(\vec{r}) = \begin{cases} 1, & \text{if site } \vec{r} \text{ is occupied by the vacancy;} \\ 0, & \text{otherwise} \end{cases}$$

$$C_a(\vec{r}) = \begin{cases} 1, & \text{if site } \vec{r} \text{ is occupied by the atom;} \\ 0, & \text{otherwise} \end{cases}$$

Moreover the condition

$$C_v(\vec{r}) + C_a(\vec{r}) = 1 \quad (2)$$

is satisfied which means that each site of the lattice is "occupied" or by the atom or by the vacancy.

Substituting $C_a(\vec{r})$ from Eq.(2) into Eq.(1) we obtain the energy per lattice site with $c_v = N_v / N$ in the form

$$E = \frac{1}{2N} \sum_{\vec{r}, \vec{r}'} \tilde{V}(\vec{r}, \vec{r}') C_v(\vec{r}) C_v(\vec{r}') + \frac{1}{2} [1 - 2c_v] V_{aa}(0) + c_v V_{va}(0) \quad (3)$$

Here

$$\tilde{V}(\vec{r}, \vec{r}') = V_{vv}(\vec{r}, \vec{r}') + V_{aa}(\vec{r}, \vec{r}') - 2V_{va}(\vec{r}, \vec{r}') \quad (4)$$

is the potential of mixing. In Eq.(3) the following definitions are used

$$\sum_{\vec{r}, \vec{r}'} V_{aa}(\vec{r}, \vec{r}') = V_{aa}(0), \quad (5a)$$

$$\sum_{\vec{r}, \vec{r}'} V_{va}(\vec{r}, \vec{r}') = V_{va}(0), \quad (5b)$$

and

$$\sum_{\vec{r}} C_v(\vec{r}) = N_v, \quad (6)$$

Solid State Physics

with N_v and N - the total number of vacancies and lattice sites, respectively. The formation of a mono-vacancy at zero pressure in an elementary system is usually described within a canonical ensemble, i.e. for fixed temperature and fixed number of atoms. The distribution of vacancies in considered binary atom-vacancy "alloy" may be described by single occupation probability function $n(\bar{r})$ that is the probability to find the vacancy at the site \bar{r} of the crystal lattice

$$n(\bar{r}) = \langle C_v(\bar{r}) \rangle, \quad (7)$$

where the averaging is done over the Gibbs canonical ensemble. Performing such averaging and adding the configurational entropy term it is possible to represent the Helmholtz free energy in a form

$$\begin{aligned} F &= E - TS = \\ &= \frac{1}{2N} \sum_{\bar{r}, \bar{r}'} \tilde{V}(\bar{r}, \bar{r}') n(\bar{r}) n(\bar{r}') + \frac{1}{2} [1 - 2c_v] V_{aa}(0) + c_v V_{va}(0) + \\ &+ kT \sum_{\bar{r}} [n(\bar{r}) \ln(n(\bar{r})) + (1 - n(\bar{r})) \ln(1 - n(\bar{r}))]. \end{aligned} \quad (8)$$

This approach was used in Ref.[26] to describe the ordering effects in binary substitutional solid solution and in Ref.[23] for the atom-VTD alloy. Eq.(8) is written in a form neglecting the correlation effects in the atom-vacancy solid solution. To account for these effects we will use the generalization of the Kirkwood's approach [29] which was formulated in Ref.[30]. The results of Ref.[30] are applicable to binary substitutional alloys and consider the long-range interactions. The partition function for the atom-VTD solid solution with the pair-wise interaction at any fixed temperature may be given as

$$Z = \sum_{c_v(\bar{r}_1)=0}^1 \sum_{c_v(\bar{r}_2)=0}^1 \dots \sum_{c_v(\bar{r}_n)=0}^1 \exp \left[-\frac{1}{2kT} \sum_{\bar{r}, \bar{r}'} \tilde{V}(\bar{r}, \bar{r}') C_v(\bar{r}) C_v(\bar{r}') \right]. \quad (9)$$

Using the definition (7) Eq.(9) takes the form

$$Z = Z_0 \exp \left[-\frac{1}{2kT} \sum_{\bar{r}, \bar{r}'} \tilde{V}(\bar{r}, \bar{r}') n(\bar{r}) n(\bar{r}') \right] \times \left\langle \exp \left[-\frac{1}{2kT} \sum_{\bar{r}, \bar{r}'} \tilde{V}(\bar{r}, \bar{r}') \Delta C_v(\bar{r}) \Delta C_v(\bar{r}') \right] \right\rangle_0, \quad (10)$$

where $\Delta C_v(\bar{r}) = C_v(\bar{r}) - n(\bar{r})$, $\langle \dots \rangle_0$ is the average over the non-interacting ensemble of particles, Z_0 is defined as

$$\ln Z_0 = -\sum_{\bar{r}} \{ n(\bar{r}) \ln[n(\bar{r})] + [1 - n(\bar{r})] \ln[1 - n(\bar{r})] \}, \quad (11)$$

and

$$\begin{aligned} &\left\langle \exp \left[-\frac{1}{2kT} \sum_{\bar{r}, \bar{r}'} \tilde{V}(\bar{r}, \bar{r}') \Delta C_v(\bar{r}) \Delta C_v(\bar{r}') \right] \right\rangle_0 = \\ &= Z_0^{-1} \sum_{c_v(\bar{r}_1)=0}^1 \sum_{c_v(\bar{r}_2)=0}^1 \dots \sum_{c_v(\bar{r}_n)=0}^1 \exp \left[-\frac{1}{2kT} \sum_{\bar{r}, \bar{r}'} \tilde{V}(\bar{r}, \bar{r}') \Delta C_v(\bar{r}) \Delta C_v(\bar{r}') \right]. \end{aligned} \quad (12)$$

The free energy of the atom-VTD alloy that corresponds the partial function (10) is

$$F_1 = F - kT \ln \left\langle \exp \left[-\frac{1}{2kT} \sum_{\bar{r}, \bar{r}'} \tilde{V}(\bar{r}, \bar{r}') \Delta C_v(\bar{r}) \Delta C_v(\bar{r}') \right] \right\rangle_0, \quad (13)$$

Solid State Physics

where F is the sum of the first and the last terms of Eq.(8) and represents the free energy in the mean-field approximation, neglecting the correlations. The second term in Eq.(13) represents the contribution of the correlation effects to the free energy of an alloy, $\Delta F = F_1 - F$.

$$\Delta F = -kT \ln \left\langle \exp \left[-\frac{1}{2kT} \sum_{\vec{r}, \vec{r}'} \tilde{V}(\vec{r}, \vec{r}') \Delta C_v(\vec{r}) \Delta C_v(\vec{r}') \right] \right\rangle_0. \quad (14)$$

This expression may be expanded in series on cumulants $M_n(X)$

$$\Delta F = -kT \sum_{n=1}^{\infty} \frac{(-1/kT)^n M_n(X)}{n!}, \quad (15)$$

where $X = \frac{1}{2} \sum_{\vec{r}, \vec{r}'} \tilde{V}(\vec{r}, \vec{r}') \Delta C_v(\vec{r}) \Delta C_v(\vec{r}')$ and several first cumulants have the form

$$\begin{aligned} M_1(X) &= \langle X \rangle_0, \\ M_2(X) &= \langle X^2 \rangle_0 - \langle X \rangle_0^2, \\ M_3(X) &= \langle X^3 \rangle_0 - 3\langle X^2 \rangle_0 \langle X \rangle_0 + 2\langle X \rangle_0^3, \\ M_4(X) &= \langle (X - \langle X \rangle_0)^4 \rangle_0 - 3\langle (X - \langle X \rangle_0)^2 \rangle_0^2. \end{aligned}$$

As shown in Ref.[30] the term in Eq.(15) which contains M_l may be neglected and

$$\begin{aligned} M_2 &= \sum_{1,2} \tilde{V}^2(1,2) \langle \Delta C_v^2(1) \rangle_0 \langle \Delta C_v^2(2) \rangle_0, \\ M_3 &= \frac{1}{2} \sum_{1,2} \tilde{V}^3(1,2) \langle \Delta C_v^3(1) \rangle_0 \langle \Delta C_v^3(2) \rangle_0 + \sum_{1,2,3} \tilde{V}(1,2) \tilde{V}(2,3) \tilde{V}(3,1) \langle \Delta C_v^2(1) \rangle_0 \langle \Delta C_v^2(2) \rangle_0 \langle \Delta C_v^2(3) \rangle_0, \\ M_4 &= \frac{1}{2} \sum_{1,2} \tilde{V}^4(1,2) \left(\langle \Delta C_v^4(1) \rangle_0 - 3\langle \Delta C_v^2(1) \rangle_0^2 \right) \left(\langle \Delta C_v^4(2) \rangle_0 - 3\langle \Delta C_v^2(2) \rangle_0^2 \right) + \\ & 3 \sum_{1,2,3,4} \tilde{V}(1,2) \tilde{V}(2,3) \tilde{V}(3,4) \tilde{V}(4,1) \langle \Delta C_v^2(1) \rangle_0 \langle \Delta C_v^2(2) \rangle_0 \langle \Delta C_v^2(3) \rangle_0 \langle \Delta C_v^2(4) \rangle_0 - \\ & 6 \sum_{1,2,3} \tilde{V}^2(1,2) \tilde{V}^2(2,3) \langle \Delta C_v^2(1) \rangle_0 \langle \Delta C_v^2(2) \rangle_0^2 \langle \Delta C_v^2(3) \rangle_0 + \\ & 6 \sum_{1,2,3} \tilde{V}(1,2) \tilde{V}^2(2,3) \tilde{V}(3,1) \langle \Delta C_v^2(1) \rangle_0 \langle \Delta C_v^2(2) \rangle_0^2 \langle \Delta C_v^3(3) \rangle_0. \end{aligned} \quad (16)$$

Here the numbers 1,2,3,...etc. are used instead of $\vec{r}_1, \vec{r}_2, \vec{r}_3, \dots$ etc. Calculating the expressions of the type

$\langle \Delta C_v^n(\vec{r}) \rangle_0^m$, where n and m are integer numbers and substituting Eq. (16) into Eq. (15) we obtain

$$\begin{aligned} \Delta F &= -\frac{1}{4kT} \sum_{1,2} \tilde{V}^2(1,2) f_1(1) f_1(2) + \frac{1}{12(kT)^2} \left\{ \sum_{1,2} \tilde{V}^3(1,2) f_1(1) f_2(1) f_2(2) + \right. \\ & 2 \sum_{1,2,3} \tilde{V}(1,2) \tilde{V}(2,3) \tilde{V}(3,1) f_1(1) f_1(2) f_1(3) \left. \right\} - \frac{1}{48(kT)^3} \left\{ \sum_{1,2} \tilde{V}^4(1,2) f_1(1) f_1(2) f_3(1) f_3(2) + \right. \\ & 6 \sum_{1,2,3,4} \tilde{V}(1,2) \tilde{V}(2,3) \tilde{V}(3,4) \tilde{V}(4,1) f_1(1) f_1(2) f_1(3) f_1(4) - 12 \sum_{1,2,3} \tilde{V}(1,2) \tilde{V}(2,3) f_1(1) f_1^2(2) f_1(3) + \\ & \left. 12 \sum_{1,2,3} \tilde{V}(1,2) \tilde{V}^2(2,3) \tilde{V}(3,1) f_1(1) f_1(2) f_1(3) f_2(2) f_2(3) \right\} + \dots, \end{aligned} \quad (17)$$

where

$$\begin{aligned} f_1(\bar{r}) &= n(\bar{r})[1 - n(\bar{r})] \\ f_2(\bar{r}) &= 1 - 2n(\bar{r}), \\ f_3(\bar{r}) &= 1 - 6n(\bar{r}) + 6[n(\bar{r})]^2. \end{aligned} \tag{18}$$

Let us consider the case when all positions of the crystal lattice sites $\{\bar{r}\}$ are described by one Bravais lattice. The function $n(\bar{r})$, which determines a distribution of solute atoms (or vacancies, in our description) in an ordering phase, can be expanded in Fourier series. It can be presented as a superposition of concentration waves (CW)

$$n(\bar{r}) = c_v + \frac{1}{2} \sum_j \left[Q(\bar{k}_j) e^{i\bar{k}_j \bar{r}} + Q^*(\bar{k}_j) e^{-i\bar{k}_j \bar{r}} \right], \tag{19}$$

where $\exp(i\bar{k}_j \bar{r})$ is a concentration wave, \bar{k}_j is a nonzero wave vector defined in the first Brillouin zone of the disordered "vacancy-atom" alloy, the index j denotes the wave vectors in the Brillouin zone, and $Q(\bar{k}_j)$ is a concentration wave amplitude. As shown in Ref.[26], all $Q(\bar{k}_j)$ are linear functions of the long-range-order parameters of the super-lattices that may be formed on the basis of the Ising lattice of the disordered solid solution. In the alloy with small concentration of one of components it is possible to assume the existence of a disordered solid solution. The concentration of vacancies is very small ($c_v \approx 10^{-3} \div 10^{-5}$) and the disappearance of the ordering state immediately leads to the statement that all $Q(\bar{k}_j)$ are equal to zero. Thus Eq. (8) may be rewritten in the following form (per lattice site)

$$F = E(c_v) + kT [c_v \ln(c_v) + (1 - c_v) \ln(1 - c_v)], \tag{20}$$

where

$$E(c_v) = \frac{1}{2} \tilde{V}(0) c_v^2 + \frac{1}{2} [1 - 2c_v] V_{aa}(0) + c_v V_{va}(0), \tag{21}$$

and

$$\begin{aligned} \Delta F = & -\frac{1}{4kT} \sum_{1,2} \tilde{V}^2(1,2) [c_v(1 - c_v)]^2 + \frac{1}{12(kT)^2} \left\{ \sum_{1,2} \tilde{V}^3(1,2) [c_v(1 - c_v)]^2 (1 - 2c_v)^2 + \right. \\ & \left. 2 \sum_{1,2,3} \tilde{V}(1,2) \tilde{V}(2,3) \tilde{V}(3,1) [c_v(1 - c_v)]^3 \right\} - \frac{1}{48(kT)^3} \left\{ \sum_{1,2} \tilde{V}^4(1,2) [c_v(1 - c_v)]^2 [1 - 6c_v + 6c_v^2] + \right. \\ & \left. 6 \sum_{1,2,3,4} \tilde{V}(1,2) \tilde{V}(2,3) \tilde{V}(3,4) \tilde{V}(4,1) [c_v(1 - c_v)]^4 - 12 \sum_{1,2,3} \tilde{V}(1,2) \tilde{V}(2,3) [c_v(1 - c_v)]^4 + \right. \\ & \left. 12 \sum_{1,2,3} \tilde{V}(1,2) \tilde{V}^2(2,3) \tilde{V}(3,1) [c_v(1 - c_v)]^3 (1 - 2c_v)^2 \right\} + \dots \end{aligned} \tag{22}$$

Restricting ourselves only by the terms of the second order in c_v , we obtain ΔF in a more compact form:

$$\begin{aligned} \Delta F = & \left[-\frac{1}{4kT} \sum_{1,2} \tilde{V}^2(1,2) + \frac{1}{12(kT)^2} \sum_{1,2} \tilde{V}^3(1,2) - \frac{1}{48(kT)^3} \sum_{1,2} \tilde{V}^4(1,2) + \dots \right] c_v^2 = \\ & \frac{1}{2} kT \sum_{1,2} \left\{ -\frac{1}{2(kT)^2} \tilde{V}^2(1,2) + \frac{1}{6(kT)^3} \tilde{V}^3(1,2) - \frac{1}{24(kT)^4} \tilde{V}^4(1,2) + \dots \right\} c_v^2. \end{aligned} \tag{23}$$

In the nearest neighbor approximation this equation transforms to

Solid State Physics

$$\Delta F = \frac{1}{2} kT n_1 \left\{ -\frac{1}{2(kT)^2} \tilde{V}_1^2 + \frac{1}{6(kT)^3} \tilde{V}_1^3 - \frac{1}{24(kT)^4} \tilde{V}_1^4 + \dots \right\} c_v^2 = \frac{1}{2} kT n_1 \left\{ \exp\left(-\frac{\tilde{V}_1}{kT}\right) - 1 + \frac{\tilde{V}_1}{kT} \right\} c_v^2. \quad (24)$$

Here n_1 and \tilde{V}_1 are the number of the nearest neighbors and the mixing potential on the first coordination shell, respectively.

Using Eqs. (13,20,24) together with the equilibrium condition $\partial F_1 / \partial c_v = 0$ we immediately obtaine

$$c_v = \left[1 + \exp\left(\left(\frac{\partial E}{\partial c_v} + \frac{\partial \Delta F}{\partial c_v}\right) / kT\right) \right]^{-1}. \quad (25)$$

This expression is more general than the Boltzmann distribution

$$c_v \sim \exp\left(-\frac{E_v}{kT}\right), \quad (26)$$

that usually describes the temperature dependence of the concentration of vacancies. Eq. (25) may be reduced to Eq.(26) if one neglects the correlation effects and assumes the linear approximation for the concentration dependence of E ,

$$E(c_v) = E_0 + c_v E_v, \quad (27)$$

with E_v independent on c_v and $E_v \gg kT$. It is easy to see that Eq.(25) reflects the Pauli principle for vacancies in a crystal lattice and is a Fermi-type distribution function for vacancies in a disordered atom-vacancy solid solution with correlations.

The Boltzmann distribution function is obtained from this Fermi-type distribution when

$(\tilde{V}(0)c_v - V_{aa}(0) + V_{va}(0)) + \frac{\partial \Delta F}{\partial c_v} \gg kT$. Thus the term in the left side of this expression represents the vacancy formation energy in the Boltzmann distribution, accounts for the correlation effects and includes the concentration dependent terms $\tilde{V}(0)c_v$ and $\frac{\partial \Delta F}{\partial c_v}$.

Let us turn to the Eq. (27) which is usually treated as the definition of the energy of formation of vacancies. It may be considered as the first term of the power expansion series on the small parameter that is the vacancy concentration:

$$E(c_v) = E(0) + c_v E_v^{(0)} + \frac{1}{2} c_v^2 E_v^{(1)} + \dots \quad (28)$$

Here $E_v^{(0)}$ and $E_v^{(1)}$ are the expansion coefficients. Restriction of this expansion by the linear term will lead to the Eq.(27). Including the square term allows to account the pair-wise interaction of vacancies (see for example Ref. [31]):

$$E_v = \frac{dE(c_v)}{dc_v} = E_v^{(0)} + c_v E_v^{(1)} + \dots \quad (29)$$

Confining these series by the first two terms and comparing with Eqs.(21,27) we obtain

$$E_v^{(0)} = -V_{aa}(0) + V_{va}(0) \quad (30)$$

and

$$\frac{1}{2}E_v^{(1)} = \frac{1}{2}\tilde{V}(0). \quad (31)$$

The expression (31) gives a physical meaning of the additional term $\frac{1}{2}E_v^{(1)}c_v^2$, that is simply determined by the energy of mixing in the uncorrelated atom-vacancy solid solution.

3. Interaction parameters from the self-diffusion data

The necessary experimental information about the value and the sign of the effective potential of mixing may be obtained from the self-diffusion experiment. As was shown in Refs. [32,33], the curvature of the dependence of the logarithm of diffusivity on the reverse temperature may be explained on the basis of the assumption that the energy of formation of vacancies is concentration dependent. It may be presented in the form of Eq.(28). The diffusion coefficient, D , of the Arrhenius-type formula may be written as

$$D \sim c_v \exp\left(-\frac{E_\mu}{kT}\right), \quad (32)$$

where E_μ is the migration energy. Using Eqs. (23,24,29) D may be expressed in the following form

$$\ln D \sim -\frac{1}{kT} \left[E_v^{(0)} + E_\mu + \frac{E_v^{(1)} - kTn_1 \left[\exp\left(-\frac{\tilde{V}_1}{kT}\right) - 1 + \frac{\tilde{V}_1}{kT} \right]}{1 + \exp\left(\frac{E_v^{(0)}}{kT}\right)} \right]. \quad (33)$$

Recalling Eq. (31) and keeping in mind that in the nearest neighbors approximation $E_v^{(1)} = n_1\tilde{V}_1$

$$\ln D \sim -\frac{1}{kT} \left[E_v^{(0)} + E_\mu - \frac{kTn_1 \left[\exp\left(-\frac{\tilde{V}_1}{kT}\right) - 1 \right]}{1 + \exp\left(\frac{E_v^{(0)}}{kT}\right)} \right]. \quad (34)$$

Here the last term reflects the correlation effects in the atom-VTD solid solution and it is given in a form of the Mayer's function (see, for example, [34]). In Eq.(33) we keep only the $E_v^{(1)}$ term from Eq. (29) and correlation term and neglect all terms, except $E_v^{(0)}$ in the denominator of the exponent. If the interaction in the atom-VTD solid solution is neglected ($\tilde{V}_1 = 0$), we obtain from Eq. (34) the usual Arrhenius law. Inclusion of interaction leads to the appearance of the temperature dependence, represented by the last term in this equation. This temperature dependence is a possible reason for the curvature of $\ln D$ vs $1/T$. If $|\tilde{V}_1| \ll kT$ the exponent in Eq. (34) may be expanded in the series. A simple analysis of Eq. (34) shows that if \tilde{V}_1 is negative, we have a normal behavior for diffusion coefficient with the positively curved Arrhenius plot. If \tilde{V}_1 is positive, the negatively curved Arrhenius plot will be obtained.

4. Results and discussion

To illustrate the described thermodynamic approach we calculated the effective potential of mixing on the first coordination shell, \tilde{V}_1 , for the atom-vacancy alloy from the self-diffusion data for Nb. To represent numerically, $E_v^{(0)}$ and \tilde{V}_1 are computed by fitting the Eq. (34) for the self-diffusion temperature dependence to experimental data [35]. From this fitting we obtain $E_v^{(0)} = 1.82$ eV and $\tilde{V}_1 = -$

Solid State Physics

0.22 eV. The result for $E_v^{(0)}$ corresponds well with that of the fitting the usual Arrhenius law for self-diffusion to the results of measurements. In Ref. [36] this value is $E_v=2.0$ eV. Summarizing the values and the signs of the Nb energy parameters we may conclude that the negative sign of \tilde{V}_1 reflects the tendency for the bonding of vacancies in complexes. These complexes may be di-vacancies, triple-vacancies, etc. Formation of such complexes was suggested previously (see Ref.[14]) as possible explanation of the curvature of $\ln D$ vs $1/T$ in high-temperature region for metals. In this case the question arises why these complexes have to be formed at high temperatures. Contrary, it seems that in such conditions the dissociative process has to be dominating as compared with the bonding process. The increase of the temperature has to destroy the bonds between vacancies instead of formation of such bonds. Our thermodynamic approach that is applied to the atom-VTD solid solution solves this contradiction in a natural way. We obtain the formation of the complexes of vacancies as a result of accounting for the correlation effects in this solution. These effects become sufficient in some temperature interval near the phase transition. For Nb and other metals showing the change in the slope of $\ln D$ vs $1/T$ in high-temperature region this phase transition is the melting of a metal. The same arguments seem to be applicable to some *bcc* metals (for example, Ti, Zr, Hf) that are known as "anomalous" *bcc* metals. In these metals the continuous curvature of $\ln D$ vs $1/T$ is observed in a wide temperature interval that is the interval of existence of *bcc* phase. The usual explanation of this effect is based on the idea of "phonon softening" of the lattice [37]. At the same time above mentioned metals undergo the polymorphous phase transition to the hexagonal close-packed (*hcp*) lattice when the temperature decreases (for Ti, for example, the critical temperature of phase transformation, $T_c \sim 1180$ K). So for $T_{\text{melt}} > T > T_c$ these metals have *bcc* structure while at lower temperatures the *hcp* structure is observed. In spirit of the formulated thermodynamic approach the correlation effects may be meaningful in the whole temperature interval, ΔT , of the existence of *bcc* phase (for Ti $\Delta T = T_{\text{melt}} - T_c \sim 660$ K). These temperatures are close to the temperature of the phase transition (that is either melting or polymorphic transformation) where correlations may play significant role and have to be taken into consideration in the thermodynamic description of the atom-vacancy solid solution. This will lead to the temperature dependence of the activation energy thus describing the continuous curvature of $\ln D$ vs $1/T$. This result in some sense corresponds to the result obtained by Sanchez and de Fontaine [38]. In Ref. [38] the deviation of $\ln D$ vs $1/T$ from the straight line in β -Zr was explained by the low-temperature phase transition.

In conclusion, one methodological aspect should be mentioned. It concerns the applicability of Kirkwood's approach to the study of the correlation effects in the atom-VTD solid solution. This method represents a regular procedure that accounts the additional correlation-dependent terms that are included in the free energy of solid solution. Actually this procedure is one of the methods of thermodynamic perturbation theory. Eq.(15) gives the free energy of correlations in the form of expansion series and demands the existence of small parameter. It is usually assumed that these expansion series are converged rapidly if the condition $\tilde{V}(\bar{r}, \bar{r}')/(kT) \ll 1$ is satisfied. This corresponds to relatively high temperatures. Thus traditionally it is assumed that Kirkwood's method to account the correlation effects works well in the high-temperature region. At the same time in a special case of the atom-vacancy solid solution in metals there is an additional small parameter that is the concentration of vacancies. The extreme smallness of c_v is provided in the solid phase of a metal for all temperatures where this phase exists. The convergence of the cumulants expansion series (Eq. (15)) is more rapid for systems with low concentration of one of components (that is VTD in our case). If we restrict ourselves by square terms in concentration of vacancies the cumulants expansion series may be summed up in nearest neighbor approximation. The result given by Eq.(24) may be used at any reasonable finite temperature (which corresponds to the solid state) and shows the contribution of correlations in the free energy of the atom-VTD "alloy".

Acknowledgements

This research was supported in part by the grant N^o G-617-16.10/1999 from the German-Israel Science Foundation (GIF). Author is thankful to Dr. S. Dorfman for numerous useful discussions and to Prof. Dr. H. Mehrer for his constant interest in this activity.

References

- [1] Girifalco L.A. (1973) *Statistical Physics of Materials*. John Wiley and Sons, New York
- [2] Polak M., Deng J., Rubinovich L. (1997) *Phys. Rev. Lett.* **78**, 1058
- [3] Jensen P. J., Dreyse H., Bennemann K. H. (1992) *Europhys. Lett.* **18**, 463
- [4] Polak M., Rubinovich L., Deng J. (1995) *Phys. Rev. Lett.* **74**, 4059
- [5] Teraoka Y. (1991) *Surf. Sci.* **242**, 113
- [6] Ruban A. V., Abrikosov I. A., Kats D. Ya., Gorelikov D., Jacobsen K. W., Skriver H. L. (1994) *Phys. Rev. B* **49**, 11383
- [7] Rousset J. M., Saul A., Rubinovich L., Polak M. (1999) *J. Phys.: Condens. Matter* **11**, 9909; Polak M., Rubinovich L. (2000) *Surf. Sci. Rep.* **38**, 127
- [8] Wang H. Y., Najafabadi R., Srolovitz D. J., Le Sar R. (1992) *Phys. Rev. B* **45**, 12028
- [9] Najafabadi R., Srolovitz D. J. (1993) *Surf. Sci.* **286**, 104
- [10] Saul A., Legrand B., Treglia G. (1994) *Phys. Rev. B* **50**, 1912
- [11] Bozzolo G., Good B., Ferrante J. (1993) *Surf. Sci.* **289**, 169
- [12] Hou M., Azzaoui M. L. (1997) *Surf. Sci.* **380**, 210
- [13] Binder K. (1995) *Phase transitions at surfaces*, in *Cohesion and Structure of Surfaces*, Ed. D. Pettifor, Elsevier, Amsterdam
- [14] *Diffusion in Solid Metals and Alloys* (1990) H.Mehrer, ed., v. 26. Landolt-Börnstein, Springer-Verlag,
- [15] D.N.Siedman (1986) *Encyclopedia of Materials Science and Engineering* **5**, 3591. Ed. Michael B. Bever, Pergamon Press, New York
- [16] Hirsch B., Silcox J., Smallman R.E., Westmacott K.H. (1958) *Philos. Mag.* **3**, 897.
- [17] *Lattice Defects in Quenched Metals* (1965). Eds R.M.J.Cotterill, M.Doyama, J.J.Jackson, and M.Meshii, Academic Press, New York
- [18] Chik K.P (1970) In: *Vacancies and Interstitials in Metals*. Proceedings of the International Conference, Jülich, 1968, Eds. A.Seeger, D.Schumacher, W.Schilling, and J.Diehl, North-Holland, Amsterdam, 183
- [19] Franklin A.D. (1972) *Point Defects in Solids* **1**. Eds. J.H.Crawford and L.M.Slifkin, Plenum Press, New York, 1
- [20] Reller A., Thomas J.M., Jefferson D.A, Uppal M.K. (1984) *Proc.Roy.Soc.London A* **394**, 223
- [21] Frangis N., van Tendeloo G., van Landuyt J., Amelinckx S. (1986) *J.Sol.State Chem.* **61**, 369
- [22] Vaipolin A. A. (1990) *Sov.Phys.Solid State* **32**, 2109
- [23] Fuks D., Dorfman S. (1994) *Phys.Rev. B* **50**, 16340
- [24] Chang R. (1976) *Scr. Metall.* **10**, 861
- [25] Flocken J.W., Hardy J.R. (1969) *Phys.Rev.* **177**, 1054
- [26] Khachaturyan A.G. (1983) *Theory of Structural Transformations in Solids*. John Wiley, New-York
- [27] De Vita A., Gillan M.J. (1991) *J.Phys.:Condens.Matter* **3**, 6225
- [28] Ferreira S., Frota-Pessoa S. (1995) *Phys.Rev. B* **51**, 2045
- [29] Kirkwood J.G. (1938) *J.Chem.Phys.* **6**, 70
- [30] Badalyan D.A., Khachaturyan A.G. (1970) *Sov.Phys.Solid State* **12**, 346
- [31] Leibfried G., Brener N. (1978) *Point Defects in Metals. I. Introduction to the Theory*. Springer-Verlag, Berlin
- [32] Fuks D., Pelleg J., Dorfman S., Rashkeev S. (1993) *Solid State Commun.* **87**, 405
- [33] Fuks D., Pelleg J., Rashkeev S.N., Dorfman S. (1994) *Z.Phys. B* **95**, 189
- [34] R. Balescu (1975) *Equilibrium and nonequilibrium statistical mechanics*. John Wiley and Sons, New-York-London
- [35] Einzinger R.E., Mundy J.N., Hoff H.A. (1978) *Phys.Rev. B* **17**, 440
- [36] Balluffi R.W. (1978) *J.Nucl.Mater.* **69&70**, 240
- [37] Köhler U., Herzog Ch. (1987) *phys.stat.sol.(b)* **144**, 243
- [38] Sanchez M., de Fontaine D. (1975) *Phys.Rev.Lett.* **35**, 227

Received on the 17th of December 2002

DEA SUPER EFFICIENCY MULTISTAGE RANKING

Y. HADAD^a, L. FRIEDMAN^b, Z. SINUANY-STERN^{b,c}, A. MEHREZ⁺

^a *Department of Industrial Engineering and Management, Negev Academic College of Engineering, Beer Sheva, 84100, Israel, E-Mail: yossi@nace.ac.il*

^b *Department of Industrial Engineering and Management, Ben-Gurion University of the Negev, Beer Sheva, 84105, Israel*

^c *Academic College of Judea and Samaria, Ariel, 44837, Israel*

⁺ *Professor Mehrez passed away on February 5th, 2000 after a courageous struggle with cancer*

In this paper a new ranking method is presented within the Data Envelopment Analysis (DEA). Based on the super efficiency ranking method of Anderson and Peterson, which ranks only the efficient units, we developed here a multistage process which ranks also the inefficient units using a similar procedure at each stage. The model is applied to an example from the literature. Moreover, several ranking methods are compared to the new multistage method and nonparametric statistical tests are utilized to compare the various ranking methods. In this example, as expected, all the ranking methods were significantly correlated.

General topics covered by this paper include the following areas:

- * Data Envelopment Analysis- procedure designed to measure the relative efficiency.
- * The Technical and Scale Efficiency.
- * The Technical Efficiency
- * Ranking Methods.

Keywords: Data Envelopment Analysis (DEA), Rank-Scaling, Cross Efficiency Matrix, Multi-Criteria Decision Analysis (MCDA).

1. Introduction

Ranking organizational units in the context of Data Envelopment Analysis (DEA) has become an acceptable approach recently, as done in Multi-Criteria Decision Analysis (MCDA). See for example Belton and Stewart [5] and Green and Doyle [9]. If we consider the availability of a model in commercial software as an indication of its popularity then we can point that the super efficiency ranking method developed by Anderson and Peterson (A&P) [2] is the most widespread ranking method. For example, it appears in the Warwick DEA code [23]. Moreover, this ranking method was cited more often than others.

In spite of its popularity there were several criticisms about the A&P ranking method. A&P accepts the DEA score as a rank scale for the inefficient units. In order to differentiate between the efficient units (which receive score 1 in DEA), they developed a method to score them with values greater than 1. Cooper and Tone [7] argue that the DEA only classify the units into two dichotomic sets: efficient and inefficient. They do not rank the efficient unit since they claim that they all are on the efficient frontier. Moreover, they do not accept the DEA score as a ranking score for the inefficient units since their weights vary from unit to unit. However, they suggest another ranking method based on the slack variables of the dual problem (the improvements of each variable). Wilson [24] argues that the A&P ranking model does not provide ranking, it mainly identifies outliers; namely, efficient units that receive very high scores by A&P are identified as outliers.

In our paper we present a new ranking method, G/DEA, based on the A&P approach, which responds to both criticism mentioned above. G/DEA is a multistage procedure where the A&P method is applied several times on subsets of the units. G/DEA does not receive the DEA score for ranking, it ranks them in stages. Furthermore, we show by example that A&P does not necessarily identify outliers.

There are several ranking methods in the DEA literature (see Adler et al. [1]). In this paper we refer to two other ranking methods. The ranking method developed the first is based on the cross efficiency matrix (Sexton, [14]), and a more recent one, the discriminant analysis of ratio (Sinuany-Stern and Friedman, [17]). Both methods rank all the units.

In this paper we first present advantages of ranking in the DEA context, then the super efficiency rank scaling method of A&P, is given. Afterwards we present the new super efficiency multistage ranking. In section 5 an example from the literature is presented and analysed. In Section 6 we compare the ranking of several methods. Finally a summary and conclusions are given.

2. Data Envelopment Analysis and ranking in the DEA context

2.1. DATA ENVELOPMENT ANALYSIS

DEA is a procedure designed to measure the relative efficiency in situations when there are multiple inputs and multiple outputs and no obvious objective how to aggregate both inputs and outputs into a meaningful index of productive efficiency. DEA was developed by Charnes Cooper and Rhodes (CCR) [5]. The method provides a mechanism for measuring Decision-Making Unit (DMU) Pareto efficiency compared with other DMUs. The mechanism is extensively employed in diverse industries and environments (an extensive review of DEA applications is provided by Seiford [13]). In the service sector, applications of DEA include education (Sexton et. al. [15]), recreation and health care management to name just a few.

The efficiency in DEA is termed Technical and Scale Efficiency (TSE) and the relative efficiency of a DMU is defined as the ratio of its total weighted output to its total weighted input. The question is how to select the weights if no unit values can be assigned to the inputs and outputs? Here lies the seed of DEA procedure. DEA permits each DMU to select any weight that it wants for each input and output, provided that they satisfy certain reasonable conditions: first that no weights can be negative, and second that the weights must be universal, which means that the resulting ratio should not exceed 1. The BCC model, named after Banker, Charnes and Cooper (BCC) [3] allows the production function to exhibit non-constant return to scale (Banker and Chang, [4]) while the CCR model imposes the additional assumption of constant returns to scale on the production function.

The Technical and Scale Efficiency (TSE) with constant return to scale is computed according to the CCR model (Charnes, Cooper & Rhodes [5]).

Consider n DMUs, when each DMU j ($j=1, \dots, n$) uses m inputs $X_j = (X_{1j}, X_{2j}, \dots, X_{mj})^T > 0$ for producing s outputs $Y_j = (Y_{1j}, Y_{2j}, \dots, Y_{sj})^T > 0$. The CCR model is as follows:

$$\text{Max } E_k = \frac{\sum_{r=1}^s U_r^k Y_{rk}}{\sum_{i=1}^m V_i^k X_{ik}}$$

subject to

$$\frac{\sum_{r=1}^s U_r^k Y_{rj}}{\sum_{i=1}^m V_i^k X_{ijk}} \leq 1 \quad j = 1, 2, \dots, n \quad (1)$$

$$U_r^k \geq 0 \quad V_i^k \geq 0$$

$$r = 1, 2, \dots, s \quad i = 1, 2, \dots, m$$

The weights are all positive and the ratios are bounded by 100%. Each unit k is assigned the highest possible efficiency score by choosing the most optimal weights. If a unit reaches the maximum possible value of 100% it is efficient, otherwise it is inefficient.

The formulation of (1) can be translated into a linear program, which can be solved relatively easily, and a complete DEA solves n linear programs, one for each unit.

$$\begin{aligned}
 & \text{maximize } h_k = \sum_{r=1}^s U_r Y_{rk} \\
 & \text{subject to} \\
 & \sum_{i=1}^m V_i X_{ik} = 1 \\
 & \sum_{r=1}^s U_{rj} Y_{rj} - \sum_{i=1}^m V_{ij} X_{ij} \leq 0 \quad j=1,2,\dots,n \\
 & U_r \geq \varepsilon \quad r=1,2,\dots,s \\
 & V_i \geq \varepsilon \quad i=1,2,\dots,m
 \end{aligned} \tag{2}$$

Where ε is defined as an infinitesimal constant (a non-Archimedean quantity). According to the model, h_k denotes the TSE efficiency for DMUK . If $h_k = 1$ DMUK is defined efficient and if $h_k < 1$ then DMUK is not efficient.

The dual to (2) is:

$$\begin{aligned}
 & \text{minimize } \theta_k - \varepsilon \left(\sum_{r=1}^s S_{rk}^+ + \sum_{i=1}^m S_{ik}^- \right) \\
 & \text{subject to} \\
 & \sum_{j=1}^n X_{ij} \lambda_j + S_{ik}^- = \theta X_{ik} \quad i=1,2,\dots,m \\
 & \sum_{j=1}^n Y_{rj} \lambda_j - S_{rk}^+ = Y_{rk} \quad r=1,2,\dots,s \\
 & \lambda_j \geq 0 \quad j=1,2,\dots,n \\
 & S_{rk}^+, S_{ik}^- \geq 0 \quad r=1,2,\dots,s, \quad i=1,2,\dots,m
 \end{aligned} \tag{3}$$

The BCC model (Banker et. al. [3]) computes Technical Efficiency (TE) with increasing return to scale. It can be defined by adding the constraint $\sum_{j=1}^n \lambda_j = 1$.

2.2. RANKING METHODS

Ranking is a well established approach in social science (see Young and Hammer [25]), historically much more established than the dichotomic classification of DEA to efficient and inefficient organizational units (see Adler et al. [1]). Also, economics applied the classical measurement of efficiency which rank-scales economic units. Rank scaling in the DEA context has become well established in the last decade. Sexton [14] was the first to introduce full rank scaling of organizational units in the DEA context, by utilizing the Cross-Efficiency Matrix. Anderson and Peterson [2] developed the super efficiency approach for rank-scaling that was followed by other researchers. The ranking in relation to rank-scaling has the advantage that it can be tested statistically by a nonparametric analysis. (See for example Friedman and Sinuany-Stern [10],[11] Sinuany-Stern and Friedman [17] and Sueyoshi and Aoki [22]). Practical examples are given by: (1) In general it is common to rank universities, because this type of information is very important in academia. Doyle and Green [8] rank-scaled 20 universities in the UK; (2) Sinuany-Stern et al [16] rank scaled 22 academic departments in a university; (3) Friedman and Sinuany-Stern [10] rank-scaled industrial branches in Israel; (4) Sinuany-Stern and Friedman [18] rank scaled towns in Israel; (5) Sueyoshi and Kirihara [21] uses linear discriminant analysis for classification of Japanese Banking Institutes, they extended the method in 2001 [22]; (6) Sueyoshi [20], where he ranked Japanese agriculture cooperatives Note that every year the National Statistical Bureau in Israel publishes in the media the ranking of towns in Israel.

In summary, decision-makers often prefer a full ranking of the organizational units rather than a dichotomic classification, because the average manager is not familiar with the DEA or the super-efficiency analysis. Thus the actual super-efficiency score does not mean much to them. However, stating the rank of each unit is common knowledge to all of them, and can be very helpful in marketing the DEA.

But it does not replace the other by-product of DEA, such as, improvement needed in each input-output for each unit, bench marking and the Pareto frontier analysis (see, for example, Sinuany-Stern et al, [16]).

3. Super efficiency ranking

Anderson and Peterson (A&P) [2] view the DEA score for the inefficient units as their rank scale. In order to rank scale the efficient units they suggest to allow the efficient units to receive a score greater than 1 by dropping the constraint that bounds the score of the evaluated unit k; namely the primal problem of A&P of unit k will be formulated as follows:

$$\begin{aligned}
 h'_{kk} &= \text{Max} \sum_{r=1}^s u_{rk} y_{rk} \\
 \text{subject to} \\
 \sum_{r=1}^s u_{rk} y_{rj} - \sum_{i=1}^m v_{ik} x_{ij} &\leq 0 \quad \text{for } j = 1, \dots, n, \quad j \neq k \\
 \sum_{i=1}^m v_{ik} x_{ik} &= 1 \\
 u_r &\geq \epsilon \quad \text{for } r=1, \dots, s \\
 v_i &\geq \epsilon \quad \text{for } i=1, \dots, m
 \end{aligned} \tag{4}$$

where x_{ij} is input i of unit j , there are m inputs and n units; y_{ij} is output r of unit j , there are s outputs; u_{rk} is the ideal weight assigned to output r of unit k ; v_{ik} is the ideal weight assigned to input i of unit k ; $\epsilon > 0$ is a non-Archimedean infinitesimal; and h'_{kk} is the A&P score of unit k .

The dual problem, as stated by Anderson and Peterson [2] is given below:

$$\begin{aligned}
 \text{Min } E_k - \epsilon \left(\sum_{i=1}^m s_i^- + \sum_{r=1}^s s_r^+ \right) \\
 \text{subject to} \\
 E_k x_k = \sum_{\substack{j=1 \\ j \neq k}}^n \lambda_j x_{ij} + s_i^- \quad i = 1, \dots, m ; \\
 y_k = \sum_{\substack{j=1 \\ j \neq k}}^n \lambda_j y_{rj} - s_r^+ \quad r = 1, \dots, s ; \\
 \lambda_j, \quad s^+, \quad s^- \geq 0.
 \end{aligned} \tag{5}$$

The basic idea is to compare the unit under evaluation (k) with a linear combination of all other units in the sample, i.e. the unit itself is excluded. Intuitively, this means that unit k is removed from the frontier and h'_{kk} measures its distance from the new frontier.

4. Super efficiency multistage ranking

As shown above, Anderson & Peterson [2] rank all the efficient units by a score greater than 1 and the inefficient units by the DEA score. In this section, we suggest a new ranking model, G/DEA. This model is multistage, it ranks the inefficient units in a procedure similar to the super efficiency A&P. In the first stage we rank the efficient units using A&P procedure. In the next stage we repeat the A&P procedure only for the inefficient units of the previous stage (not including the efficient units of the previous stage). We continue the ranks so that the rank of the most efficient unit in the current stage is less than the rank of the least efficient unit of the previous stage (by one). Obviously, always in the last stage we remain with the least efficient group who are all as “bad” in comparison to previous sets but are as “good” in comparison to each other to the extent that they all are “efficient” when compared to its other. As shown in Figure 1, the new ranking algorithm follows here:

Step 0: Initialization

Set $J = \{\text{all } n \text{ units}\}$

Set $I = 0$

Step 1: A&P Run

Run A&P primal model for set J .

Step 2: Ranking

Let J^* be the set of n^* "efficient" units found in step 1.

Rank the units in set J^* so that the maximal A&P score h'_{kk} receives the rank $I+1$, the

second maximal $I+2$, etc., the last one receives the rank $I+n^*$, set $I = I + n^*$.

Set $J = J - J^*$, the set of inefficient units from step 1.

Step 3: Termination

If $J \neq \emptyset$ then we repeat the process. Go to step 1.

If $J = \emptyset$ we stop.

In the second stage of our G/DEA procedure as described above, we obtain a new set of "efficient" units which is the second best set after we delete the original set of efficient units. In every stage all the sets of efficient units from the previous stages are deleted.

Note that in our G/DEA the ranks of each stage are lower than the next stage. However, the ranks in our G/DEA procedure may differ from the ranks received by A&P. In the first stage the ranks of our G/DEA ranking are identical to A&P ranking.

Since that the process terminates in the last stage when all the remaining units become efficient. Obviously, when the number of variables (inputs plus outputs) is large in relation to the sample size, the number of stages is expected to be smaller.

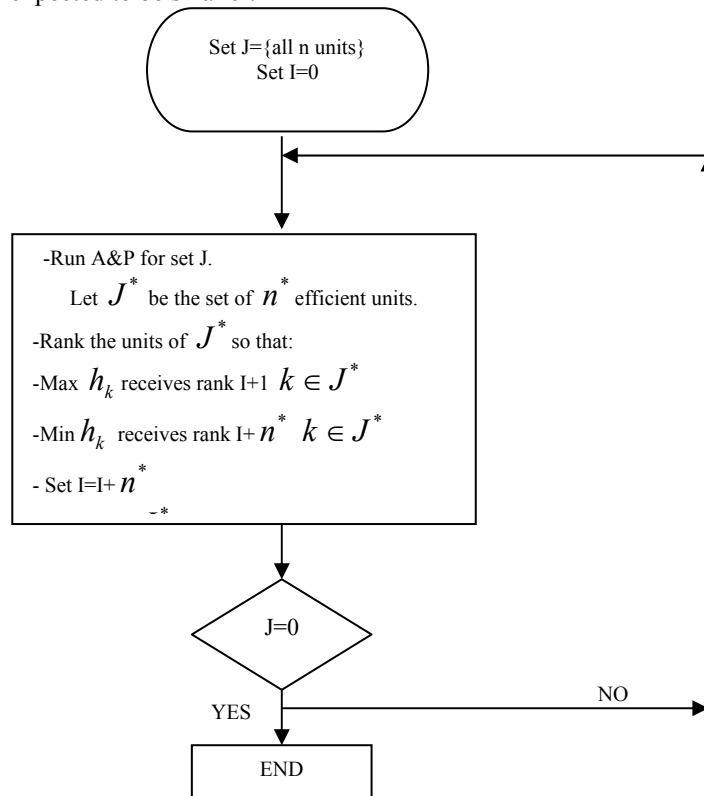


Figure 1. G/DEA Ranking Procedure

5. Example

In order to demonstrate the new ranking method G/DEA we used Sueyoshi's [19] example of 35 cities in China. He used 3 inputs and 3 outputs.

The input are:

X₁ Industrial labor force.

X₂ Working fund.

X₃ Investment.

The outputs are:

Y₁ Gross industrial output value.

Y₂ Profit and taxes.

Y₃ Retail sales.

Table 1 presents the rank of the G/DEA procedure; 5 stages were needed in order to rank all the 35 cities.

TABLE 1 . Scores and ranking of the chine cities

Stage	DMU	SCORE					RANKING				
		G/DEA	A&P	DR/DEA	CE/DEA	MAV.	G/DEA	A&P	DR/DEA	CE/DEA	AVE.
1	Lhasa	4.449	4.449	1.613	0.708	0.430	1	1	1	10	2.5
	Nanning	1.977	1.977	1.573	0.833	0.208	2	2	2	4	1
	Zhuhai	1.614	1.614	0.971	0.479	1.156	3	3	5	29	6
	Shanghai	1.480	1.480	0.995	0.962	0.040	4	4	4	1	2.5
	Nanchang	1.204	1.204	0.437	0.794	0.269	5	5	29	7	8
	Ningbo	1.183	1.183	1.006	0.946	0.059	6	6	3	2	4
	hangzhou	1.022	1.022	0.703	0.880	0.140	7	7	10	3	5
2	Shenzhen	4.760	0.951	0.802	0.401	1.509	8	8	6	32	14
	Changsha	1.258	0.755	0.576	0.648	0.171	9	20	19	16	17
	Guangzhou	1.198	0.791	0.751	0.682	0.165	10	16	8	13	9
	Wuhan	1.155	0.944	0.597	0.794	0.201	11	9	16	6	7
	Tianjin	1.151	0.756	0.674	0.676	0.212	12	13	11	14	11
	Beijing	1.127	0.731	0.767	0.636	0.155	13	22	7	19	15
	Shijiazhuang	1.126	0.944	0.555	0.795	0.199	14	10	22	5	12.5
	Changchun	1.084	0.872	0.609	0.731	0.199	15	12	15	9	12.5
	Jinan	1.068	0.907	0.622	0.773	0.182	16	11	14	8	10
	Xiamen	1.011	0.717	0.748	0.452	0.614	17	24	9	30	20
3	Fuzhou	1.535	0.561	0.524	0.506	0.112	18	31	23	28	26.5
	Nanjing	1.130	0.706	0.654	0.630	0.125	19	25	12	21	19
	Lanzhou	1.119	0.756	0.509	0.647	0.176	20	19	26	17	21
	Zhengzhou	1.111	0.808	0.593	0.693	0.176	21	14	17	11	16
	Dalian	1.070	0.673	0.641	0.618	0.091	22	27	13	23	23
	Hefei	1.033	0.794	0.567	0.689	0.158	23	15	20	12	18
	Shenyang	1.025	0.774	0.441	0.663	0.177	24	17	28	15	22
	Harbin	1.021	0.764	0.387	0.625	0.243	25	18	31	22	26.5
	Chengdu	1.001	0.727	0.495	0.637	0.145	26	23	27	18	24
4	Yinchuan	1.234	0.453	0.398	0.346	0.322	27	35	30	35	32.5
	hohot	1.149	0.571	0.511	0.511	0.121	28	30	25	27	30
	kunming	1.141	0.651	0.586	0.591	0.106	29	28	18	25	28
	Chongqing	1.128	0.747	0.512	0.631	0.189	30	21	24	20	25
	Guiyang	1.028	0.591	0.559	0.523	0.134	31	29	21	26	29
	Xian	1.009	0.697	0.359	0.593	0.188	32	26	33	24	31
5	Xining	1.694	0.471	0.311	0.394	0.206	33	34	35	33	35
	Taiyuan	1.530	0.516	0.331	0.450	0.182	34	32	34	31	32.5
	Urumqi	1.341	0.478	0.386	0.374	0.305	35	33	32	34	34

The G/DEA ranking is similar to the A&P ranking, but not identical. For example, Jinan was ranked 11 by A&P but 16 by G/DEA. Another example is Changsha, which received rank 20 by A&P and 9 by G/DEA. The Spearman rank correlation between the A&P ranks and G/DEA ranks in our example was highly significant (0.861).

Table 2 summarizes the five stages of G/DEA. Although the DEA rank scaling is not completely compatible with G/DEA, the average DEA score reduces monotonically over the stages. Using the a-

Applied statistics

parametric one-way Analysis of Variance for all the five stages (the Kruskal-Wallis Test), it was found that all the five stages are significantly different with p-value less than 0.0001. Applying this a-parametric test again on the four groups it was found that all four groups are significantly different from each other, with p-value of 0.001.

TABLE 2. Statistics of each stage

STAGE	Number of ranked DMUs	DEA score	
		AVERAGE	STD
1	7	1	0
2	10	0.8368	0.0961
3	9	0.7292	0.0761
4	6	0.6183	0.1041
5	3	0.4883	0.0242

6. Comparison to other ranking methods

In the previous section we compared the G/DEA and A&P rankings. In this section, we extend the comparison to two additional ranking methods from the DEA literature.

1. The CE/DEA - Cross Efficiency ranking method (see Sexton, [14]).
2. The DR/DEA - discriminant analysis of ratio (see Sinuany-Stern and Friedman, [14]).

CE/DEA cross evaluates each unit using the optimal weights of other units, an overall score is derived from the average evaluation, as follows:

$$\bar{h}_k = \sum_{j=1}^n h_{kj} / n \quad \text{where } h_{kj} = \frac{\sum_{r=1}^s u_{rj} y_{rk}}{\sum_{i=1}^m v_{ij} x_{ik}} .$$

The advantage of CE/DEA is that the extreme weights problem is avoided by the cross evaluation procedure. Moreover, all units are evaluated by the same sets of weights, thus they are comparable.

DR/DEA is based on a set of common weights (to all the units) which are derived by maximizing the ratio between: the “between group variance” and the “within group variance” of T, the ratio between the composite output and composite input. The groups are given by the DEA dichotomic classification of efficient and inefficient units. This is not the traditional discriminant analysis, it is a ratio discriminant analysis (see Appendix for technical details). There is no closed form solution for the common weights, they are solved by a non linear search optimization. The advantage of this method is that all the units are ranked scaled with one set of common weights. Moreover, this method utilizes the DEA classification.

In Table 1 the results for all the scores and ranking methods are applied to the example we used in the previous section. Most of the ranks seem compatible. However, we identified two extreme cities, Shenzhen and Zhuhai, where a huge difference is observed between CE/DEA ranking and all the other ranking methods. Zhuhai, for example, is ranked 29 by CE/DEA and between 3–4 by the other methods, Shenzhen is ranked 32 by CE/DEA and between 6–8 by the other methods. This phenomenon happens due to the large variability of the weights. Sueyoshi [19] also highlights these units, he used various constraints on the weights (the Assurance Region), which reduced Zhuhai from efficiency 1 to 0.624 and reduced Shenzhen from 0.963 to 0.481. Similarly, according to CE/DEA, Zhuhai evaluation is 0.479, although it was DEA efficient, and Shenzhen CE/DEA evaluation is 0.401.

Wilson [24] claims that A&P is useful only for identifying outliers, namely those units that receive the highest A&P score (which is vastly more than 1). Doyle and Green [8] suggest the Maverick index for detecting outliers. In the Maverick index, M_k , the units enjoy that greatest relative increment when shifting from peer appraisal to self appraisal:

$$M_k = \left(h_{kk} - \sum_{j \neq k} h_{kj} / (n-1) \right) / \left(\sum_{j \neq k} h_{kj} / (n-1) \right) .$$

Applied statistics

According to the Maverick index that appears in Table 1, Zhuhai is an outlier (it has the highest Maverick index among the efficient units), which means that Zhuhai self-evaluation was much higher than the average evaluation given to it by other cities. However, according to Wilson [24], Zhuhai was not an outlier, Lhasa was the outlier (see Table 1). (Note that Sueyoshi [19] found that for two sets of weights Lhasa receives 100% efficiency, and for other two sets of weights Lhasa receives 20.85% efficiency). Thus, we can conclude that A&P does not necessarily identify outliers. Moreover, Shenzhen which, according to Wilson, is not an outlier (since it is inefficient), and happens to have the maximal Maverick index. This may explain the discrepancy between the ranking of CE and the other methods. Note that Charnes et al. [6] did not include Zhuhai, Lhasa and Shenzhen in their analysis!

Table 3 summarizes the Spearman Coefficients of correlation between the ranks of all pairs of ranking methods. All correlations were very significant (p -value < 0.01). In relation to the average rankings both G/DEA and A&P received the maximal correlation (0.94).

TABLE 3. Correlations of ranking methods

	G/DEA	A&P	DR/DEA	CE/DEA
G/DEA		0.861	0.769	0.632
A&P			0.660	0.796
DR/DEA				0.453
AVERAGE	0.942	0.938	0.806	0.797

6. Summary and conclusions

In this paper, we present a new ranking method, G/DEA. This multistage method is based on the A&P ranking. In the first stage G/DEA rank scales the efficient units in the same way as A&P. In the next stage the efficient set is deleted and the A&P method is applied again. Basically, also the inefficient units are rank scaled in a similar process while in A&P they receive the DEA score.

Identifying outliers is analysed here by the Maverick index which is compared to A&P extreme values. We can conclude that the A&P score for the efficient units is not enough to identify outliers.

The problem of possible unfeasibility of the A&P values is resolved by Mehrabian [12]. Moreover, in order to limit the super efficiency score to a scale with a maximum of 2, Sueyoshi [20] developed an Adjusted Index Number to resolve the problem.

Although there are many ranking methods in the DEA context (see Adler et al. [1]), we chose three ranking methods representing the range of ranking methods in the DEA context: first Anderson and Peterson [2] ranking which is the basis for our new ranking method G/DEA. The second is CE/DEA which is the first ranking method in the DEA context (see Sexton [14]) based on all the weights of all the units mutually. The third ranking method is DR/DEA based on multivariate statistical analysis providing common weights for all the units (see Sinuany-Stern and Friedman, [17]).

We show in our example that there are differences between A&P and G/DEA ranking. Both A&P and G/DEA ranking methods suffer from the use of weights which vary from unit to unit. Consequently, we compared them to two other ranking methods which are based on the same sets of weights, CE/DEA and DR/DEA and the average of all the methods.

All four ranking methods were highly correlated in our example. As expected, the average of all the methods is best correlated with each method; which indicates that combining several ranking methods should be considered in practice (see Friedman and Sinuany-Stern[17]).

Acknowledgment

This paper was partially supported by the Paul Ivanier Center for Robotics and Production Management, Ben-Gurion University of the Negev.

References

- [1] Adler, N., L. Friedman and Z. Sinuany-Stern. (2002) Review of Ranking Methods in the DEA Context. *European Journal of Operational Research* **140**, 249–265.
- [2] Anderson, P. and Peterson, N.C. (1993) A procedure for ranking efficient units in Data Envelopment Analysis. *Management Sciences* **39** (10), 1261–1264.

- [3] Banker, R.D., A. Charnes, and Cooper W.W. (1984) Some Models for Estimating Technical and Scale Inefficiencies in Data Envelop Analysis. *Management Science* **30**, 1078-1092
- [4] Banker, R.D. and Chang H. (1995) A Simulation Study of Hypothesis Tests for Differences in Efficiencies. *International Journal Production Economist* **39**, 37-54.
- [5] Belton, V. and Stewart, T.J. (1999) DEA and MCDA: competing or complementary approaches In: Meskens, N., Roubens, M. (Eds.), *Advances in Decision Analysis*. Kluwer Academic Publications Norwell.
- [6] Charnes, A. and Cooper, W.W (1989) Using DEA to evaluate efficiency in the economic performance of Chinese cities. *Socio-Econ. Plann. Sci.* **23**, 325-344.
- [7] Cooper, W.W. and Tone, K. (1997) Measures of inefficiency in DEA and stochastic frontier estimation. *European Journal of Operational Research*, **99** 72–88.
- [8] Doyle, J.R. and Green, R.H. (1994) Efficiency and cross-efficiency in DEA: derivatives meaning and uses. *Journal of Operational Research Society* **45** (5), 567–578.
- [9] Green, R.H. and Doyle, J.R. (1995) On maximizing discrimination in multiple criteria decision making. *Journal of Operation Research Society* **46** (2), 192–204.
- [10] Friedman, L. and Sinuany-Stern, Z. (1998) Combining ranking scales and selecting variables in the data envelopment analysis context: The case of industrial branches. *Computers and Operations Research* **25** (9), 781–791.
- [11] Friedman L. and Sinuany-Stern Z. (1997) Scaling units via the canonical correlation analysis in the DEA context, *European Journal of Operational Research* **100** (3), 629-637.
- [12] Mehrabian, S., Alirezaee, M.R. and Jahanshohloo G.R. (1999) A complete efficiency ranking of decision making units in Data Envelopment Analysis. *Computational Optimization and Applications* **14**, 261–266.
- [13] Seiford, L.M.. (1996) ‘The evolution of the state-of-art (1978-1995)’, *Journal of Productivity Analysis* **7**, 99-137.
- [14] Sexton, T.R., (1986) The methodology of DEA. In *Measuring Efficiency: An Assessment of DEA*. Ed. R.H. Silkman. San Francisco: Jossey-Bass, 7–29.
- [15] Sexton, T. R., Sleeper, S. and Taggart, R. E. Jr. (1994) Improving pupil transportation in North Carolina”, *Interfaces*, Jan/Feb 24 (1), 87-104.
- [16] Sinuany-Stern, Z., Mehrez, A. and Barboy, A. (1994) Academic departments efficiency via DEA. *Computer and O.R.* **21** (5), 543–556.
- [17] Sinuany-Stern, Z. and Friedman L. (1998) DEA and the discriminant analysis of ratios for ranking units. *European Journal of Operations Research* **111**, 470–478.
- [18] Sinuany-Stern, Z., and Friedman, L. (1998b) Rank Scaling in the DEA Context:. *Studies in Regional & Urban Planning* **6**, 135–140.
- [19] Sueyoshi, T. (1992) Measuring the industrial performance of Chinese cities by DEA. *Socio-Econ. Plan. Sci.* **26** (2), 75-88.
- [20] Sueyoshi, T. (1999) DEA non-parametric ranking test and index measurement: Slack-adjusted DEA and an application to Japanese agriculture cooperatives. *Omega* **27**, 315–326.
- [21] Sueyoshi, T. and Kirihara A. (1998) Efficiency measurement and strategic classification of Japanese Banking Institutes. *International Journal of Systems Science* **29** , 1249-1263
- [22] Sueyoshi, T., Aoki L. (2001) A use of nonparametric statistic for DEA frontier shift: the Kruskal and Wallis rank test, *Omega* **29**, 1-18.
- [23] Warwick Windows DEA Version 1.02, 1998. Warwick Business School, England.
- [24] Wilson, P.W., 1995. Protecting influential observations in Data Envelopment Analysis. *Journal of Productivity Analysis* **4**, 27–45.
- [25] Young, F. and Hammer, R. M. (1987) *Multidimensional scaling. Theory and application*, London: Lawrence Erlbaum Associates Publishers.

APPENDIX

Discriminant Analysis of Ratios for Ranking

Sinuany-Stern and Friedman [18] developed a technique in which discriminant analysis of ratios was applied to DEA (DR/DEA). Instead of considering a linear combination of the inputs and outputs in one equation (as in the traditional discriminant analysis of the two groups), they constructed a ratio

Applied statistics

function between a linear combination of the inputs and a linear combination of the outputs. In some ways this ratio function is similar to the DEA efficiency ratio, however whilst DEA provides weights for the inputs and outputs, which vary from unit to unit, DR/DEA provides common weights for all units. In principle, DR/DEA determines the weights such that the ratio score function discriminates optimally between two groups of observations (DMUs) on a one-dimensional scale (in our case, efficient and inefficient units predetermined by DEA). The ratio, T_j , and the arithmetic means of the ratio scores of the efficient and inefficient groups are:

$$T_j = \frac{\sum_{r=1}^s u_r Y_{rj}}{\sum_{i=1}^m v_i X_{ij}}, \quad j=1, \dots, n \quad \bar{T}_1 = \sum_{j=1}^{n_1} \frac{T_j}{n_1} \quad \text{and} \quad \bar{T}_2 = \sum_{j=n+1}^n \frac{T_j}{n_2},$$

where n_1 and n_2 are the number of efficient and inefficient units in the DEA model respectively. The weighted mean of the entire n units ($n=n_1+n_2$) will be denoted by $\bar{T} = \frac{n_1 \bar{T}_1 + n_2 \bar{T}_2}{n}$.

Our problem is to find the common weights v_i and u_r such that the ratio of the between-group variance of T , ($SS_B(T)$) and the within group variance of T , ($SS_W(T)$) will be maximized, as shown in model as follows

$$\max_{\substack{u, v \\ r, i}} \lambda = \max_{\substack{u, v \\ r, i}} \frac{SS_B(T)}{SS_W(T)},$$

$$SS_B(T) = n_1(\bar{T}_1 - \bar{T})^2 + n_2(\bar{T}_2 - \bar{T})^2 = \frac{n_1 n_2}{n_1 + n_2} (\bar{T}_1 - \bar{T}_2)^2$$

$$SS_W(T) = \sum_{j=1}^{n_1} (T_j - \bar{T}_1)^2 + \sum_{j=n+1}^n (T_j - \bar{T}_2)^2$$

DR/DEA constructs the efficiency score for each unit j as T_j , the ratio between the composite output and composite input. Thus it rank scales the DMUs so that the unit with the highest score receives rank 1 and the unit with the lowest score ranks n . If any weight is negative then non-negativity constraints ought to be added to the optimization problem. To solve this problem, they used a non-linear search optimization algorithm, however there is no guarantee that the solution found is globally optimal.

Received on the 20th of December 2002

DECISION-MAKING SIMULATION MODEL FOR CONTROLLING SEVERAL STOCHASTIC PROJECTS

Z. LASLO^a, D. GOLENKO-GINZBURG^{b,c}, A. GONIK^c, A. MALISHEVA^c

^a *Department of Industrial Engineering and Management, Negev Academic College of Engineering, Beer-Sheva, 84100, Israel, E-Mail: zohar@nace.ac.il*

^b *Department of Industrial Engineering and Management Academic College of Judea and Samaria, Ariel, 44837, Israel*

^c *Department of Industrial Engineering and Management, Ben-Gurion University of the Negev, Beer-Sheva, 84105, Israel*

Several simultaneously realized projects under random disturbances are considered. Each project has a high level of indeterminacy and consists of a chain of operations to be processed in a definite sequence. For each operation, its duration is a random variable with given density function. Each operation utilizes several non-consumable related resources with fixed capacities, e.g. manpower (engineers) of different specialties. Each project has its due date, together with the chance constraint to meet the deadline. Processing costs to utilize all resources per time unit and per resource unit (separately for each type of resources) are pre-given as well. All resources participate in the system beginning from the first project's starting moment and until the last project is actually completed. For each type of resources its total limit remains unchanged throughout the projects' duration. The problem is to determine the optimal total capacities of each resource at the management's disposal in order for each project to meet its due date on time subject to the chance constraint. The objective is to minimize the total expenses of hiring and maintaining resources. A heuristic search algorithm in combination with a simulation model based on the minimax principle is suggested. A decision rule to reallocate free available resources among the operations is embedded in the simulation model.

Key words: Resource reallocation, simulation model, minimax decision rule, chance constraint, coordinate descent search method.

1. Introduction

There is no lack of publications in the area of controlling several projects in a design office (see, e.g. Butera and Thurman [1984], Hajek [1984], Gonik [2000], etc.). At the initial stage of any complicated project with no similar prototype in the part, the model may be restricted to a source and a sink nodes connected by a chain of several intermediate consecutive operations of random duration. Thus, at the initial stage, a detailed *network* model does not exist.

We are considered with several simultaneously realized preliminarily projects (PP) consisting of a chain of operations to be processed in a definite technological sequence. Each project's operation utilizes qualified manpower of various specialties, i.e., several non-consumable resources, with fixed capacities. Each type of resource at the management's disposal is in limited supply, with a resource limit that remains unchanged at the same level throughout the projects' duration, i.e., until the last project is actually completed. Thus, due to the limited resource levels, projects' operations may have to wait in lines for resource supply, in order to start functioning. Since for each operation its duration is a random variable with given density function, a deterministic schedule of the moment's operations actually start cannot be determined.

The general problem is to determine:

- Optimal *deterministic* total resource capacities for each type of resource at the management's disposal (beforehand), and
- Random values of the moments operations actually start (in the course of the projects' realization and conditioned on our decisions),

to minimize the average of the total expenses of hiring and utilizing all resources subject to the chance constraints of meeting the projects' due dates on time.

The problem is solved via a heuristic algorithm by a combination of the cyclic coordinate descent method (at the upper level) and a simulation model (at the lower level). Resource reallocation between the projects waiting in lines is carried out via decision rule based on a minimax principle. The latter enables support to "weaker" projects from the "stronger" ones in the course of the projects' realization.

2. Notation

Let us introduce the following terms:

- n - number of projects of preliminarily type PP_i , $1 \leq i \leq n$, to be realized simultaneously in a design office;
- O_{ic} - the c -th operation of the i -th project in the form of a consecutive chain, $1 \leq c \leq m_i$;
- m_i - number of operations in project PP_i ;
- t_{ic} - random duration of operation O_{ic} (a random value);
- \bar{t}_{ic} - average value of t_{ic} (pregiven);
- V_{ic} - variance of t_{ic} (pregiven);
- R_k - the total capacity of the k -th type of resources, $1 \leq k \leq d$, at the disposal of the design office (a deterministic value to be optimized);
- d - number of resources;
- r_{ick} - the k -th resource capacity to be assigned to operation O_{ic} (pregiven);
- D_i - the due date for project PP_i (pregiven);
- p_i^* - chance constraint to meet the due date D_i on time (pregiven);
- S_{ic} - the moment operation O_{ic} actually starts (a random value, to be determined by the simulation model via a decision rule in the course of realizing the projects);
- F_{ic} - the moment operation O_{ic} terminates (a random value);
- F_i - the moment project PP_i terminates, $F_i = S_{im_i} + t_{im_i}$ (a random value);
- F - the moment the last project terminates, $F = \text{Max}_i F_i$;
- $p_i \{R_k, D\}$ - actual probability of meeting D_i on time on condition that R_k total resource capacities, $1 \leq k \leq d$, are hired by the design office;
- $W_k \{S_{ic}, t\}$ - the summarized capacity of the k -th resource assigned to operations at moment t , on condition that operations O_{ic} start at moments S_{ic} , $1 \leq k \leq d$;
- $R_k(t) = R_k - W_k(S_{ic}, t)$ - free available resources of k -th type at moment t ;
- S_k - the cost of hiring, maintaining and utilizing the k -th resource unit at the time unit, $1 \leq k \leq d$ (pregiven, a constant value);
- ΔR_k - the positive search step value to optimize variable R_k , $1 \leq k \leq d$ (pregiven);
- ε - the relative accuracy value to obtain an optimal solution (pregiven);
- $R_{k \text{ mi}}$ - the minimal possible level for the total capacity R_k , $1 \leq k \leq d$ (pregiven);
- $R_{k \text{ ma}}$ - the maximal possible level for value R_k , $1 \leq k \leq d$ (pregiven);

Q - the system's total resource expenses.

Note that relations

$$R_{k \text{ min}} \geq \text{Max}_i \text{Max}_c r_{ick}, \quad (1)$$

$$R_{k \text{ max}} \leq \sum_i \left\{ \text{Max}_{1 \leq c \leq m_i} r_{ick} \right\}, \quad (2)$$

$$R_{k \text{ min}} \leq R_k \leq R_{k \text{ max}}, \quad 1 \leq i \leq n, \quad 1 \leq c \leq m_i, \quad 1 \leq k \leq d, \quad (3)$$

hold.

Restriction (1) is evident since otherwise some of the projects cannot be realized at all. If (2) does not hold a certain part of resources will not participate in the projects' realization.

3. The problem formulation

The general problem is to determine both optimal *deterministic* values R_k , $1 \leq k \leq d$, (before the projects' realization) and *random* values S_{ic} (in the course of the projects' realization and conditioned on our decisions), $1 \leq i \leq n$, $1 \leq c \leq m_i$, to minimize the average of the total resource expenses

$$\left\{ \underset{\{R_k, S_{ic}\}}{\text{Min}} E \left\{ \sum_{k=1}^d S_k R_k \cdot \left[\underset{i}{\text{Max}} F_i - \underset{i}{\text{Min}} S_{il} \right] \right\} \right\} \quad (4)$$

subject to (3) and

$$W_k \{S_{ic}, t\} \leq R_k \quad \forall t : t \geq \underset{i}{\text{Min}} S_{il}, \quad (5)$$

$$p_i \{R_k, D_i\} \geq p_i^*, \quad 1 \leq i \leq n, \quad 1 \leq k \leq d, \quad 1 \leq c \leq m_i. \quad (6)$$

Note that problem (3-6) is a very complicated stochastic optimization problem which does not provide an analytical solution. We suggest solving the problem by using a two-level heuristic algorithm. The latter comprises a simulation model and a subalgorithm to carry out the coordinate descent optimization method.

Note, in conclusion, that to simplify the problem, we will henceforth assume that $\underset{i}{\text{Min}} S_{il} = 0$ holds.

4. Simulation model

The input data of the simulation model is the vector of total resource capacities $\overset{1}{R}_k$, $1 \leq k \leq d$, which is determined in the course of the coordinate descent algorithm's work. Thus, in the course of a routine simulation run vector $\{R_k\}$ is fixed and remains unchanged. It goes without saying that vector $\overset{1}{R}_k$ satisfies (1-3).

The main task of the simulation model is to determine (in the course of a simulation run) random starting moments S_{ic} of all operations O_{ic} , $1 \leq i \leq n$, $1 \leq c \leq m_i$, entering the projects, with respect to a minimax objective

$$I = \underset{\{S_{ic}\}}{\text{Max}} \underset{i}{\text{Min}} \left[\frac{p_i \{ \overset{r}{R}_k, D_i \} - p_i^*}{p_i^*} \right] \quad (7)$$

and subject to (5). Value $p_i \{ \overset{1}{R}_k, D_i \}$ can be evaluated by means of undertaking numerous simulation runs in order to obtain representative statistics and, later on, calculating frequencies for the probability value $\text{Pr}\{F_i \leq D_i\}$. As to the minimax objective, it is imbedded in the outlined below decision rule to reallocate restricted resources among projects ready to be operated and waiting in lines.

A routine simulation run starts functioning at $t=0$ and terminates with the completion of the last project. The simulation model comprises three submodels as follows:

Submodel I actually governs most of the procedures to be undertaken in the course of the projects' realization, namely:

- determines essential moments (decision points) when projects may be supplied with free available resources. A routine essential moment usually coincides either with the moment an operation is finished and additional resources become available, or when a subset of new operations O_{ic} becomes ready to be processed;
- singles out (at a routine decision point) all the operations that are ready to be processed;
- checks the possibility of supplying these operations with available resources without undertaking a competition;
- supplies the chosen operations O_{ic} with resources and later on simulates the corresponding durations t_{ic} ;
- returns the utilized non-consumable resources to the design office store (at the moment an operation is finished);
- updates the remaining projects at each routine decision point;
- determines the completion moment for each projects,

together with several other, less important, procedures.

Submodel II calculates auxiliary decision rule values in case when there is a lack of available resources and not all the operations ready to be processed and waiting in line for resources at a routine decision point t , can start to be realized. Assume that at moment t q operations $O_{i_1c_1}, O_{i_2c_2}, \dots, O_{i_qc_q}$ are

ready to be processed and at least for one type k of resources, relation $\sum_{v=1}^q r_{i_v c_v k} > R_k(t)$ holds. For each

PP_{i_v} waiting in line, Submodel II calculates value

$$\Pr\{F_{i_v} \leq D_{i_v}\} = \Phi \left\{ \frac{D_{i_v} - t - \sum_{r=c_v}^{m_{i_v}} t_{i_v r}}{\sqrt{\sum_{r=c_v}^{m_{i_v}} V_{i_v c_v}}} \right\}, \quad 1 \leq v \leq q, \quad (8)$$

where

$$\Phi(x) = \frac{1}{\sqrt{2\pi}} \int_{-\infty}^x e^{-\frac{z^2}{2}} dz. \quad (9)$$

Thus, value (8) is an approximate probability estimate for project PP_{i_v} to meet its target on time on condition that the project will obtain needed resources at moment t and will not wait in lines henceforth. Such an assumption has been successfully used for many control problems in project management and manufacturing systems [5-7].

After determining the values of deviation from the target by

$$\gamma_{i_v} = \frac{\Pr\{F_{i_v} < D_{i_v}\} - p_{i_v}^*}{p_{i_v}^*}, \quad 1 \leq v \leq q, \quad (10)$$

we sort the latter in ascending order. Denote the newly reordered operations

$$O_{j_1 f_1}, O_{j_2 f_2}, \dots, O_{j_q f_q}, \gamma_{j_\xi f_\xi} < \gamma_{j_{\xi+1} f_{\xi+1}}, \quad 1 \leq \xi \leq q-1. \quad (11)$$

It can be well-recognized that the less value γ_{i_v} is the more urgent becomes the problem of supplying PP_{i_v} with resources as soon as possible. Here we make no difference between project PP_{i_v} and the operation $O_{i_v c_v}$ in the list (11) since only one operation of any project may wait in line for resources at a certain decision moment t . Thus, priority value γ_{i_v} refers both to project PP_{i_v} and to the operation $O_{i_v c_v}$.

Submodel III undertakes reallocation of free available resources $R_k(t)$, $1 \leq k \leq d$, among project PP_{i_v} , $1 \leq v \leq q$. All the sorted operations in the list (11) are examined, one after another, in the ascending order of values γ , to check, for each operation, the possibility that it can be supplied with remaining available resources. If, for a certain operation $O_{j_\xi f_\xi}$, $1 \leq \xi \leq q$, relations $r_{j_\xi f_\xi k} \leq R_k(t)$, $1 \leq k \leq d$, hold, the needed resources $r_{j_\xi f_\xi k}$ are passed to the operation while the remaining resources $R_k(t)$ are updated, $R_k(t) - r_{j_\xi f_\xi k} \Rightarrow R_k(t)$, $1 \leq k \leq d$. Then, the next operation $O_{j_{\xi+1} f_{\xi+1}}$ is examined. If not all relations $r_{j_\xi f_\xi k} \leq R_k(t)$ hold, we proceed straightforward examining the next operation. The procedure terminates either when all the available resources are reallocated among the operations or all the q operations have been examined. The procedure is simple in usage and has been used in various scheduling problems [5-6].

It can be well-recognized that since decision rule (10) is imbedded in decision-making for resource reallocation, the outlined above simulation models honors objective (7).

Note that the general idea of the minimax approach is as follows. In the course of projects' realization the design office takes an urgent care of "weaker" projects which deviate from their trajectories and their chance constraints more than other projects. Those projects have to be supplied with

resources in the first place at the expense of other, “stronger” projects. Thus, the general idea of the minimax objective (7) is to raise the weakest project as much as possible in order to balance all the projects under realization.

5. Cyclic coordinate descent sub-algorithm

As mentioned above, the suggested heuristic algorithm to solve the problem (3-6) comprises two levels. At the lower level the simulation model undertakes numerous simulation runs in order to manage the projects’ realization on the basis of the minimax principle. At the upper level the heuristic search subalgorithm undertakes cyclic coordinate optimization in order to obtain the optimal vector \hat{R}_k . The procedure of the optimization is based on minimizing objective (4) cyclically with respect to coordinate variables R_1, R_2, \dots, R_d . Coordinate R_1 is optimized first, then R_2 , and so forth through R_d . The coordinate descent method is widely known [4] and is very efficient in various optimization problems with complicated, mostly non-linear, objectives [5]. The enlarged step-by-step procedure of the optimizing subalgorithm is as follows:

STEP 1. Determine the initial search point $X^0 = \{R_k^0\}$ by taking deliberately overstating values, e.g. $R_k^0 = R_{k \max}$, $1 \leq k \leq d$. It can be well-recognized that setting $X^0 = \{R_{k \max}\}$ results in

$$p_i \{ \hat{R}_k^0, D_i \} > p_i^*, 1 \leq i \leq n, \quad (12)$$

and, thus, X^0 is a feasible solution. Note that for any initial search point X^0 relation (12) can be checked via simulation, on the basis of numerous simulation runs, by comparing the corresponding statistical frequency rates with pre-given values p_i^* , $1 \leq i \leq n$. If at least for one index i relation (12) does not hold, problem (3-6) has no solution. Otherwise apply the next step.

STEP 2. Fix the initial values $\{R_k\}$, $\hat{R}_k = \hat{X}^0$, and start diminishing value R_1 by ΔR_1 consecutively, i.e., $R_1 - r \cdot \Delta R_1 \Rightarrow R_1$, $r = 1, 2, \dots$, while all other coordinates R_2, R_3, \dots, R_d are fixed and remain unchanged. Each newly determined search point $(R_1 - r \cdot \Delta R_1, R_2, \dots, R_d)$ has to be examined via simulation in order to verify the following statements:

- A Checking a new search point results in decreasing objective (4);
- B Restrictions (6) remain valid.

In order to formalize the procedure of verification via a simulation model, we suggest

- to undertake M simulation runs in order to obtain representative statistics ($M \div 500 - 1000$);
- to modify objective (4) on the basis of M simulation runs as follows:

$$Q^* = \left(\sum_{k=1}^d s_k R_k \right) \cdot \left\{ \frac{1}{M} \sum_{m=1}^M F^{(m)} + \sum_{i=1}^n K_i \cdot \beta \left(\left[\frac{1}{M} \sum_{m=1}^M \alpha (F_i^{(m)} - D_i) \right] - p_i^* \right) \right\}, \quad (13)$$

where

$$\alpha(x) = \begin{cases} 1 & \text{if } x \leq 0 \\ 0 & \text{otherwise} \end{cases}, \quad \beta(x) = \begin{cases} 1 & \text{if } x < 0 \\ 0 & \text{otherwise} \end{cases}$$

$F^{(m)}$ is the moment the last project terminates in the m -th simulation run, $1 \leq m \leq M$,

$F_i^{(m)}$ is the moment the i -th project terminates in the m -th simulation run,

K_i is a very large positive value (usually taken [5] close to 10^{17}) in order to prohibit automatically cases $p_i \left\{ \overset{r}{R}_k, D_i \right\} < p_i^*$ for any $i, 1 \leq i \leq n$.

Thus, verifying the validity of statements A and B independently from each other is substituted by checking the validity of the monotonous decrease of one objective (13). Note that for the sake of simplicity we have taken $\text{Min} S_{i1} = 0$ in (13).

STEP 3. We proceed examining the monotonous decrease of estimate Q^* in the course of diminishing consecutively the first coordinate R_1 , until either:

- 1 The diminished value R_1 reaches its lower bound $R_{1 \min}$, or
- 2 The monotonous decrease of objective (13) ceases to hold for $R_{1 \min} \leq R_1 \leq R_{1 \max}$.

In any case value R_1 which corresponds to the minimal value of Q^* , is fixed, and we start diminishing the second coordinate, R_2 , by step ΔR_2 (with fixed values R_1 (newly obtained), R_3, \dots, R_d). The process proceeds for other coordinates, etc., until the last coordinate, R_d , is examined.

Note that in the course of undertaking a coordinate search each successive search results always in decreasing objective (13). Otherwise, i.e., if a routine search step does not result in decreasing (13), the corresponding routine coordinate R_k is fixed and the next, the $(k+1)$ -th coordinate R_{k+1} , starts to be examined.

STEP 4. Obtaining a new search vector $\left\{ \overset{r}{R}_k \right\}$ in the course of optimizing *all the coordinates separately*, results in realizing the first iteration to determine the quasi-optimal values $\left\{ R_k \right\}$. All search steps ΔR_k have to be diminished (mostly by dividing by two), and we proceed to minimize (13) cyclically with respect to the new coordinate variables, beginning from R_1 .

STEP 5. For all next iterations in the course of the coordinate optimization, a search is realized for each routine coordinate $R_k, 1 \leq k \leq d$, in two opposite directions, namely $R_k - \Delta R_k$ and $R_k + \Delta R_k$, to determine the direction of objective's (13) decline. The direction which results in the highest objective's decrease has to be chosen. The search process proceeds in that direction until the objective's decrease ceases to hold.

STEP 6. After undertaking a routine search iteration $v, v=1,2,\dots$, the objective value (4), Q^v , referring to that iteration, has to be compared with the results of the previous, $(v-1)$ -th iteration, by calculating

$$\Delta^{(v)} = \frac{Q^{(v-1)} - Q^{(v)}}{Q^{(v-1)}}. \quad (14)$$

Thus, at least two iterations have to be undertaken.

STEP 7. If relation $\Delta^{(v)} < \varepsilon$ holds, i.e., if the relative difference between two adjacent iterations $Q^{(v-1)}$ and $Q^{(v)}$ becomes less then the pre-given tolerance $\varepsilon > 0$, the algorithm terminates. Otherwise, step 2 has to be applied.

6. Numerical example

In order to check the fitness of the developed minimax control model experimentation has been undertaken. Three simultaneously realized preliminarily projects are considered. The first project comprises two consecutive operations, while both the second and the third projects comprise three consecutively realized operations. Two types of non-consumable resources participate in the system.

The projects' parameters are as follows:

Applied statistics

PROJECT No. 1

$$\begin{aligned} r_{111} &= 15; & r_{121} &= 17; \\ r_{112} &= 60; & r_{122} &= 51; \\ O_{11} &= U(31, 40); & O_{12} &= U(48, 55). \end{aligned}$$

PROJECT No. 2

$$\begin{aligned} r_{211} &= 15; & r_{221} &= 20; & r_{231} &= 27; \\ r_{212} &= 73; & r_{222} &= 88; & r_{232} &= 85; \\ O_{21} &= U(30, 38); & O_{22} &= U(18, 30); & O_{23} &= U(28, 39). \end{aligned}$$

PROJECT No. 3

$$\begin{aligned} r_{311} &= 20; & r_{321} &= 26; & r_{331} &= 18; \\ r_{312} &= 64; & r_{322} &= 78; & r_{332} &= 80; \\ O_{31} &= U(30, 45); & O_{32} &= U(16, 28); & O_{33} &= U(20, 30). \end{aligned}$$

Other system's parameters are as follows:

$$\begin{aligned} R_{1 \min} &= 27; & R_{1 \max} &= 50; & s_1 &= 50 \text{ \$}; \\ R_{2 \min} &= 88; & R_{2 \max} &= 160; & s_2 &= 30 \text{ \$}; \\ p_1 &= 0.75; & p_2 &= 0.80; & p_3 &= 0.85; \\ D_1 &= 127; & D_2 &= 140; & D_3 &= 150. \end{aligned}$$

The optimization process is presented in Table 1. A conclusion can be drawn that the cyclic coordinate descent algorithm needs only two iterations with 23 search steps. Thus, the two-level heuristic algorithm performs well.

TABLE 1. Illustrative Performance of the Algorithm

Search step number	R_1	R_2	No. of iteration	Total resource expenses	Feasibility
1	50	160	1	1,043,900	feasible
2	49	160	1	1,036,750	feasible
3	48	160	1	1,029,600	feasible
4	47	160	1	1,022,450	feasible
5	46	160	1	1,015,300	feasible
6	45	160	1	1,008,150	feasible
7	44	160	1	1,001,000	feasible
8	43	160	1	1,070,300	non-feasible
9	44	159	1	996,710	feasible
10	44	158	1	992,420	feasible
11	44	157	1	988,130	feasible
12	44	156	1	983,840	feasible
13	44	155	1	979,550	feasible
14	44	154	1	975,260	feasible
15	44	153	1	970,970	feasible
16	44	152	1	966,680	feasible
17	44	151	1	962,390	feasible
18	44	150	1	958,100	feasible
19	44	149	1	953,810	feasible
20	44	148	1	949,520	optimal
21	44	147	2	945,230	non-feasible
22	43	148	2	1,014,860	non-feasible
23	45	148	2	956,670	feasible

7. Conclusions and future research

1. The developed optimization problem covers a realistic situation in a design office, at the stage of developing preliminary projects.
2. The problem can be solved by using a two-level algorithm. At the upper level a heuristic cyclic optimization procedure is suggested. At the lower level a simulation model is realized.
3. The developed model undertakes cost-optimization and can be used both in planning and monitoring several preliminary projects.
4. The backbone of the simulation model is the newly developed decision rule which is based on the minimax principle. The latter enables resource support to the “weakest” projects which deviate essentially from their targets, at the expense of “stronger” projects, which are more successful in the course of their realization.
5. The model can be modified for the case of projects with different priorities. This seems to be a perspective and interesting research since cost parameters have to be restricted while the objective is based on analyzing the projects different importance.
6. The developed model is easy in usage and can be implemented on a PC.

Acknowledgments

This research has been partially supported by the Paul Ivanier Center for Robotics Research and Production Management, Ben-Gurion University of the Negev.

References

- [1] Butera F. and Thurman J. eds. (1984) *Automation and Work Design. International Labour Organization*. New York - London.
- [2] Hajek, V.G. (1984) *Management of Engineering Projects*. McGraw-Hill Book Co., New York.
- [3] Muth, E.M. and Thompson, G.L. eds. (1963) *Industrial Scheduling*. Prentice Hall Englewood Cliffs, New Jersey.
- [4] Luenberger, D.G. (1973) *Introduction to Linear and Non-Linear Programming*. Addison Wesley Co., Massachusetts.
- [5] Gonik, A. (2000) A generalized resource constrained scheduling model for stochastic network projects. *Communications in Dependability and Quality Management* **3(1)**, 74-89.
- [6] Golenko-Ginzburg, D. and Gonik, A. (1997) Stochastic network project scheduling with non-consumable limited resources. *International Journal of Production Economics* **48**, 29-37.
- [7] Golenko-Ginzburg, D., Kesler, S.Sh. and Landsman, Z. (1995) Industrial job-shop scheduling with random operations and different priorities. *International Journal of Production Economics* **40**, 185-195.

Received on the 20th of December 2002

**ONE SIMPLE METHOD FOR SOLUTION
OF SOME CLASS OF INVERSE PROBLEMS**

S. GUSEINOV

*Transport and Telecommunication Institute
1 Lomonosov's Str., Riga LV-1019, LATVIA
and*

*Institute of Mathematics, Latvian Academy of Sciences and University of Latvia,
1 Academia's Square, Riga, LV-1524, LATVIA
E-mail: sharifg@tsi.lv*

As a rule, direct problems of heat transfer, in particular, the boundary-value problems of thermal conductivity with the boundary conditions of the first, second, third types and also the mixed type are well-posed problems. The corresponding coefficient inverse problems, in general case, are ill-posed and in order to determine the required unknown coefficients, the conforming additional condition is necessary. In this work we consider a certain class of nonhomogeneous one-dimensional on spatial variable coefficient inverse problems of thermal conductivity in the bounded domain under some additional information. In this work author offers one simple method for determination in the analytical form as required coefficient of thermal diffusivity, so the heat spreading in considered domain. Let us note that offered method is suitable for solution of a certain of nonlinear coefficient, boundary-value and retrospective inverse problems of mathematical physics.

Keywords: problem of thermal conductivity, inverse problems

Let us consider the following one-dimensional boundary-value problem:

$$\frac{\partial u}{\partial t} = a^2 \cdot \frac{\partial^2 u}{\partial x^2} + f(x,t), 0 < x < L, 0 < t < T, \quad (1)$$

$$u(x,t)|_{t=0} = h(x), 0 \leq x \leq L, \quad (2)$$

$$u(x,t)|_{x=L} = \gamma_2(t), 0 \leq t, \quad (3)$$

$$\frac{\partial u(x,t)}{\partial x} \Big|_{x=0} = 0, 0 \leq t. \quad (4)$$

Let there is the additional information, that

$$u(x,t)|_{x=0} = \gamma_1(t), 0 \leq t, \quad (5)$$

Inverse problem consists of the determination of constant thermal diffusivity coefficient a and the distribution of the temperature $u(x,t)$ in the field $D := [0, L] \times [0, T]$ under known $h(x)$, $\gamma_1(t)$, $\gamma_2(t)$ and $f(x,t)$.

Mathematical physics

For the solution of presented inverse problem we will represent the unknown function $u(x, t)$ in the following form:

$$u(x, t) = U^{(1)}(t) + x \cdot U^{(2)}(t) + \int_0^x (x - \xi) \cdot U^{(3)}(\xi, t) d\xi . \quad (6)$$

Now we will determine $U^{(1)}(t)$, $U^{(2)}(t)$ and $U^{(3)}(t)$ in expansion (6).

Considering additional information (5) in (6) we receive that

$$U^{(1)}(t) = \gamma_1(t) . \quad (7.1)$$

Similarly, considering boundary condition (4) in (6):

$$U^{(2)}(t) \equiv 0 . \quad (7.2)$$

Now considering (7.1) and (7.2) in (6) we receive that

$$u(x, t) = \gamma_1(t) + \int_0^x (x - \xi) \cdot U^{(3)}(\xi, t) d\xi . \quad (7.3)$$

Now in formula (7.3) let us replace the parameter t on τ and substitute obtained expression in initial equation (1) (where the parameter t is replaced on τ also):

$$\gamma_1'(\tau) + \int_0^x (x - \xi) \cdot \frac{\partial U^{(3)}(\xi, \tau)}{\partial \tau} d\xi = f(x, \tau) + a^2 \cdot U^{(3)}(x, \tau) .$$

Let us integrate this equality on τ from 0 till t :

$$\gamma_1(t) - \gamma_1(0) + \int_0^x (x - \xi) \cdot [U^{(3)}(\xi, t) - U^{(3)}(\xi, 0)] d\xi = a^2 \cdot \int_0^t U^{(3)}(x, \tau) d\tau + \int_0^t f(x, \tau) d\tau ,$$

or in another form

$$\gamma_1(0) + \int_0^x (x - \xi) \cdot U^{(3)}(\xi, 0) d\xi = \gamma_1(t) - \int_0^t f(x, \tau) d\tau + \int_0^x (x - \xi) \cdot U^{(3)}(\xi, t) d\xi - a^2 \cdot \int_0^t U^{(3)}(x, \tau) d\tau . \quad (8)$$

Now let us consider initial condition (2) in (7.3):

$$h(x) = \gamma_1(0) + \int_0^x (x - \xi) \cdot U^{(3)}(\xi, 0) d\xi .$$

Considering the last equality in (8) we get

$$\gamma_1(t) + \int_0^x (x - \xi) \cdot U^{(3)}(\xi, t) d\xi - h(x) = a^2 \cdot \int_0^t U^{(3)}(x, \tau) d\tau + \int_0^t f(x, \tau) d\tau . \quad (9)$$

From here

$$\int_0^T dt \int_0^L dx \gamma_1(t) + \int_0^T dt \int_0^L dx \int_0^x (x - \xi) \cdot U^{(3)}(\xi, t) d\xi -$$

Mathematical physics

$$-\int_0^T dt \int_0^L h(x) dx = a^2 \cdot \int_0^T dt \int_0^L dx \int_0^t U^{(3)}(x, \tau) d\tau + \int_0^T dt \int_0^L dx \int_0^t f(x, \tau) d\tau$$

After some simple transformations from last equality we will receive

$$\begin{aligned} & L \cdot \int_0^T \gamma_1(t) dt + \frac{1}{2} \cdot \int_0^L (L-x)^2 dx \int_0^T U^{(3)}(x, t) dt - T \cdot \int_0^L h(x) dx - \int_0^L dx \int_0^T (T-t) \cdot f(x, t) dt = \\ & = a^2 \cdot \int_0^L dx \int_0^T (T-t) \cdot U^{(3)}(x, t) dt . \end{aligned}$$

From here for the analytical determination of the coefficient of thermal diffusivity a we can write the following formula:

$$a^2 = \frac{L \cdot \int_0^T \gamma_1(t) dt + \frac{1}{2} \cdot \int_0^L (L-x)^2 dx \int_0^T U^{(3)}(x, t) dt}{\int_0^L dx \int_0^T (T-t) \cdot U^{(3)}(x, t) dt} - \frac{T \cdot \int_0^L h(x) dx + \int_0^L dx \int_0^T (T-t) \cdot f(x, t) dt}{\int_0^L dx \int_0^T (T-t) \cdot U^{(3)}(x, t) dt} . \quad (10)$$

It is evident from (10) that the coefficient a^2 is determined unambiguously, if function $U^{(3)}(x, t)$ is known. In the meanwhile unknown function $U^{(3)}(x, t)$ is determined by following simple procedure: at first, let us consider boundary condition (3) in (7.3):

$$\gamma_1(t) + \int_0^L (L-x) \cdot U^{(3)}(x, t) dx = \gamma_2(t) .$$

From here

$$\int_0^L (L-x) \cdot U^{(3)}(x, t) dx = \gamma_2(t) - \gamma_1(t) . \quad (11)$$

The equation (11) is Fredholm's first kind integral equation for determination of unknown function $U^{(3)}(x, t)$ in the field D .

After designating

$$\gamma(t) \stackrel{def}{=} \gamma_2(t) - \gamma_1(t) ,$$

$$A \bullet \stackrel{def}{=} \int_0^L (L-x) \bullet dx , \quad (12)$$

we can rewrite equation (11) in the following operator form:

$$(AU)(t) = \gamma(t) .$$

The equation (12) is first kind operator equation and, consequently, it is ill-posed problem. Having applied to (12) one of regularizing method, for example, the Tychonoff's regularization method, we can find the regularized solution $U_{REGUL}(x, t)$ of this problem. Further, considering $U_{REGUL}(x, t)$ in (10), we will easily find unknown coefficient of thermal diffusivity a , and then according to formula (7.3) also unknown function $u(x, t)$.

Remark 1. The operator equation (12) can be solved with the a priori assigned accuracy by the regularizing iterative process, described in the work [1]. Moreover, the order of convergence of this offered iterative method and also the optimum parameter of iteration are estimated in [1].

Mathematical physics

Remark 2. In the work [2] analogous with (2) problem was all over again solved by the regularizing discreteness of that problem, and then using of Tychonoff's smoothing out functional is solved in analytical form. Thus, the coefficient of thermal diffusivity a and $u(x, t)$ are located as in the analytical form according to formulas (10) and (11), (7.3), so and in the discrete form.

Remark 3. Offered method and the course of solution without essential changes is also transferred to similar boundary-value problems of the first, second and third types. The modified variant of this method also allows to solve some class of the nonlinear inverse problems of mathematical physics.

References

- [1] Guseinov Sh., Volodko I. (2003) On the order of convergence estimate of one regularizing method. *Journal of Mathematical Modelling and Analysis* **8**, 1
- [2] Guseinov Sh., Buikis A. (2001) Calculation of the thermal diffusivity for two layer media. *Latvian Journal of Physics and Technical Sciences*, No.4

Received on the 20th of December 2002

Authors' index

BROWN G.	24
FRIEDMAN L.	37
FUKS D.L.	24, 28
GOLENKO-GINZBURG D.	47
GONIK A.	47
GUSEINOV S.	55
JACOBS P.W.M.	7,18
HADAD Y.	37
KIV A.E.	24
KOVALEVSKA A.	7,18
KUTSENKO L.YU.	24
LASLO Z.	47
MALISHEVA A.	47
MEHREZ A.	37
SHUNIN YU.N.	7,18
SINUANY-STERN Z.	37
TALIANKER M.M.	37
ZHUKOVSKII YU.F.	7,18

Personalia



Yuri N. Shunin (b. March 6, 1951 in Riga)

- Computer simulation of semiconductor technologies, the Head of Department of natural sciences and computer modelling (Information System Institute). *Director of speciality:* Information Systems; professor of General and Applied Physics Department (Transport and Telecommunication Institute, Riga). *Director of specialities:* Semiconductor Electronics & Technologies,
- **University study:** Moscow physical and technical institute (1968-1974).
- Ph.D. (physics & mathematics) on solid state physics (1982, Physics Institute of Latvian Academy of Sciences), Dr. Sc. Habil (physics & mathematics) on solid state physics (1992, Ioffe Physical Institute of Russian Academy of Sciences).
- **Publications:** 220 publications, 1 patent.
- **Scientific activities:** solid state physics, physics of disordered condensed media, amorphous semiconductors and glassy metals, semiconductor technologies, heavy ion induced excitations in solids, mathematical and computer modelling, system analysis



Igor V. Kabashkin (born in Riga, 1954)

- Vice-rector for Research and Development Affairs of Transport and Telecommunication Institute, Professor, Director of Telematics and Logistics Institute,
- PhD in Aviation (1981, Moscow Institute of Civil Aviation Engineering), Dr.Sc.Habil. in Aviation (1992, Riga Aviation University), Member of the International Telecommunication Academy, Member of IEEE, Corresponding Member of Latvian Academy of Sciences (1998)
- **Publications:** 290 scientific papers and 67 patents.
- **Research activities:** information technology applications, operations research, electronics and telecommunication, analysis and modelling of complex systems, transport telematics and logistics



Yuri F. Zhukovskii (b. February 2, 1949, Riga, Latvia),

Theoretical Laboratory of Institute Solid State Physics, University of Latvia

Education: 1966-75. **B.S. + M.S. degrees:** Department of Physics and Mathematics, the University of Latvia, Riga, Latvia. 1986-92. **Ph.D. degree (Dr. chem.):** Institute of Inorganic Chemistry, Latvian Academy of Sciences, Latvia, and Institute of Physics, St. Petersburg State University, Russia.

Advisors: Dr. chem. A.K. Lokenbach (Riga) and Dr. phys. E.P. Smirnov (St. Petersburg).

Title of the Thesis: "Quantum-chemical investigations of water chemisorption on aluminum surface".

Publications: 80 papers and conference abstracts dealing with the quantum chemistry.

CONFERENCES: 32 presentations dealing with the quantum chemistry were prepared for 27 international conferences, meetings, seminars and symposiums organized in 12 countries (with 28 published abstracts).

01-03.2000. Visiting scientist, Centre for Materials Research, University College London, Great Britain; 04-05. and 10-11.2000. Visiting scientist, the Ångström Laboratory, Inorganic Chemistry, Uppsala University, Sweden



Arnold E. Kiv, professor, Dr. Sc. Habil (phys&math)

- Chief of Theoretical Physics Department and Computer Modelling Laboratory South Ukrainian Pedagogical University, professor of the Department of Materials Engineering, Ben-Gurion University of the Negev P.O.B. 653, Beer-Sheva, 84105, Israel
- Scientific activities:** sub-threshold radiation effects in solids. Present scientific activities: computer modelling of processes in physics, psychology and social sciences.

Personalia



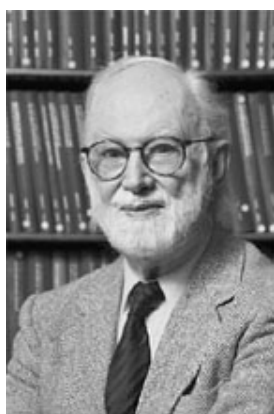
David Fuks (b. December, 1948, Odessa, Ukraine)

Professor, Dr. Sc. Habil. Prof. of the Department of Materials Engineering of the Ben-Gurion University of the Negev (Israel).

University study: Mechnikov Odessa State University, Department of Theoretical Physics, 1971

Publications: One book, six chapters in collective volumes and more than 200 papers.

Scientific interests: Phase transitions in metal alloys and compounds, structure of solids, diffusion processes in solids, computer modelling in materials science.



Patrick W.M. Jacobs (b. on September 15, 1923, Durban, South Africa)

Dr.Sc., Professor Emeritus, Department of Chemistry and Centre for Chemical Physics, The University of Western Ontario, London, ON, Canada, N6A 5B7

Publications: More than 315 papers in the fields of solid state reactions, electrical and optical properties of ionic crystals, energies and entropies of formation, migration and association of point defects in ionic crystals

Scientific interests: Current projects in computer simulation of condensed matter include: molecular dynamics of ionic crystals, especially fast-ion conductors, and quantum chemistry of solids, especially ionic crystals, light metals and metal/ceramic interfaces.

Sharif Guseinov, Dr.Sc. in Mathematics

Education: 1983-1985 Student of Faculty of Applied Mathematics, Azerbaijan State University

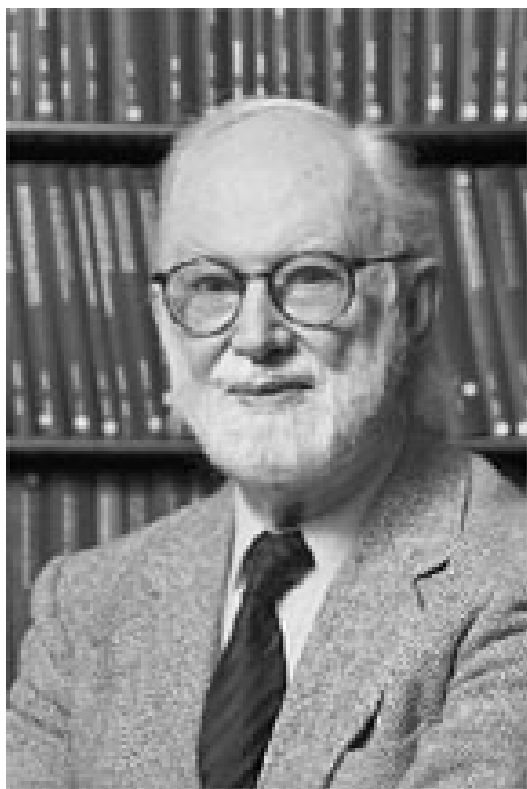
1987-1991 Student of Department of Mathematics and Cybernetics, Lomonosov's Moscow State University, 1991-1994 Ph.D. student of Lomonosov's Moscow State University. Dissertation thesis: "The methods of solution of inverse problems of magneto - telluric sounding."

Professional Experience: 1995-1997 Lomonosov's Moscow State University, lecturer

1997-1999 International Institute of Nuclear Physics, assistant scientist, since 2001 - The Main Scientific Employee of Institute of Mathematics of Latvian University and Latvian Academy of Sciences; senior lecturer of Transport and Telecommunication Institute.

Publications: Since 1991 till 2003 were published 42 scientific articles and contributions to conferences.

Patrick W.M. JACOBS - 80



Patrick W.M. JACOBS was born on September 15, 1923, Durban, South Africa, Dr.Sc., Professor Emeritus, Department of Chemistry and Centre for Chemical Physics, The University of Western Ontario, London, ON, Canada, N6A 5B7

More than 315 papers in the fields of solid state reactions, electrical and optical properties of ionic crystals, energies and entropies of formation, migration and association of point defects in ionic crystals¹. Current projects in computer simulation of condensed matter include: molecular dynamics of ionic crystals, especially fast-ion conductors, and quantum chemistry of solids, especially ionic crystals, light metals and metal/ceramic interfaces.

Editorial board of CM&NT sends best wishes to professor Patrick Jacobs.

¹ **Patrick W. M. Jacobs** - Professor Emeritus M.Sc. (Natal) DIC, Ph.D., D.Sc. Imperial College, University of London
Office: Rm 126, Lab Rm 26, Chemistry Building, Office: 661-3933, ext. 83933, Lab: 661-2111, ext. 86661,
pjacobs@uwo.ca

COMPUTER MODELLING & NEW TECHNOLOGIES

ISSN 1407-5806 & ISSN 1407-5814(on-line)

EDITORIAL BOARD:

Prof. Igor Kabashkin (Chairman of the Board), *Transport & Telecommunication Institute, Latvia;*

Prof. Yuri Shunin (Editor-in-Chief), *Transport & Telecommunication Institute, Latvia;*

Prof. Adolfas Baublys, *Vilnius Gediminas Technical University, Lithuania;*

Dr. Brent Bowen, *University of Nebraska at Omaha, USA;*

Prof. Olgierd Dumbrajs, *Helsinki University of Technology, Finland;*

Prof. Eugene Kopytov, *Transport & Telecommunication Institute, Latvia;*

Prof. Arnold Kiv, *Ben-Gurion University of the Negev, Israel;*

Prof. Anatoly Kozlov, *Moscow State University of Civil Aviation, Russia;*

Prof. Juris Zakis, *University of Latvia;*

Prof. Edmundas Zavadskas, *Vilnius Gediminas Technical University, Lithuania.*

Technical editor:

MS Christina Hamroon, *Transport & Telecommunication Institute, Latvia*

MS Cyril Budilov, *Transport & Telecommunication Institute, Latvia*

Host Organization:

Transport and Telecommunication Institute - Eugene Kopytov, Rector

Co-Sponsor Organizations:

PAREX Bank, Latvia - Valery Kargin, President

Supporting Organization:

Latvian Transport Development and Education Association - Andris Gutmanis, President

Latvian Academy of Sciences - Juris Ekmanis, Vice-president

Latvian Operations Research Society – Igor Kabashkin, President

University of Nebraska at Omaha , USA - Brent Bowen, Director of Aviation Institute

The Khaim Kordonsky Charitable Foundation

**THE JOURNAL IS DESIGNED FOR PUBLISHING PAPERS CONCERNING THE
FOLLOWING FIELDS OF RESEACH:**

- mathematical and computer modelling
- mathematical methods in natural and engineering sciences
- physical and technical sciences
- computer sciences and technologies
- semiconductor electronics and semiconductor technologies
- aviation and aerospace technologies
- electronics and telecommunication
- navigation and radar systems
- telematics and information technologies
- transport and logistics
- economics and management
- social sciences

Computer Modelling & New Technologies Preparation of Publications

Articles are presented in the journal in English (preferably), Russian, German and Latvian languages (at the option of authors). All articles are reviewed.

EDITORIAL CORRESPONDENCE

Transporta un sakaru institūts (Transport and Telecommunication Institute)
Lomonosova iela1, LV-1019, Riga, Latvia. Phone: (+371)-7100593. Fax: (+371)-7100535.
E-mail: journal@tsi.lv, <http://www.tsi.lv>

COMPUTER MODELLING AND NEW TECHNOLOGIES, 2003, Vol.7, No.1
Scientific and research journal of Transport and Telecommunication Institute (Riga, Latvia).
The journal is published since 1996.

The Camera-Ready Copies

PREPARATION OF CAMERA-READY TYPESCRIPT: COMPUTER MODELLING AND NEW TECHNOLOGIES

A Guide for Authors

A.N. AUTHOR

Affiliation

Institute address

Abstract reviews the main results and peculiarities of a contribution. Abstract is presented always in English or in English and the second (presentation) language both.

Keywords: main terms, concepts

1. Introduction

These instructions are intended to provide guidance to authors when preparing camera-ready submissions to a volume in the **CM&NT**. Please read these general instructions carefully before beginning the final preparation of your camera-ready typescript.

Two ways of preparing camera-ready copy are possible:

- (a) preparation on a computer using a word processing package;
- (b) printed copy fitted for scanning.

2. Printer Quality, Typing Area and Fonts

IMPORTANT:

If you produce your camera-ready copy using a laser printer, use a 15 x 23 cm typing area (in A4 format: 30 mm - left, 30 mm- right, 30 mm- top, 30 - bottom, line spacing - single), as in these instructions, in combination with the **10 points Times** font. The pages will then be reproduced one to one in printing.

Fonts

The names and sizes of fonts are often not the same on every computer system. In these instructions the Times font in the sizes 10 points for the text and 8 points for tables and figure legends are used. The references section should be in the 10 points font.

3. Format and Style

The text should be in clear, concise English (or other declared language). Please be consistent in punctuation, abbreviations, spelling (**British English**), headings and the style of referencing.

Camera-ready copy will be printed exactly as it has been submitted, so please make sure that the text is proofread with care.

Computer Modelling & New Technologies Preparation of Publications

In general, if you prepare your typescript on a computer using a word processing package, use styles for the font(s), margin settings, headings, etc., rather than inserting these layout codes every time they are needed. This way, you will obtain maximum consistency in layout. Changes in the layout can be made by changing relevant style(s).

4. Layout of the Opening Page

A sample for the opening page of a contribution is shown in Figure 1 on page 3. Requirements for the opening page of a contribution are (see also Figure 1) : the titles should always be a centered page and should consist of: the title in capital letters, bold font, flush center, on the fourth text line; followed by the subtitle (if present) in italics, flush center, with one line of white above. The author's name(s) in capitals and the affiliation in italics, should be centered and should have two lines of white space above and three below, followed by the opening text, the first heading or the abstract.

5. Headings

Please distinguish the following four levels of headings:

1. First-order Heading

This heading is in bold, upper and lowercase letters, numbered in arabic figures, and has two lines of space above and one line below. The text begins full out at the left margin.

1.1. SECOND-ORDER HEADING IN CAPITALS

This heading is in roman capitals, numbered in arabic figures and has one line of space above and below. The text begins full out at the left margin.

1.1.1. *Third-order Heading in Italics*

This heading is in italics, upper and lower case letters, numbered in arabic figures and has one line of space above and no space below. The text begins full out at the left margin.

Fourth-order Heading in Italics. This heading is in italics, upper and lowercase letters, with one line of space above the heading. The heading has a full stop at the end and the text runs on the same line.

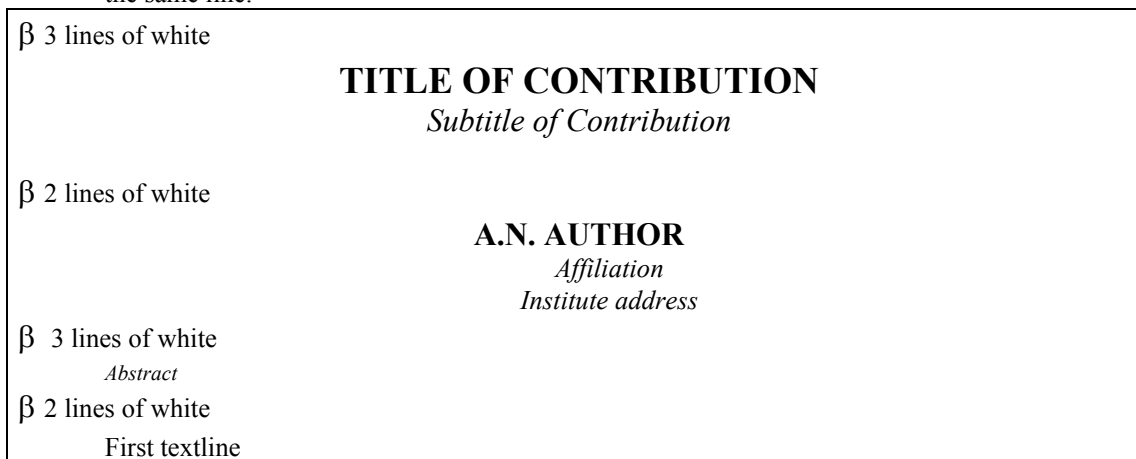


Figure 1. Example of an opening part of contribution to a Volume of CM&NT.

6. Figures and Photographs

- *Line drawings* must be submitted in original form, on good quality tracing paper, or as a glossy photographic print.

- *Halftone photographs* must be supplied as glossy prints.

- *Colour illustrations.* Colour illustrations are more expensive and the author is expected to cover the extra costs . Please consult with Editors about this.

Mount all illustrations directly into the text at the appropriate places. Alternatively, it is acceptable to leave the appropriate space blank in the text, and submit the illustrations separately. In this case You

Computer Modelling & New Technologies Preparation of Publications

must put the figure numbers in pencil in the open spaces in the text and on the back of the figures. Also indicate the top of the illustration.

For computer plotting the ORIGIN Software is preferable.

- Legends for figures/illustrations should not be incorporated in the figure itself and they should be listed in numerical order (headed as "Figure 1.", "Figure 2.", etc.). The legends should be set centered, below the figure.

7. Displayed Equations

Displayed equations should be in the left side of the page, with the equation number in parentheses, flush right.

$$E_{int} = \iint \psi^+(\mathbf{x})\psi(\mathbf{x})K(\mathbf{x}-\mathbf{x}')(-div\mathbf{P}(\mathbf{x}'))d^3x d^3x', \quad (1)$$

$$K(\mathbf{x}-\mathbf{x}') = C_0 \frac{\exp(-\lambda(|\mathbf{x}-\mathbf{x}'|))}{|\mathbf{x}-\mathbf{x}'|}. \quad (2)$$

Font sizes for equations are: 12pt -full, 7pt - subscripts/superscripts, 5pt - sub- subscripts/superscripts, 18pt - symbols, 12pt - subsymbols .

8. Tables

Please center tables on the page, unless it is necessary to use the full page width. Exceptionally large tables may be placed landscape (90° rotated) on the page, with the top of the table at the left-hand margin. An example of a table is given below:

TABLE 1. National programs of fusion research [1]

Experiment	Type	Laboratory	Task	Begin of operation
JET	tokamak	Joint European Torus, Culham, UK	Plasma physics studies in the region close to ignition	1983
TEXTOR	tokamak	FA, Jülich. Germany	Studies of plasma-wall interaction	1982
TORE SUPRA	tokamak	CEA, Cadarache, France	Testing of super-conducting coils, stationary operation	1988
ASDEX Upgrade	tokamak	IPP, Garching, Germany	Plasma boundary studies in divertor plasmas	1990
WENDELSTEIN 7-AS	stellarator	IPP, Garching, Germany	Testing the principles of "advanced stellarator"	1988
WENDELSTEIN 7-X	stellarator	IPP, Greifswald, Germany	Testing feasibility of "advanced stellarator" for power station	2004

9. References

The References should be typeset in a separate section as a numbered list at the end of your contribution in the following style:

Journal articles should consist of: author's name, initials, year, title of article, journal title, volume number, inclusive page numbers, e.g.:

- [1] Dumbrajs O. (1998) Nuclear Fusion. *RAU Scientific Reports & Computer Modeling & New Technologies* **2**, aa-zz
- [2] Kiv A.E. , Polozovskaya I.A., Tavalika L.D. and Holmes S. (1998) Some problems of operator-machine interaction.. *RAU Scientific Reports & Computer Modelling & New Technologies* **2**, aa-zz
- [3] Shunin Yu.N. (1996) Elementary excitations and radiation defects in solids induced by swift heavy ions. *RAU Scientific Reports & Solid State Electronics & Technologies* **1**, 15-35
- [4] Schwartz K. (1996) Excitons and radiation damage in alkali halides. *RAU Scientific Reports* &

Computer Modelling & New Technologies Preparation of Publications

Solid State & Electronics & Technologies 1, 3-14

Book references should consist of: author's name, initials, year, title of book, publisher, place of publication, e.g.:

[5] Schwartz K. (1993) *The Physics of Optical Recording*. Springer-Verlag, Berlin Heidelberg New York

[6] Shunin Yu.N. and Schwartz K.K. (1997) Correlation between electronic structure and atomic configurations in disordered solids. In: R.C. Tennyson and A.E. Kiv (eds.). *Computer Modelling of Electronic and Atomic Processes in Solids*. Kluwer Academic Publishers, Dordrecht, pp. 241-257 .

Unpublished papers should consist of: author's name, initials, year (or: in press), title of paper, report, thesis, etc., other relevant details, e.g.:

[7] Shunin Yu.N. (1995) Elementary Excitations in amorphous solids accompanying the swift heavy ions passages. Private communication. GSI Seminar. Darmstadt

The references above should be cross-referenced by numbers within square brackets:

...as cited in [1], or Kiv *et al.* [2]... The use of author initials for cross-references is not encouraged.

10. Authors Index

Editors form the author's index of a whole Volume . Thus , all contributors are expected to present personal colour photos with the short information on the education , scientific titles and activities.

11. Submission

Check your typescript very carefully before it is submitted. Submit two copies of the typescript to the Editors of the Volume. Always retain a copy of all material submitted as backup.

11.1. DISK FORMATS AND WORD PROCESSING PACKAGES

If you want to present contributions electronically please before submitting accord with the Editors the details on your computer system, your word processing package and version (MS Word 6 and above versions are preferable) and the way of transfer on the information (disk or Internet).

Acknowledgements

Acknowledgements (if present) mention some specialists , grants and foundations connected with the presented paper. The first page of the contribution should start on page 1 (right-hand, upper, without computer page numbering). Please paginate the contributions, in the order in which they are to be published. Use simple pencil only.